Robot Manipulator Skill Learning and Generalising through Teleoperation

Weiyong Si

A thesis submitted in partial fulfilment of the requirements of the University of the West of England, Bristol for the degree of Doctor of Philosophy

PhD Dissertation

School of Engineering

University of the West of England, Bristol

August 10, 2023

Abstract

Robot manipulators are widely used in industrial settings for simple and repetitive tasks but are challenging to use in human-centred environments for complex manipulation tasks. Advances in collaborative robotics and machine learning have increased interest in robot skill learning, but learning complex and compliant manipulation skills remains challenging. In addition, teleoperation allows precise control of robots and human intelligence to perform safety-critical tasks from a distance. Various human-robot collaboration interfaces based on augmented and virtual reality have been developed to integrate robot control and telemanipulation by human operators. In this dissertation, we study human-robot skill transfer and generalisation through intuitive teleoperation interfaces for contact-rich manipulation tasks, including medical examinations, manipulating deformable objects, and composite layup in manufacturing.

This thesis has three main parts. Part 1 (Chapter 3) focuses on the development and controller design of teleoperation systems with multimodal feedback, forming the foundation for robot learning from human demonstration and interaction. In this chapter, we compare the two different teleoperation interfaces and propose a comparative metric to evaluate the interface for a specific task, robot-assisted medical examination. In Part 2 (Chapters 4, 5, 6), we investigated various methods to model the manipulation skills and improve the generalisation capability to new tasks. Part 2 proposed primitive skill library theory (Chapter 4), human-in-the-loop mechanism (Chapter 5), and perception-enhanced method (Chapter 6) to improve the generalization capability of learning from human demonstration. In Part 3 (Chapters 7, 8), two typical applications, composite layup (Chapter 7) and robot-assisted

ultrasound scanning (Chapter 8), are used to evaluate the effectiveness of the proposed methods. In addition, we investigate deep multimodal neural networks to encode manipulation skills, particularly multimodal perception information, for ultrasound scanning skills. Finally, Chapter 9 summarizes this thesis's main work, contributions, and potential directions.

Keywords: Learning from demonstration; Teleoperation; Multimodal interface; Human-in-the-loop; Compliant control; Human-robot interaction; Robot-assisted sonography.

Acknowledgements

I would like to thank my supervisors for giving me the opportunity to pursue my PhD in such an amazing Lab - Bristol Robotics Lab (BRL). Prof. Chenguang Yang taught me so much invaluable research and life experience, and this thesis would not have been possible without his continuous support, patience, insights and availability. Dr Ning Wang has offered guidance, valuable advice, and the opportunity to participate in teaching. BRL is an exciting place to work, and I am thankful for having been part of it for the past 3 years.

My progression reviewers Prof. Quanmin Zhu and Dr Shancang Li have also played an important role in the development of my work. Their annual comments and advice have helped shape and improve my thesis. And thanks to my external examiner for his time and effort. I also would like to thank the FET department and graduate school staff for supporting the administration of my PhD study.

I would like to thank collaborators during my PhD study, from whom I have learned various skills and insights about research: Tianqi Yue, Yuan Guan, Xueyan Xing, Zhenyu Lu, Zhehao Jin, Jiale Dong, Guanyi Zhao, Xian Li, Cheng Guo, Tianjian Zhong and Dandan Zhang. I would like to thank to Nicola and Rebecca for their support on ultrasound scanning. And I also would like to thank ORCA Medical Ltd for its support of the ultrasound machine. Especially, I would like to thank Prof. Yang again to allow me and provide the possibilities to have all these different collaborations.

I felt really lucky to have worked with my colleagues in Teleoperation Group, Zhenyu Lu, Donghao Shi, Yuan Guan, Jimmy Bostock, Xueyan Xing, Chen Jia, Lan Huang, Yanlei Li, Suhas, Arturs, Zhehao Jin, Tong Zhao. I truly thank them for all the interesting conversations on various topics and for the

inspiring working environment they have built.

I would like to dedicate this thesis to my parents, my old sister and my wife. Without them the infinite mental support, I would have never reached the place where I am now. Many thanks to my nephew and niece for bringing me so much joyful time together.

Finally, I am very grateful to the University of the West of England for providing me with the research scholarship to undertake the PhD study.

Publication list

Journal papers

1. Si, W., Wang, N. and Yang, C., 2021. A Review on Manipulation Skill Acquisition through Teleoperation-based Learning from Demonstration. Cognitive Computation and Systems, 3(1), pp.1-16. (IET Premium Awards 2022)

2. Si, W., Wang, N. and Yang, C., 2021. Composite Dynamic Movement Primitives based on Neural Networks for Human–robot Skill Transfer. Neural Computing and Applications, pp.1-11.

3. Yue, T., Si, W., Partridge, A., Yang, C., Conn, A., Gadelha, H., Rossiter, J. A Semi-active, 2022 Contact-triggered Universal Soft Suction Cup. IEEE Robotics and Automation Letters.

4. Si, W., Guan, Y. and Wang, N, 2022. Adaptive Compliant Skill Learning for Contact-Rich Manipulation with Human in the Loop. IEEE Robotics and Automation Letters.

5. Si, W., Wang, N., Li, Q., Yang, C. (2022). A Framework for Composite Layup Skill Learning and Generalizing Through Teleoperation. Frontiers in Neurorobotics, 1-16.

6. Dong, J., Si, W., and Yang, C. "A novel human-robot skill transfer method for contact-rich manipulation task." Robotic Intelligence and Automation (2023).

7. Xing, X., Burdet, E., Si, W., Yang, C., Li, Y. (2023). Impedance Learning for Human-Guided Robots in Contact With Unknown Environments. IEEE Transactions on Robotics.

Conference papers

1. Si, W., Wang, N. and Yang, C., 2021. Reactive and Constrained Motion Primitive Merging and Adaptation. 26 International Conference on Automation and Computing (ICAC2021).

2. Dong, J, Si, W. and Yang, C., 2021. A DMP-based Online Adaptive Stiffness Adjustment Method. In IECON 2021 Annual Conference of the IEEE Industrial Electronics Society.

3. Si, W., Yue, T., Guan, Y., Wang, N., Yang, C. (2022, August). A Novel Robot Skill Learning Framework Based on Bilateral Teleoperation. In 2022 IEEE 18th International Conference on Automation Science and Engineering (CASE) (pp. 758-763). IEEE.

4. Si, W., Guo, C. , Dong, J. , Lu, Z. and Yang, C., 2022. Deformation-aware Contact-rich Manipulation Skills Learning and Compliant Control. 15th International Workshop on Human-Friendly Robotics, included within Springer Proceedings in Advanced Robotics.

5. Li, X., Si, W., Yang, C. (2022, June). An Observation Based Method for Human Robot Writing Skill Transfer. In 2022 IEEE 17th International Conference on Control and Automation (ICCA) pp. 412-417.

6. Si, W., Zhong, T, Wang, N. and Yang, C, (ICM2023). A Multimodal Interface-based Framework for Human-robot Collaboration. IEEE International Conference On Mechatronics, 2023.

7. Tian, J., Si, W., Wang, N. Yang, C. A Vision-based Target Localization Method for Robot-assisted Sonography. In 2023 28th International Conference on Automation and Computing.

8. Dong, J., Si, W., Wang, N. Yang, C. Robot Learning from Multiple Demonstrations Based on Generalized Gaussian Mixture Model. In 2023 28th International Conference on Automation and Computing.

Contents

List of Figures

List of Tables

Nomenclature

AR Augmented reality

Cobots Collaborative robots

DMPP DMPs with perceptual term

DMPs Dynamic Movement Primitives

EMG Electromyography

F/T sensor 6-axis force/torque sensor

FCI Franka Control Interface

GMM Gaussian mixture model

HITL Human-in-the-loop

HMM Hidden Markov Model

HRC Human-robot collaboration

KMP Kernelized movement primitives

LfD Learning from demonstration

MLP Multilayer perceptron

NN Neural network

ProMPs Probabilistic movement primitives

RBFNNs Radial basis function neural networks

ROS Robot operating system

SDK Software development kit

VR Virtual Reality

1 Introduction

1.1 Background

Robot manipulators have been widely employed in various fields, including manufacturing, space exploration, material handling, rehabilitation and telemedicine robots (Zeng et al., 2018; Lamon et al., 2019; Björnsson, Jonsson, and Johansen, 2018; Gao, Zhou, and Asfour, 2020; Madhani, Niemeyer, and Salisbury, 1998). The utilization of these manipulators in structured environments is common due to their cost-effectiveness and efficiency, particularly for repetitive and simple tasks. However, performing physical contact-rich tasks, such as manipulating deformable objects or physical human-robot interaction, is still challenging for robots. These tasks require the robot to interact with its environment compliantly and adaptively. Despite recent advancements in autonomous manipulation technology, performing real-world tasks autonomously in unstructured and dynamic conditions remains a challenge. In addition, teleoperation, often referred to as the human-in-the-loop mechanism, offers a viable solution for remote manipulation, even when confronted with limited information. Therefore, this project aims to study robot manipulator skill learning and generalising through teleoperation to overcome the aforementioned challenges.

Complex and human-like manipulation skill acquisition through teleoperation-based learning from demonstration provides a solution to teach robots own human-like manipulation skills; however, it is still very challenging, such as how to capture the human skills, how to encode the manipulation skills, and how to generalise the learned skills to novel tasks and conditions etc. To tackle these challenges, we

conduct this research from the design of intuitive human-robot interfaces, teleoperation-based human-robot shared control, multimodal manipulation skill modelling and compliant control etc. There are a number of practical applications in both medical examination and flexible industry. For example, ultrasound scanning, also known as sonography, illustrate a cost-effective, convenient, and safe diagnostic approach that involves various aspects of dexterous manipulation. These tasks encompass real-time adjustments in motion, orientation, and force regulation, relying on immediate medical imaging data and patient feedback. Thus, in this project, we employed ultrasound scanning, composite layup, and daily manipulation tasks to validate the proposed framework and various algorithms.

1.2 Motivation

Why do we design an intuitive, natural and trusted teleoperation interface for efficient human-robot skill transfer?

This project focuses on learning and generalizing manipulation skills for contact-rich tasks that require physical interaction with the object and environment. The success of such tasks heavily depends on multimodal feedback, such as haptic and visual feedback etc., and safety-critical applications also require reactive and trustworthy interaction with the environment and humans. However, designing an intuitive and natural teleoperation interface for dexterous manipulation tasks is challenging, especially for contact-rich manipulation tasks like medical examinations, which can be cognitively demanding for human operators. This makes designing an intuitive and intelligent interface challenging for human-robot skill transfer. To address this challenge, we will design a multimodal human-robot interface for efficient human-robot skill transfer. In addition, we will also propose an evaluation metric to assess the performance of this interface. Physical human-robot collaboration (HRC) interfaces will be developed to integrate robot control and telemanipulation by human teachers.

Why do we adopt the teleoperation-based approach for robot skill learning and generalising?

Regarding the demonstration methods used in learning from demonstration (LfD), there are three main approaches for capturing human skills: kinesthetic teaching, teleoperation, and passive observation. Compared to kinesthetic teaching and passive observation, the teleoperation-based method has several advantages for human-robot skill transfer due to its ability to provide a multimodal interface for human teachers.

The teleoperation-based demonstration can overcome the limitations of physical workspaces, allowing human teachers to control robots that work in remote, dangerous, and inaccessible environments. The human operator can provide demonstrations remotely, without the need to share a workspace with robots. Additionally, having a separate workspace is safer for human teachers, especially in dangerous working environments and tasks, such as nuclear waste decomposition.

The teleoperation-based demonstration can easily capture the multimodal information of human manipulation, such as kinematic motion profiles, Electromyography (EMG) signals of the human arm, and interaction force. This multimodal information is essential for encoding the dexterous manipulation skills of humans and transferring these human-like manipulation skills to robots.

The teleoperation-based demonstration can combine the autonomy of the robot and the intelligence of humans, improving the quality of the demonstration data. Teleoperation-based frameworks provide a mechanism for combining the human-in-the-loop and the autonomous control of robots. Compared to kinesthetic teaching, the precision of demonstrations can be improved due to the accurate control of robots' control systems.

The teleoperation-based demonstration allows the teleoperator to telemanipulate the robot in a scale-up or scale-down to control robots. For fine manipulation, telemanipulation by scale-down can reduce the effect of human tremble and improve control accuracy. However, scale-down telemanipu-

lation will decrease the workspace of robots. For different tasks, adaptive scaling parameters can be designed to adapt to the task.

The teleoperation-based demonstration allows the human operator to interactively teach robot skills and correct the robot's behavior online. Traditional human-robot skill transfer methods mainly focus on learning from human demonstration offline. However, the process of human acquisition is gradual, and the teleoperation-based human-robot skill transfer scheme allows the human-robot skill transfer process to be more dynamic.

While teleoperation-based learning from demonstration has many benefits, there are also a few challenges to consider:

Designing an intuitive and natural teleoperation interface for dexterous manipulation tasks is challenging, especially for contact-rich manipulation tasks like medical examinations. First, the cognitive workload is huge for human operators, making it difficult to create an intuitive and intelligent interface design for human teachers. In addition, human-robot collaboration and its control algorithms to achieve high-quality demonstrations can be challenging due to uncertain tasks and environments. Allocating control subtasks for human teachers and robots during the human demonstration phase for complex and multi-step tasks is unresolved. Also, the stability and convergence of the control system must be guaranteed.

Processing data collected from teleoperation demonstrations is challenging because of the different configurations of the leader robot and the follower robot. For example, the demonstration data from the leader robot and the following robot are often in different spaces. Most teleoperation-based demonstration methods only focus on the data from the robot side, ignoring the data collected from the leader side. However, human data, such as EMG signals, can be used to describe the stiffness of the human arm. In addition, the skill recognition and segmentation of teleoperation-based demonstration are also chal-

lenging, particularly for the online processing of multimodal information. Automatic skill recognition and segmentation based on sensory feedback data are necessary for teleoperation-based human-robot skill transfer online. Last, the mapping design from the leader device to the follower robot is also challenging, particularly for tasks with multiple constraints like the medical examination that requires adjusting the position, orientation and contact force continuously to attain the desired image and ensure the patient's safety and comfort.

Why do we study the manipulation skill encoding?

Although there has been extensive research on skill encoding for motion skills, transferring human-like manipulation skills to robots remains a challenging task. In particular, encoding stiffness skills and force skills poses significant difficulties. The main challenges of skill encoding stem from contact-rich manipulation tasks and multi-step complex skills. The generalisation capability of the encoding skill model is still an open issue, and ongoing research efforts are focused on improving it. Additionally, ensuring convergence and safety during robot skill learning is also a challenging task that requires further investigation.

Ensuring the safety and convergence of contact-rich manipulation skills is a crucial challenge in skill encoding. Skill encoding is akin to a planner, encompassing orientation, motion trajectory, and force trajectory planners, among others. The dynamic system method can be employed to guarantee the convergence and safety of these manipulation skills. Multimodal skill encoding is necessary for physical human-robot interaction tasks, as unimodal motion skills alone may not suffice for contact-rich tasks. Fine manipulation tasks often require more than just motion skills, including orientation, contact force, and stiffness. Developing a composite manipulation skill model for multimodal skills is a necessary and challenging task.

1.3 Aims and objectives

This proposed PhD project aims at studying the robot manipulator skill learning and generalising through teleoperation. There are three main aims of this project.

- To design an intuitive, natural and trusted teleoperation interface to capture a range of human teachers' skills for efficient human-robot skill transfer.
- To study how to encode human teachers' complex and multi-step manipulation skills by investigating the primitive skill theory and dynamic system-based skill model.
- To enhance the generalisation ability of the skill model by investigating the human-in-the-loop mechanism, perception information and neural networks.

Specifically, the main research questions to be answered in this project are as follows.

- How to encode the human manipulation skill to achieve human-robot skill transfer efficiently?
- How to develop a control system with human-in-the-loop for the robot manipulator to achieve compliant manipulation?
- For the contact-rich tasks, how to encode the manipulation skill to guarantee robot interaction with the environment safely, reactively, and compliantly?
- How to develop a teleoperation system to achieve human-robot skill transfer effectively and intuitively?
- How to improve the skill model generalisation ability to novel tasks and environments?
- How to validate the proposed theory and algorithms through real applications, flexible manufacturing and medical examination?

1.4 Research hypothesis

- Robot manipulators can acquire dexterous manipulation skills similar to human beings through teleoperation-based learning from demonstration.
- Decomposing complex and multi-step manipulation skills into primitive skills during the modeling stage, and then merging them into a complex action during the execution stage, can greatly facilitate human-robot skill transfer.
- Combining the compliant control and learning from human demonstration is necessary for robot manipulators to perform contact-rich manipulation tasks autonomously.
- Perception information, deep neural network and human-in-the-loop mechanism can improve the generalisation and robustness of the learned skill model.

1.5 Main contribution and thesis outline

The pipeline of my PhD research project is shown in Fig. 1.1. The introduction, motivation and objectives of this thesis are introduced in Chapter 1. In Chapter 2, a literature review on manipulation skills acquisition through teleoperation-based demonstration is carried out, and the motivation and objectives of this thesis are discussed subsequently. Overall, the main contents and contributions of this thesis are as follows:

Part 1 introduces the development and controller design of teleoperation systems with multimodal feedback, which is the foundation of this project for robot learning from human demonstration and generalising to various tasks and conditions.

In Chapter 3, the hardware and software development of the multimodal teleoperation system are

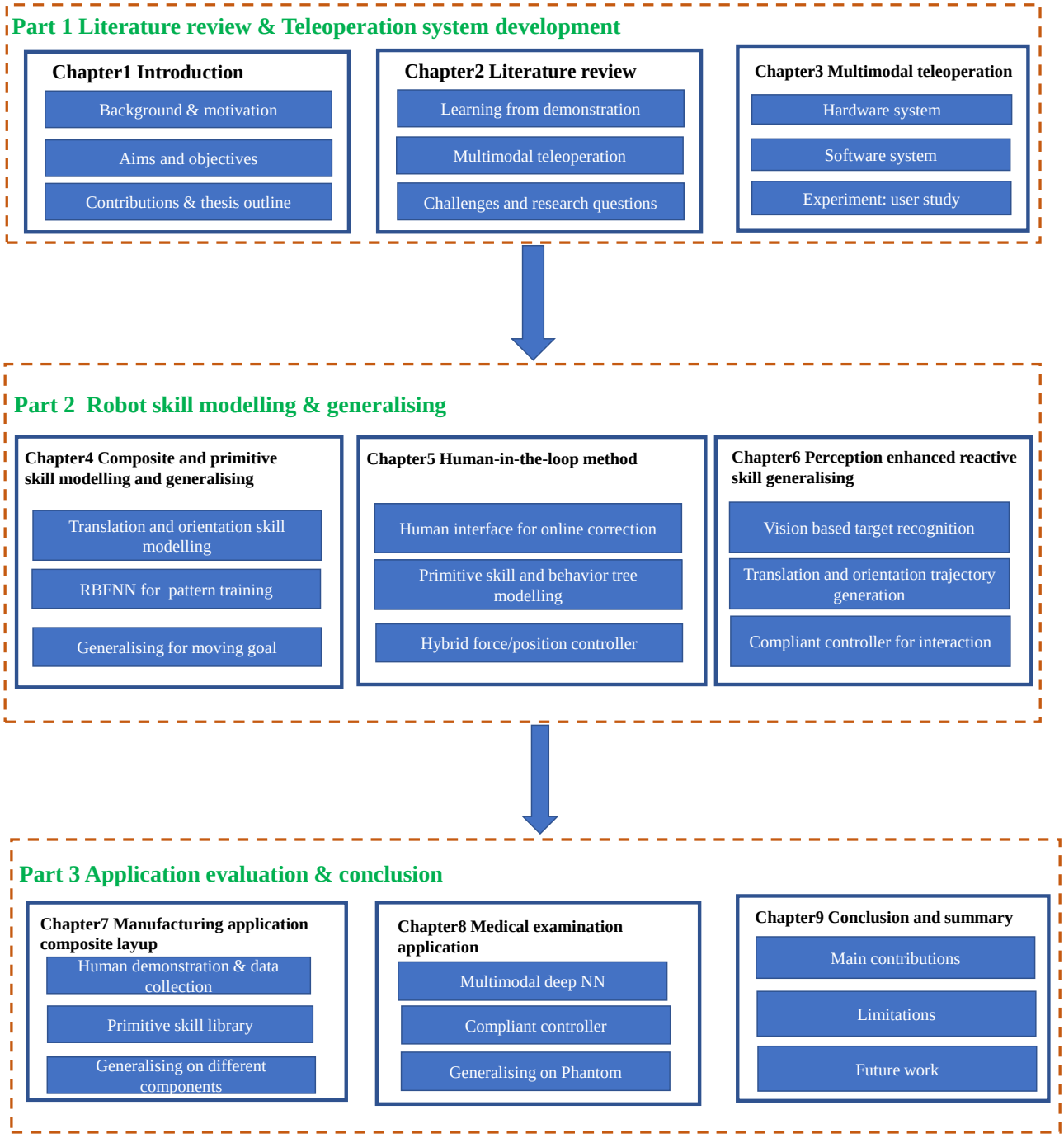

Figure 1.1: The structure of the thesis with three parts.

introduced. First, two human-robot interfaces, including a 3D mouse, haptic devices, force/torque sensor, EMG armband, depth camera etc., were developed. Second, we designed different controllers for different interfaces, respectively. Last, we proposed a quantitative evaluation for robot-assisted ultrasound tasks, including subjective and objective metrics, to compare the performance of different teleoperation interfaces.

In Part 2, we studied the dynamic movement primitive model, human-in-the-loop method, and perception-enhanced method to improve the generalisation capability of learning from human demonstrations.

In Chapter 4, we studied a composite skill modelling method, encoding translation and orientation motion simultaneously, based on radial basis function neural networks (RBFNNs) and dynamic movement primitives (DMPs). It is a common constraint in terms of position and orientation simultaneously in practice, and the target goal is always changing during the execution, such as human motion when robots perform ultrasound scanning. The skill modelling method can be applied to these tasks, requiring the translation and orientation regulation simultaneously and moving target.

In Chapter 5, a human-in-the-loop (HITL) method based on bilateral teleoperation was studied for compliant manipulation skill learning. It is hard and costly to teach robots skills for all scenarios, thus, human correction and interaction online for skills update is necessary and significant. The pizza dough rolling task is used to evaluate the human-in-the-loop method for skill generalising.

In Chapter 6, we investigated perception-enhanced skill learning and generalisation for compliant interaction. Machine vision and neural networks were used to recognise the deformation and the trajectory generation based on learning from demonstration. The impedance controller in Cartesian space is used to track the generated trajectory. The dough rolling task was used to evaluate the performance of the proposed method.

In Part 3, we evaluate the proposed framework and algorithms through manufacturing (Chapter 7) and robot-assisted medical examination tasks (Chapter 8). .

In Chapter 7, we employed the primitive skill library method and compliant control to conduct a preliminary evaluation of the robot-assisted composite layup. The performance of the proposed approach is evaluated through the robot-assisted composite layup on different shapes and orientations of the components.

Chapter 8 investigated a deep multimodal imitation learning framework for robot-assisted ultrasound scanning on the Phantom and human subject. Compared with the conventional imitation learning method, the deep multimodal imitation learning module owns better generalisation capability for the generation of reference motion and force commands for different patients. The proposed deep multimodal imitation approach is able to significantly improve the success rate of procedure completion.

Chapter 9 summarises the contributions and potential directions of this thesis.

2 Literature review

2.1 Introduction

In this chapter, we review the progress and challenges of manipulation skill acquisition through teleoperation-based learning from demonstration. Manipulation skill learning and generalisation have gained increasing attention due to the wide applications of robot manipulators and the spurt of robot learning techniques. Especially, the learning from demonstration method has been exploited widely and successfully in the robotic community, and it is regarded as a promising direction to realize the manipulation skill learning and generalisation. In addition to the learning techniques, the immersive teleoperation enables the human to operate a remote robot with an intuitive interface and achieve the telepresence. Thus, it is a promising way to transfer manipulation skills from humans to robots by combining the learning methods and the teleoperation, and adapting the learned skills to different tasks in new situations. This chapter, therefore, aims to provide an overview of immersive teleoperation for skill learning and generalisation to deal with complex manipulation tasks. To this end, the key technologies, e.g. manipulation skills learning, multimodal interfacing of teleoperation and telerobotic control, are introduced. Then, an overview is given in terms of the most important applications of immersive teleoperation platforms for robot skill learning. Finally, this chapter discusses the remaining open challenges and promising research topics.

The robot manipulator has been widely used to perform repetitive and simple tasks in certain and structured environments due to the advantages of low cost, efficiency and safety. Although the manip-

ulator has been widely used in a variety of disciplines, especially in the industrial domain, it is still difficult to perform physical in-contact tasks, e.g., manipulating deformable materials (Gao, Zhou, and Asfour, 2020; Leidner, 2019; Leidner et al., 2019), collaborating with human beings in the same workplace (Magrini, Flacco, and De Luca, 2015; Kronander and Billard, 2014), working in unknown and less structured environments (Guan, Vega-Brown, and Roy, 2018; Rodriguez et al., 2019).

(a) Assembly (Rodriguez et al., 2019).

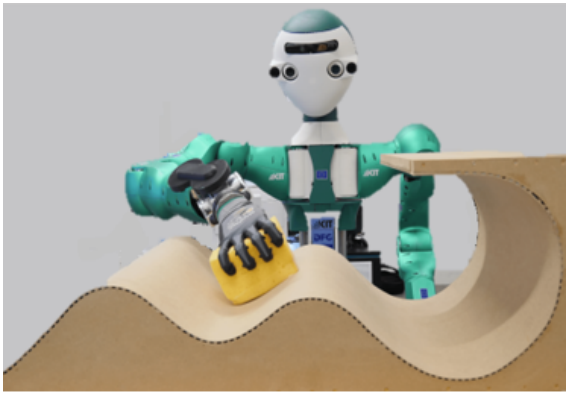

(b) Cleaning an arbitrary surface (Gao, Zhou, and Asfour, 2020).

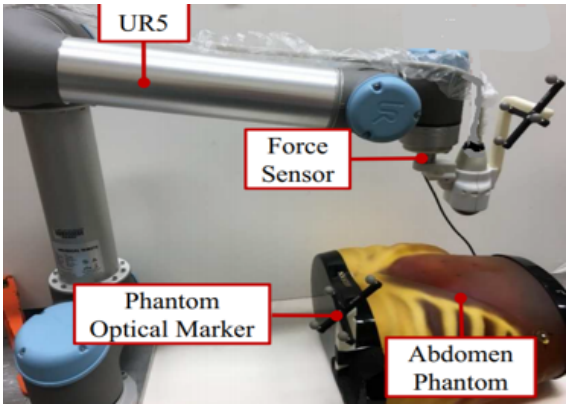

(c) Robot-assisted Echograph (Şen et al., 2016).

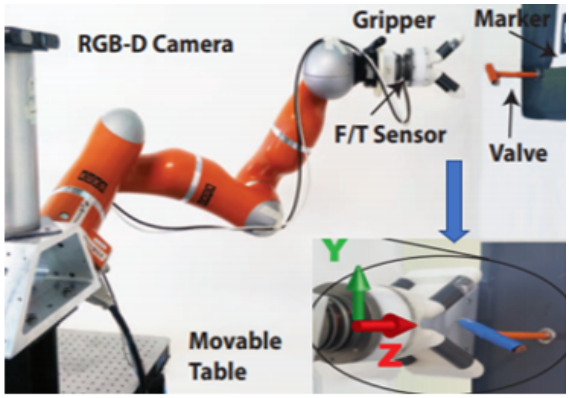

(d) Valve turning (Ahmadzadeh et al., 2014).

Figure 2.1: Illustrative examples of different in-contact manipulation tasks.

As shown in Fig.2.1, several typical in-contact tasks, including precise assembly (Rodriguez et al., 2019), cleaning a surface (Gao, Zhou, and Asfour, 2020), robot-assisted echography (Şen et al., 2016)

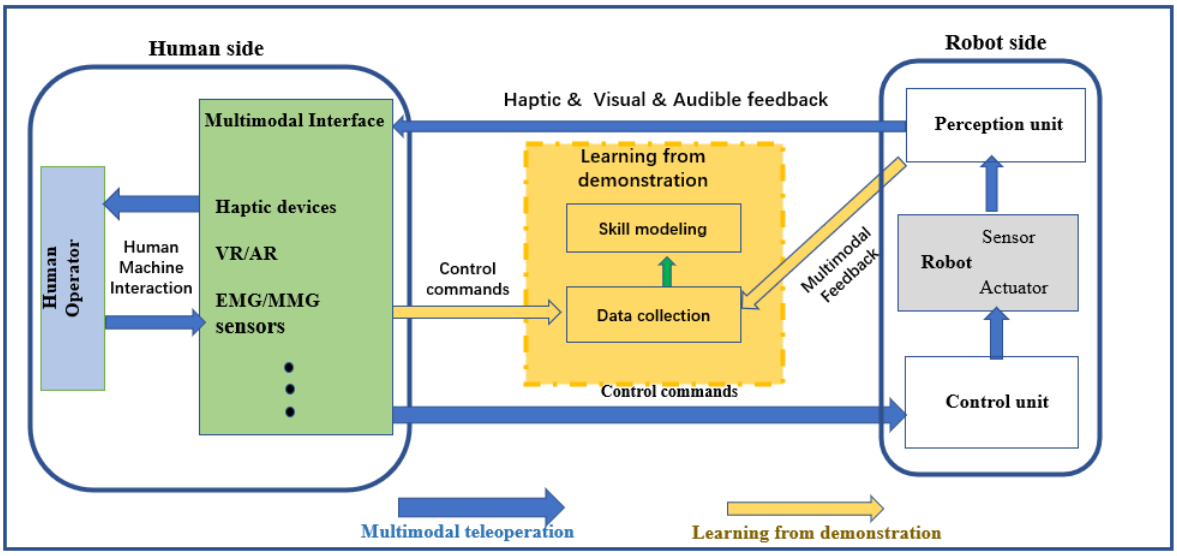

Figure 2.2: The structure of the teleoperation system for LfD.

and valve turning (Ahmadzadeh et al., 2014), are presented. When the robot manipulator performs such tasks, robots not only track desired trajectories but also interact with the environment physically. The challenges of these contact-rich tasks are attaining the accurate contact model, dealing with the uncertainty of humans' behaviours, and the safety of humans etc. All of the scenarios, as mentioned above, require robots to own human-like and compliant manipulation skills.

Recently, several machine learning techniques, e.g., reinforcement learning (Liu et al., 2020a), imitation learning (Zhang et al., 2018) and transfer learning (Matas, James, and Davison, 2018), have been successfully employed in robotic skill learning. There exist some review papers to introduce and discuss these learning methods (Kroemer, Niekum, and Konidaris, 2019). Among the learning methods, the learning from demonstration (LfD) (also named programming by demonstration, PbD or imitation learning), is one effective way to transfer manipulation skills from humans to robots (Argall et al., 2009). According to the demonstration approach, LfD can be divided into three categories: kinesthetic teaching, teleoperation and passive observation (Ravichandar et al., 2020). Compare with kinesthetic teaching and passive observation, the teleoperation could provide a multimodal interface interacting

with the human. Kinesthetic teaching method enables the human to demonstrate by physically moving the robot through the desired motions. The demonstration quality of kinesthetic teaching depends on the dexterity and smoothness of the human user, and even with experts, data obtained through this method often require smoothing or other postprocessing techniques. Besides, kinesthetic teaching is not applied in some extremely dangerous situations, such as nuclear plant and polluted areas, due to its requirement of demonstrators being present. Furthermore, the kinesthetic teaching requires the human teacher to work with robots in the same space, the safety of humans is also a concern. However, the learning through teleoperation could solve the aforementioned issues effectively. Furthermore, as the fast development of immersive teleoperation, learning from demonstration through immersive teleoperation enables the human demonstrator to teach robots with more natural demonstrations.

Teleoperation has been a key driver for robotic research, and it stems from the pragmatic need to perform tasks in remote environments (Hokayem and Spong, 2006; Lichiardopol, 2007). After the decades of development, the teleoperation technology has been widely used in various fields, e.g., space exploration (Weber et al., 2019), underwater exploration (Havoutis and Calinon, 2019), disaster relief (Cardenas and Kim, 2019), tele-echography (Santos, Cortesão, and Quintas, 2019), and surveillance (Theodoridis and Hu, 2012) due to the existence of risks to humans or unreachable physical distance. A general teleoperation system includes a human operator, leader devices, communication channel, following robot and perception module etc. It can be divided into unilateral and bilateral teleoperations, depending on whether the perception information is transmitted to the human operator from the following robot side (Yang et al., 2017b). In such a teleoperation system, the operator's performance can be improved by increasing the transparency of the system (Triantafyllidis et al., 2020b).

Currently, the multimodal interfaces, including the Virtual Reality (VR)/Augmented reality (AR) helmets (Stotko et al., 2019), joystick (Luo et al., 2019b), force/torque sensor (El Saddik, 2007), bio-

signal sensor (Luo et al., 2020; Yang et al., 2017a), have been developed and integrated into the teleoperation system, aiming to provide immersive teleoperation and increase overall human performance. Combining the auditory, haptic and visual information in the teleoperation has been proved a potential approach to increase the comfort of the human operator and the control performance of remote robots (Triantafyllidis et al., 2020b). Although many achievements have been done in the teleoperation, there exist several challenges realizing multimodal teleoperation, e.g., time delay caused by multimodal feedback, synchronization control, different configurations between the leader side and the follower side.

This chapter provides a comprehensive literature review on the key technologies, applications and challenges for robot manipulation skills learning and generalisation via teleoperation based LfD. The subsequent sections of this chapter are organized as follows. Preliminaries of the teleoperation system are presented in Section 2.2. In Section 2.3, the skill representation methods for LfD are introduced. Section 2.4 covers the multimodal teleoperation for LfD. Section 2.5 provides several typical applications. Finally, Section 8.5 discusses future directions on manipulation skill acquisition through teleoperation based LfD.

2.2 Preliminaries of multimodal teleoperation

Generally, a multimodal teleoperation system for robot skill learning includes the following parts: human operator with interactive interfaces, a communication module, teleoperation control and skill learning and generalisation. The overview of the teleoperation system is depicted in Fig. 2.2, and the description of each module is explained as follows.

- *Multimodal interfaces module*. The multimodal interface includes various devices, e.g., haptic joystick, VR/AR helmet, haptic data glove, Electromyography (EMG) sensor, Mechanomyography (MMG) sensor, enabling human operators to teleoperate the follower robot with immersive

telepresence. In addition, the interaction interface could also gather the sensor signals for LfD use.

- *Communication module*. This module aims to guarantee the communication between the leader side and the follower side, which has a significant impact on the control system due to the time delay and data package loss. When the multimodal information needs to be transmitted, the time delay may lead to the instability of control system.

- *Teleoperation control module*. Since there still exist some control issues in the teleoperation system (e.g., time delay, synchronization problem, and corresponding issue etc.), the advanced control frameworks and control algorithms are employed to tackle with these challenges.

- *Skill learning and generalizaton module*. The robot acquires the human-like manipulation skill through LfD. The demonstration data collected in the teaching stage will be used to train the skill model. The acquired skill of robots should be adapted to new situations within a given finite time.

As shown in Fig. 2.3, the key technologies of manipulation skill learning via teleoperation, including skill representation, robot skill learning, immersive teleoperation and teleoperation control, are introduced.

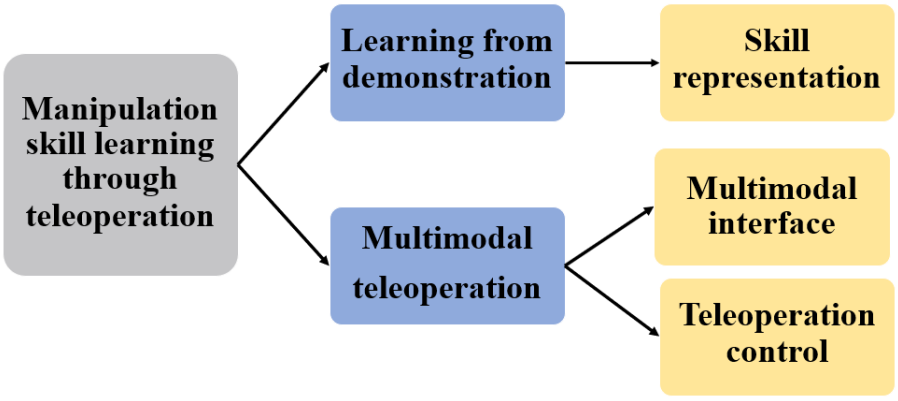

Figure 2.3: Key technologies in human-like manipulation skill learning via LfD and teleoperation.

2.3 Learning from demonstration (LfD)

2.3.1 The introduction of LfD

LfD could make robot acquire skills from the human demonstration, without much knowledge of robotics and programming (Huang et al., 2018). It offers a promising approach to transfer and refine tasks from observation of users who are not expert in robotics and computer programming. LfD provides the novice users with an intuitive method to program robots, which we human already are used to. The difference of LfD through teleoperation has multimodal interaction interfaces comparing with the kinesthetic teaching and passive observation. LfD based on teleoperation provides a user-friendly approach to transfer the skill to robots without much knowledge of robotics and programming. LfD can be used to transfer high-level symbolic reasoning skills as well as low-level motion skills (Steinmetz, Nitsch, and Stulp, 2019). There are several LfD learning strategies, such as behavioural cloning and inverse optimal control, for transferring basic motion skills and extracting the underlying objectives of optimal actions, respectively. In (Silvério et al., 2018), the task prioritization issue of bimanual operation of humanoid robot was addressed by the LfD, offering the possibility to carry out more than one manipulation task at the same time. In (Qin et al., 2019), Qin *et al.* proposed a skill learning approach based on LfD for precision assembly robot to realize effective skill transfer from teacher to the robot through several demonstrations.

Besides, the reinforcement learning (RL) technique is a different robot skill learning framework, which allows robots to explore novel skills by trial-and-error. Due to the fast development of deep learning, the RL is attaining a lot of attention from research and industry community. Further, as the robots are used in various fields, which require a large range of skills that are hard to be programmed, the advanced and flexible learning framework is necessary. The benefit of robot skills learning through

imitation is efficient by reducing the search space of feasible solution (Chatzilygeroudis et al., 2019). Combing reinforcement learning with LfD is a promising approach. In (Kim, Lee, and Kim, 2018), a skill learning framework integrating LfD and RL has been proposed to learn and generalize robotic skills. In (Rajeswaran et al., 2017), deep reinforcement learning and demonstrations has been used to learn complex dexterous manipulation.

2.3.2 Skill representation in LfD

A key research aspect of the robot skill learning and generalisation is the skill representation such that it can be analyzed and synthesized. Skill representation has a significant impact on the performance of robot skill learning and adaptation. Most generally, the skill representation approaches in LfD fall into two categories: the dynamical system method and the probability and statistical method. We will present detailed introductions of each representation approach in the following content.

In addition, the idea of movement primitive is often employed in the context of complex manipulation skill modelling due to its modularity and flexibility. The core idea of this representation is to decompose the complex behaviours into a set of movement primitives, which could be reassembled on demand to produce complex behaviours (Calinon, 2018). Often, such representation can enable the skill learning and generalisation to adapt to different tasks in new situations and environments. For instance, a complex trajectory of manipulation is segmented into several movement primitives, and the dynamical system or the statistical approach then is exploited to model the movement primitives.

Table 2.1: Comparision of various DS-based methods

Category	Characteristics	Literatures
SEDS	Global asymptotic stability; less accuracy.	(Gribovskaya, Khansari-Zadeh, and Billard, 2011) (Khansari-Zadeh and Billard, 2011) (Khansari-Zadeh, Kronander, and Billard, 2012)
Original DMP	Model is simple; Computational efficiency.	(Ijspeert, Nakanishi, and Schaal, 2001) (Ijspeert, Nakanishi, and Schaal, 2002)
DMPP	Modeling sensory feedback; Online adaptation;	(Hoffmann et al., 2009) (Chebotar, Kroemer, and Peters, 2014) (Pastor et al., 2011) (Rai et al., 2017)
Coupling DMP	Bimanual operation; obstacle avoidance.	(Hoffmann et al., 2009) (Gams et al., 2014)
RL-based DMP	Better generalisation; robust to disturbance.	(Kober, Mohler, and Peters, 2008) (Kober, Oztop, and Peters, 2011; Kober et al., 2012) (Kim, Lee, and Kim, 2018) (Stulp, Theodorou, and Schaal, 2012)

Dynamic system approach (DS)

The studies on the human motion show that the motion planning and execution of human is a coupled process, and the motion trajectory is generated by the evolution of the dynamic system over time and space (Bizzi et al., 1984; Kelso, 1995; Todorov and Jordan, 2002). Inspired by these works, the dynamical system approach can be used to robotic motion planning. Such as (Gribovskaya, Khansari-Zadeh,

and Billard, 2011), a set of non-linear autonomous dynamical systems were used to represent the manipulator motion, and its parameters were estimated by a mixture of Gaussians. In (Khansari-Zadeh and Billard, 2011), a stable estimator of Dynamical systems (**SEDS**) based on Gaussian mixture models was proposed to learn the parameters of the DS to ensure global asymptotic stability at the target. This DS-based approach was employed to model various motions, such as playing minigolf (Khansari-Zadeh, Kronander, and Billard, 2012), human handwriting motion (Khansari-Zadeh and Billard, 2011). The characteristics of various methods were compared in Table 2.1.

Dynamic Movement Primitives (DMPs) is another framework to realize the movement planning, online trajectory modification for LfD use, which was originally proposed by Ijspeert *et al.* (Ijspeert, Nakanishi, and Schaal, 2001; Ijspeert, Nakanishi, and Schaal, 2002). Recently, it also has been used to encode different modalities, such as stiffness and force profiles. According to the type of trajectory, it can be categorized into discrete DMPs and rhythmic DMPs. Take the discrete DMPs as an example, and it can be formulated as in Eq. (2.1).

$$\begin{aligned} \tau\dot{v} &= K(g-x) - Dv - K(g-x_0)s + Kf(s) \\ \tau\dot{x} &= v \end{aligned} \tag{2.1}$$

where x and v denote the position and velocity of the system, respectively. x_0 and g are the start and goal position, τ is a temporal scaling parameter. K is a spring constant, and D is a damping term. The non-linear function f depends on the phase variable s, instead of the time. The phase variable is determined by the canonical system, which often evolves from 1 to 0. The canonical system is given by,

$$\tau\dot{s} = -\alpha s \tag{2.2}$$

where α is a positive gain and $s_0 = 1$ the initial value of s. Notice that s converges exponentially to 0.

- *Advantages of DMPs*. Compare with traditional means of encoding trajectories, such as spline-based decomposition, the DMPs encoding skills has a variety of benefits (Ijspeert et al., 2013). Firstly, this motion representation can guarantee global stability, because, whatever the parameter of the function approximator we choose, the DMP is guaranteed to converge towards the target. In addition, the velocity of motion can be adapted by changing the time constant. The motion generated by DMPs is robust to strong external perturbations and can be modified on-line by additional perceptual variables. Furthermore, this approach also facilitates the motion modelling for multiple degrees of freedom (DoFs) system. They share one canonical system among all DoFs and maintain only a separate set of transformation systems.

- *Limitations of DMPs*. However, the original DMPs also has limitations on motion planning in some situations, e.g., the goal point coinciding with the start point and the goal points distributed on both sides of the start point. Due to the explicit description of the trajectory dynamics, it introduces many open parameters as well as the basis functions and its weighting coefficients. Moreover, it is still difficult to represent the high-dimensional trajectory of interaction tasks for redundant robots (Huang et al., 2019b). When it is employed to model manipulation skills, the DMPs needs to represent the sensory signals as well as motion trajectories. These sensor profiles represent the similar, but different, to different tasks. Thus, it is hard to model the correlation between the sensory value and the states of robots. In addition, the original DMP cannot achieve the force control of robots for contact tasks, such as assembly (Han et al., 2019). Therefore, since the original DMP was proposed, a variety of modified DMPs were proposed to tackle with limitations as mentioned earlier.

DMPs with perceptual term (DMPP) has been proposed to complete physical interaction tasks, which require robots to regulate the contact force, torque as well as the desired motion. The perception

information, e.g., tactile sensing and force profiles, is fundamental for these contact tasks. To take advantage of the sensory perception, a feedback term was proposed to be integrated into the DMPs model (Chebotar, Kroemer, and Peters, 2014). The modified DMPs model could be used to track the desired force profiles in grasping tasks (Pastor et al., 2011). In (Pastor et al., 2011), the authors further extended the original DMPs for online movement adaptation using the sensory feedback. The specific DMPs enhanced by previous sensor experience for particular tasks can predict the subsequent task executions. This DMPs are adaptive and robust to the external perturbations from the environments and various uncertainty from the sensors; hence it could generate a rich set of trajectories for the complex tasks. Moreover, the feedback term can be online trained using learning techniques to reactively modify previously acquired skills (Rai et al., 2017).

Coupling DMPs Some researchers extended the expression of DMPs model or added control method for realizing obstacle avoidance, interaction with external objects and bimanual operation, a majority of which added a coupling term based on the basic model. For example, Park and Khansari-Zadeh *et al.* took repulsive potential fields as coupling terms into DMPs for obstacle avoidance (Pairet et al., 2019; Rai et al., 2014). Hoffmann *et al.*, motivated by biological data and human behaviors, modified DMPs model by adding an acceleration term to avoid collisions with moving obstacle (Hoffmann et al., 2009). Composite DMPs was proposed to model both movement and stiffness features simultaneously to transfer human-like skill from humans to robots (Yang et al., 2018d; Yang et al., 2018c; Yang et al., 2018a). The coupling DMPs owns better interaction ability than the original DMPs

RL-based DMPs was proposed to increase the generalisation of original DMPs. In (Kober, Oztop, and Peters, 2011; Kober et al., 2012), RL was exploited to learn a mapping from circumstances to meta-parameters of DMPs to increase new primitive movements. To generate new bebaviors, Kim *et al.*. applied deep RL and a hierarchical strategy to optimize and generalize the skills produced

Table 2.2: Comparision of various statistical methods

Category	**Characteristics**	**Literatures**
GMM	Suitable for high-dimensional input.	(Luo et al., 2019b) (Calinon, Guenter, and Billard, 2007) (Calinon, 2016) (Calinon, 2020)
KMP	Suitable for high-dimensional input and multiple demonstrations.	(Huang et al., 2019b)
ProMPs	Better adaptation, but not suitable for high-dimensional input.	(Paraschos et al., 2013) (Conkey and Hermans, 2019)
HMM	Model the correlation between movement and sensory profiles.	(Lee and Ott, 2011) (Calinon et al., 2010)
HSMM	Encode the duration information of each HMM state and robust to perturbation.	(Calinon, Pistillo, and Caldwell, 2011) (Racca et al., 2016)

by DMPs (Kim, Lee, and Kim, 2018). The reinforcement learning technique is able to efficiently and robustly optimize the parameters of motion primitives. To further optimize the goal parameters, the path integrals algorithm was used to simultaneously optimize shape and goal parameters (Stulp, Theodorou, and Schaal, 2012). In (Kober, Mohler, and Peters, 2008), the authors proposed an augmented DMPs with a perceptual coupling, which was learned by RL. Compare with the original DMPs, the RL-based DMPs have better generalisation ability to novel situations.

Statistical modeling

Since the statistical approaches have the benefit to deal with the inherent noise in any mechanical system, they have become increasingly popular to model robotic motion. The characteristics of various statistical methods were compared in Table 2.2.

Gaussian mixture model (GMM) is one of the probabilistic mixture models, which can be used to represent the variation of human or robot motion. It is very suitable for robotic trajectory learning since it can adapt to various requirements while maintaining the core probabilistic mixture modelling strategy. It has been employed to model the joint distribution of input variables and further demonstrated motions (Calinon, Guenter, and Billard, 2007). For example, GMM was used to model both movement and force patterns for robot learning impedance behaviours in (Rozo et al., 2013). Usually, GMM is complemented with Gaussian mixture regression (GMR) (Cohn, Ghahramani, and Jordan, 1996) to retrieve the desired trajectory. To further enhance the extrapolation performance of GMM, the task-parameterized formulation has been proposed in (Calinon, 2016), which represents local trajectories and corresponding local patterns. In (Luo et al., 2019b), the GMM was utilized to encode and parametrize the smooth task trajectory to realize a task learning mechanism of the telerobots. Moreover, Calinon extended the GMM to Riemannian geometry to represent robot skills for robot learning and adaptive control in (Calinon, 2020).

Kernelized movement primitives (KMP) Although a number of advancements have been achieved to model the robot skill, dealing with unpredicted situations, e.g., unknown obstacles and external perturbations, and high-dimensional inputs are still challengable. Huang *et al.* proposed the KMP, which allows the robot to adapt the learned motor skills and while satisfying various constraints in the process of task execution (Huang et al., 2019b). Specifically, KMP is able to learn trajectories associated with high-dimensional inputs by adopting the kernel treatment technique. In contrast to

approaches relying on basis functions, its model has fewer open parameters, which make the training of models more convenient.

Probabilistic movement primitives (ProMPs) is a useful skill modelling approach for robot skill learning from humans and adapts to new tasks and environments. It is a probabilistic formulation of the movement primitives that maintains a distribution over trajectories (Paraschos et al., 2013). The property of conditioning the motion trajectory distribution on the desired point could generalize to new tasks points. The ProMPs has many good characteristics, such as blending of movement primitives, adaption to various constraints by conditioning, as well as temporal scaling and modelling the coupling between different joints. The weight of ProMPs can be learnt from the demonstration data and generalize to new tasks through probabilistic operations. The ProMPs can also deal with redundant robots' physical interaction tasks, which often needs to process various sensory data, such as force/ torque (Paraschos et al., 2015). This method enables robots to acquire complex motor skills and coordinates the motion with the perception information. In (Conkey and Hermans, 2019), the authors used active learning approach and ProMPs to generate a set of primitive skill library, capable of modelling complex skill over a given space. The active learning approach utilized uncertainty sampling techniques to generate a random task instance, and the human provides demonstrations for the task instance to enlarge the skill library. However, Callens et al., pointed out the ProMP motion models can predict motion over a short time horizon but struggle to predict motion over a longer horizon (Callens et al., 2020).

Hidden Markov Model (HMM) was used to represent the correlation between the motion state and sensory profiles by encoding a joint-probability density function over the demonstration data (Calinon, Pistillo, and Caldwell, 2011). In (Lee and Ott, 2011), the authors proposed a method based on HMM to generate continuous motion, involving the time information for each state. Combining the Gaussian regression technique with HMM is suitable for online recognition and continuous trajectory

generation, avoiding the time lag from pre-or post-processing of the data. Such as in (Calinon et al., 2010), the framework combining HMM and Gaussian Mixture Regression (GMR) was proposed to generate a probabilistic model of demonstrated data. A joint probability density function between the position and the velocity is generated by using HMM, and GMR is used to generalize the learned skills. Also, since the demonstration from human explicitly define forces and velocities, and implicitly define stiffness as well as their underlying co-relations with the positions, which are all crucial for the robot learning. An HMM-based approach is proposed and combining GMR to generate the control variables via regression (Zeng et al., 2020).

Hidden Semi-Markov Model (HSMM) was used to improve the robotic system's robustness against external perturbations in temporal space comparing with HMM (Calinon, Pistillo, and Caldwell, 2011). HSMM could also be enhanced by the GMR technique to represent the motion trajectory and force data for in-contact tasks (Racca et al., 2016). Since HSMM-GMR has been proven to be more dynamic and efficient than the vanilla HMM, it is more suitable to learn and model the correlations between the motion and other multimodal information by exploiting the collected data. In (Zeng et al., 2020), the HSMM and GMM were exploited to model the movement and stiffness simultaneously.

2.4 Multimodal teleoperation system

The purposes of exploiting multimodal interface are owing telepresence and assisting in modeling the human-like manipulation skill for in-contact tasks. A typical multimodal teleoperation framework discussed in this chapter is shown in Fig. 2.4. The human operator could teleoperate the mobile manipulator, while the multimodal perception information, e.g., video, audio and force, could be fed into the human side to increase the telepresence of operators.

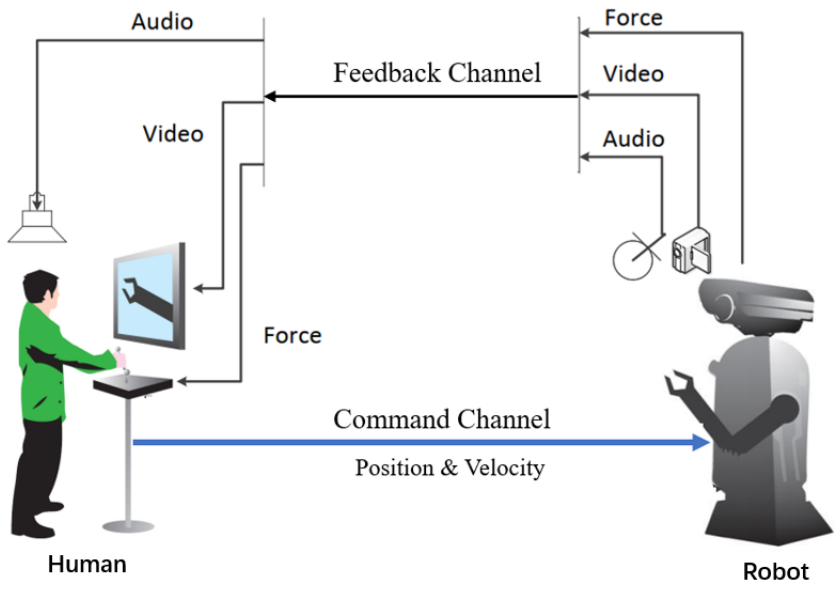

Figure 2.4: The structure of the multimodal teleoperation system adapted from (Xu et al., 2020).

2.4.1 The design of multimodal interface

To realize the immersive teleoperation, the design of multimodal interfaces is the premise. Recently, a number of researchers have proposed various schemes to implement the human-robot-interaction interfaces for a variety of applications, e.g., assembly, space exploration, teleoperated surgery, tele-rehabilitation, rescue etc. Generally, the multimodal interfaces mainly involve the haptic modality, visual modality, auditory modality and other modalities. As visual feedback is the fundamental modality, it has been well exploited to enhance the telepresence in the immersive teleoperation (Xu et al., 2018b). In (Stotko et al., 2019), a VR-based teleoperation is implemented to improve the immersion and situation awareness for live scene exploration. Under the assistance of the deep neural network, a vision-based interface realizes the end-to-end teleoperation of Shadow Dexterous hand (Li et al., 2019; Li et al., 2020). The VR headsets and hand tracking hardware are used to naturally teleoperate robots to perform complex tasks (Zhang et al., 2018).

However, only the visual feedback is unable to complete the in-contact task requiring the force

control, and the haptic feedback is essential for the in-contact teleoperation. The haptic feedback has been well studied in the teleoperation. In (Bimbo et al., 2017), the authors proposed a robotic teleoperation system with wearable haptic feedback for telemanipulation in cluttered environments. Moreover, the haptic interface is also employed in the precise telemanipulation, such as the surgical robot, micromanipulation, micro assembly. In addition to the vision and tactile touch, the auditory information is also utilized to localize the sounding object (Wang et al., 2019).

Although the unimodal feedback can complete basic tasks in structured and predictable situations, combining these diverse modalities to deal with complex contact task is essential, which is gaining increasing attention of researchers. In (Lee and Park, 2018), an enhanced teleoperator interface incorporating multi-modal augmented reality is proposed to address the dexterous manipulation of heavy materials. Although some achievements have been achieved in the immersive teleoperation, there still exist several challenges to accomplish the multimodal teleoperation due to many factors such as the effects of time delay caused by the communication link, the requirement of high packet rate in the real-time control loop, and the synchronization of different modalities.

2.4.2 Improving telepresence of teleoperation

The multimodal interfaces in teleoperation aim to provide immersive solutions and increase overall human performance (Triantafyllidis et al., 2020a). In this review, we focus on the bilateral teleoperation, where the multimodal information feedback could transmit to the operator to improve the telepresence. Extensive comparisons (Triantafyllidis et al., 2020b) have been done to show that regardless of task complexity, using multimodal interface could improve the performance. Research in cognitive psychology also suggests that utilizing multisensory stimuli enhances human perceptual learning (Shams and Seitz, 2008). Indeed, when we learn from others, we utilize a variety of multimodal information,

including verbal and nonverbal cues, to make sense of what is being taught.

Teleoperation systems enhanced by haptic feedback enable human demonstrators to perceive the remote environment and the robot interacting with the environment. The high requirement of packet rate and stability are challengeable for the teleoperation system with haptic feedback under the time delay of the communication module. Therefore, several strategies on the integration of communication and control have been proposed to deal with the above issues. Such as (Xu et al., 2020), reducing the haptic data and stability-ensuring control strategy is used to guarantee teleoperation's stability for practical tasks under the time delay of the communication. The model-mediated teleoperation for the complex environment is adopted, in which the point cloud model is estimated online to avoid transmitting irrelevant information (Xu et al., 2014).

2.4.3 Collecting demonstration data for skill learning

In addition to increasing the telepresence of human operator, the multimodal interface contributes to the high-quality demonstration that is essential to LfD successfully. For some scenarios such as car driving (Pomerleau, 1989; Bojarski et al., 2016) and helicopter control (Abbeel, Coates, and Ng, 2010), it is much easier to implement demonstration data collection since the intuitive operation interfaces for human demonstrators exist. However, it is hard to collect high-quality demonstration data for manipulators because of the correspondences between the demonstrator's operational spaces and the robot configuration (Ravichandar et al., 2020).

As the VR-based teleoperation method maps the observations into actions directly between the demonstrator and the robot, it can avoid the correspondence issue (Stotko et al., 2019). Also, the human demonstrator can perceive the remote environment by the VR headset, which could improve the performance of teleoperation. Moreover, the haptic devices have proved to be an essential interface for

learning from demonstration.

In (Luo et al., 2019a), the joystick was used to control remote Baxter robot, enabling humans to sense the contact torque and force. It is essential for the demonstrator to know the feasibility of the commands against the robot based on the feedback information. Hence, a haptic guidance approach is proposed, which allows the human teacher to perceive the various constraints on the telerobot.

Touch and visual information are ofter significant for compliant manipulation, such as robot performing in-contact tasks. The haptic and visual feedback are also necessary for contact-rich manipulation tasks in uncertain situations (Lee et al., 2020). A compact representation for multimodal sensory inputs is attained by using the self-supervision approach to improve the learning efficiency. In (Hogan and Rodriguez, 2020), the multiple contact modalities are siginificant to the reactive manipulation skills. In (Falco et al., 2019), the problem of cross-modal visuo-tactile object recognition was proposed to improve the objection recognition performance.

Most currently, the bio-signal sensors, e.g. EMG and MMG, have been exploited in LfD. It is hard to learn the human-like skill for physical human-robot interaction tasks if the human impedance feature is less considered. In (Yang et al., 2018d; Yang et al., 2018c; Yang et al., 2017a), Yang *et al.* develop a framework that enables the robot to learn both movement and stiffness features from the human tutor. In (Zeng et al., 2019), multiple sensor data has been encoded for robot skill learning to achieve multimodal demonstration learning. In (Yang et al., 2018d), EMG signal was utilized to estimate the stiffness of human arm in LfD to achieve the human-like skills transfer from humans to the robot. It is difficult for collaborative robots to learn in-contact tasks, requiring to guarantee the position and force requirements simultaneously. In (Chua et al., 2020), a multimodal system is built for force-dominant tasks, which is used to transfer skill from human to robots.

2.4.4 Teleoperation control

The stabilization of multimodal teleoperation system is essential to achieve manipulation skill learning through teleoperation. There exist control issues for the bilateral teleoperation to assist the human-like manipulation skill learning, e.g. teleoperation control, manipulation control. A large number of control methods were proposed to enhance the performance of teleoperation system (Wang, Chen, and Di Nuovo, 2020; Yang et al., 2018b).

According to control mode, the teleoperation system can be divided into three categories: direct control, supervised control and shared control (Luo, He, and Yang, 2020). For the direct control mode, the follower robot is controlled by human operator directly without autonomous abilities. When the robot works in the supervised mode, it executes the tasks according to the pre-programmed code, in which human merely supervise the execution process. However, the shared control is a hybrid strategy, combing the direct control and supervised manipulation, in which the human operator collaboratively work with robots based on a mechanism. The shared control framework has been well studied in human-robot shared manipulation (Aronson et al., 2018; Dragan, Srinivasa, and Lee, 2013; Nikolaidis et al., 2017; Javdani et al., 2018), robot skill learning through teleoperation (Xu et al., 2018a). For instance, in (Luo et al., 2019a), a hybrid shared control method based on EMG and haptic device is proposed to tele-control the mobile robot's motion and achieve obstacles avoidance. Similarly, in (Wang et al., 2015), a human robot shared control strategy is developed to realize the autonomous obstacle avoidance.

Shared control has proved to be a useful approach to designing intuitive teleoperation interfaces for human operators, which could reduce human operators' workload when they carry our complex tasks. Shared control in teleoperation system makes it possible to share the available degrees of freedom of a robotic system between the operator and an autonomous controller, to facilitate the task for the hu-

man operator and improve the overall efficiency of the system. The cutting task by robots has a high requirement of dexterity and safety. Prada et al. exploited geometric virtual fixture approach to assist with robot cutting. Besides, the shared control strategy has been employed to obstacle avoidance, in which the human operator only needs to consider the motion of the end-effector of the manipulator (Wang et al., 2015). Moreover combining the shared control method with the EMG sensor has been proposed to enable human to teleoperate a mobile robot and achieve obstacles avoidance synchronously (Luo et al., 2019a). The force feedback based on muscle activation can be transmitted into the human to update their control intention with predictability. In (Selvaggio et al., 2019), a passive task prioritized shared-control method is used to telemanipulate the redundant robots. Further, combining haptic feedback and guidance with shared control has proved effective for challenging tasks. For instance, haptic cues can increase situation awareness and effectively steer the human operator towards the safe execution of some tasks.

Impedance control is a significant control architecture when robots need to interact with environments or human physical or respond appropriately to unforeseen perturbation. The impedance even can be adjusted based on various tasks. The variable impedance control is well studied to deal with the in-contact task under less predive and structured environments. Hogan initially studied the impedance control for manipulator (Hogan, 1985), and since then, a number of improved methods were proposed to deal with various challenges of robotic control. In addition, Yang *et al.* proposed a human-like learning controller to achieve variable impedance when robots interacting with unknown environments (Yang et al., 2011). In (Kronander and Billard, 2016), the authors studied the stability considerations for variable impedance control. Kronander *et al.* studied the online learning of varying stiffness when robot learning skill through LfD (Kronander and Billard, 2012).

2.5 Applications of skill acquisition through teleoperation

Over the last decade, since the immersive teleoperation provides a number of advantages mentioned above, the multimodal teleoperation system has been widely exploited in different fields. In addition, the immersive teleoperation provides an intuitive and flexible interface to transfer the complex manipulation skills, especially robot performing in-contact manipulation tasks under uncertainty and less structured environments. Many researchers have proposed various intuitive and flexible teleoperation platforms to realize the robot skills learning and generalisation, as shown in Figs.2.5-2.8. In this section, we will introduce several typical applications of the multimodal teleoperation in various domains, e.g.,assembly, rehabilitation, palpation.

2.5.1 Medical robots

As shown in Fig.5, robots learn palpation skill through human interaction with a haptic device, the surgeon console. Although the teleoperation originally was designed to address the industrial nuclear wastes and space explorations, it has been widely utilized in medical surgery. Telemedicine diagnosis and telesurgery enable the remote and poor areas to access the start-of-the-art medical resources in developed countries. Especially, in the current situation of pandemics, the potential roles of robotics are becoming increasingly clear. Teleoperation provides feasible solutions for the remote dexterous manipulation in the medical fields. Specifically, three areas, logistics (e.g., handling of contaminated waste and delivery), clinical care (e.g., decontamination and telemedicine), and reconnaissance (e.g., monitoring compliance with voluntary quarantines) are identified to make a difference for robot application in the medical domain. From a technical point of view, to achieve the dexterous manipulation of robot manipulator in the above applications involves skill learning, robotic control, sensing the environment,

decision making etc. Although these applications are being actively explored, the actual situation is still far from the expected scenes. In this context, the teleoperation provides a feasible and effective solution to tackle with these challenges.

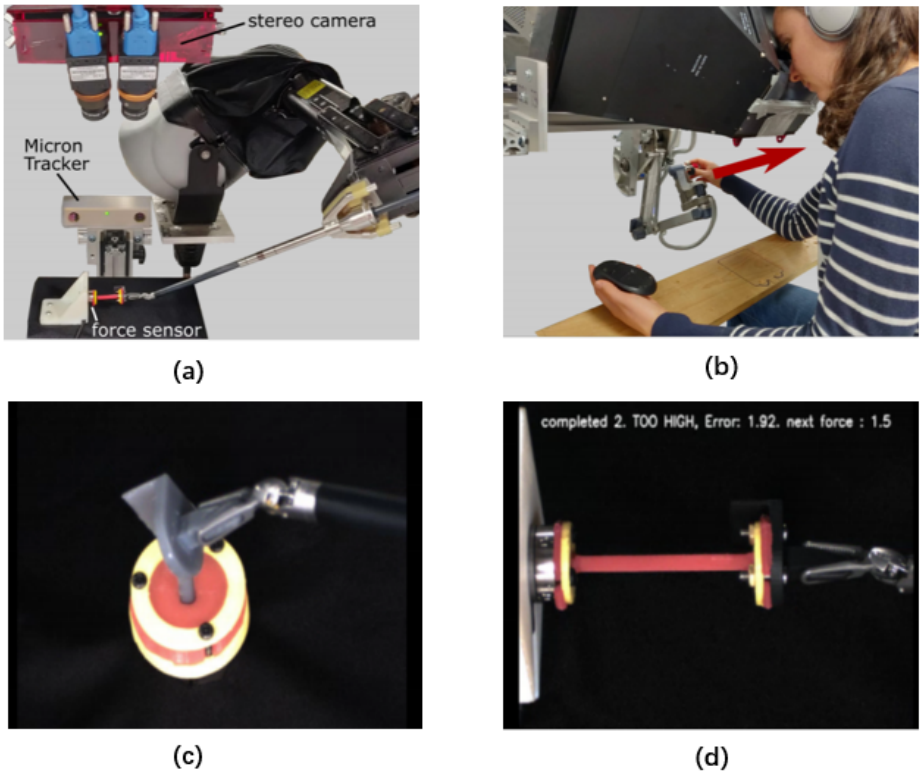

Figure 2.5: Robot learning the palpation skill adapted from (Chua et al., 2020). (a) Setup for the manipulation of the silicone sample. (b) Human interact with the haptic device. (c) and (d) The task environment through the surgeon console

After the decades of developments of the medical robot, a number of start-of-the-art teleoperation platforms for surgery have been developed. For instance, the da Vinci robotic surgical telemanipulator is a mature and commercialized surgical platform, and it has been utilized in several surgical specialties for various procedures. It is reported that more than 5,000 da Vinci systems are installed and nearly 6 million procedures performed by the end of 2018 (Black, Hosseinabadi, and Salcudean, 2020). The da Vinci system used in the clinic is not equipped with haptic feedback, although the haptic feedback

is significant to improve the teleoperation performance (Saracino et al., 2019; Freschi et al., 2013). However, researchers try to use the force/torque sensors to detect the interaction force to provide the surgeon's haptic experience (Black, Hosseinabadi, and Salcudean, 2020). Besides, a deformation tactile feedback device is developed to provide haptic to the teleoperators, which can be integrated into the da Vinci surgical teleoperation system (Quek, Provancher, and Okamura, 2018). Its effectiveness of improving teleoperation manipulation performance has been evaluated by comparison experiment; 20 participants carried out manipulation tasks using deformation tactile feedback, force feedback and the combination of both feedback respectively. The performance of teleoperation with all feedback is better than the one without haptic feedback.

To further increase the teleoperation performance of surgical robotics, Su *et al.* proposed an improved human-robot collaborative control scheme, based on a hierarchical operational space formulation of a seven-degree-of-freedom redundant robot, to provide a compliant behavior for the medical staff (Su et al., 2018; Su et al., 2019).

2.5.2 Industrial robots

Robotic assembly has been widely exploited in manufacture due to the efficiency, safety and low-cost (Zhu and Hu, 2018), however, achieving highly precise assembly and performing tasks under unpredicted situations is still open. The robot learning assembly skill through teleoperation is shown in Fig.6.

A dexterous teleoperation interface based on haptic and visual feedback was proposed to precisely control and manipulate micro objects (Kim et al., 2001). In (Bolopion et al., 2012), the authors proposed an intuitive teleoperation system with haptic and visual feedback to realize the telemanipulation of microspheres (with a diameter of less than 2 um) between France and Germany. The visual feedback

is used to derive the relative positions between the objects and the tools from the scene, while the relative information is transmitted through the haptic feedback. Further, due to limitations of the visual feedback, Bolopion *et al.* implemented a haptic interface to realize the 3-D micro assembly of spherical objects (Bolopion et al., 2010).

Recently, combining the machine learning techniques and the multimodal feedback system has been used to realize the robotic skill learning. In (Qin et al., 2019), a skill learning approach for precision assembly was proposed to realize efficient skill transfer from human to robot through the force and visual feedback. In order to transfer the human-like manipulation skill, the modulation of human impedance is essential to deal with tasks under unpredictable and unstructured environments. Therefore, in (Peternel, Petrič, and Babič, 2018), a human-in-the-loop approach based on a stiffness control interface is proposed for robots to learn assembly tasks in unstructured environments. As shown in Fig.2.6, this approach combines the end-effector force feedback with an interface controlled by the human finger for modulation of the robot end-effector stiffness. Two assembly tasks, sliding a bolt fitting inside a groove and driving a self-tapping screw into a material of unknown properties were conducted to validate the superiority of this skill learning approach based on multimodal feedback. It should be noted that multimodal feedback is essential for robot manipulators to transfer micro manipulation skill. In this regard, multimodal teleoperation is a promising approach for robotic skill learning.

2.5.3 Healthcare - Tele-rehabilitation

Stroke is becoming increasingly common worldwide, and rehabilitation training is an essential part of post-stroke care. For instance, Baek *et al.* proposed a wireless active finger rehabilitation approach based on electromagnetic manipulation for hand rehabilitation (Baek et al., 2017). A bilateral rehabilitation training scheme based on the fusion of visual and haptic feedback enables the patient to involve

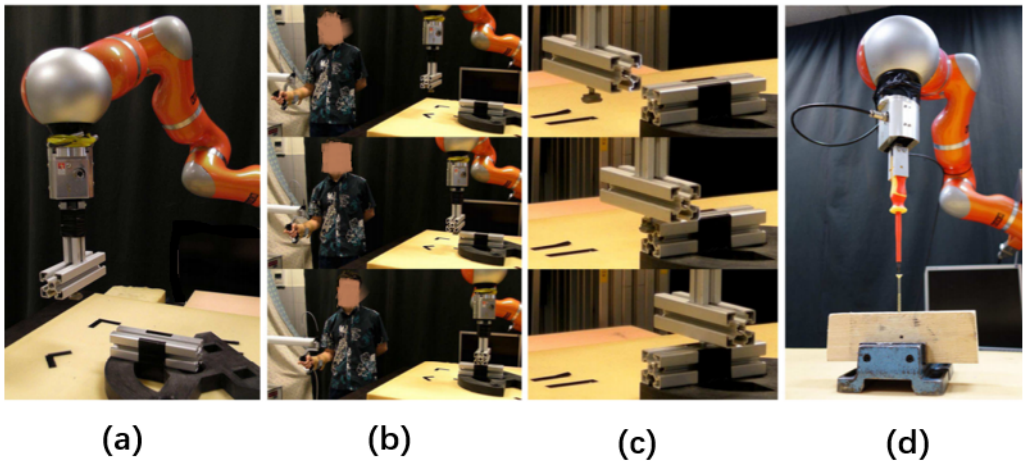

Figure 2.6: Robot learning assemby by teleoperation adapted from (Peternel, Petrič, and Babič, 2018). (a) Experimental setups for slide-in-the-groove assembly task. (b) Human teaching. (c) The autonomous robot operation of the learnt task. (d) Setup for bolt-screwing task.

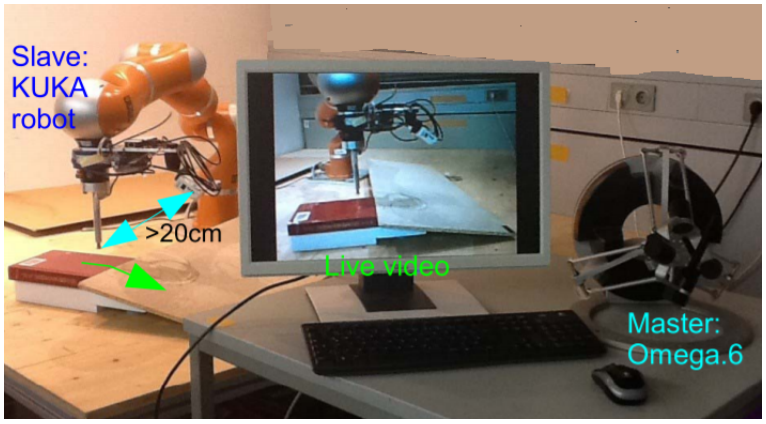

Figure 2.7: Peg-in-hole by teleoperation adapted from (Xu et al., 2014).

in the rehabilitation training actively (Yu et al., 2016). The tele-rehabilitation has recently gained increasing attention, as it allows a physical therapist to rehabilitate a patient who is far away from the physical therapist. In (Bae, Zhang, and Tomizuka, 2012), researchers developed a remote rehabilitation system with motor-assisted devices, and the physical therapist can use the images or data information to check the patient's condition by the tele-rehabilitation system. To enhance the telepresence, a bilateral tele-rehabilitation system with visual and haptic interfaces is used to rehabilitate the human lower limb

(Kawai et al., 2017). As shown in Fig.8, a healthy hand's motion is tracked by a leap motion sensor, and the Omega.7 device is used to assist the impaired hand with force feedback.

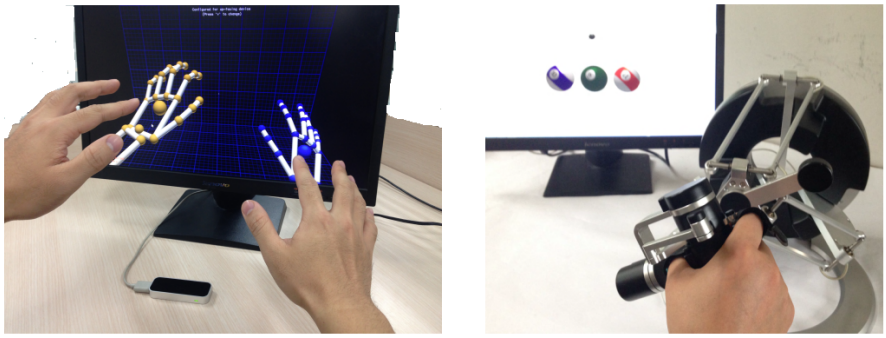

(a) (b)

Figure 2.8: Tele-rehabilition by multimodal teleoperation adapted from (Yu et al., 2016). (a) The Leap Motion sensor tracks the motion of a healthy hand. (b) The omega.7 device assists the impaired hand with force feedback.

2.5.4 Rescue and search

Robots have significant advantages over the human for complex tasks in dangerous environments. The rescue and search environments are often dangerous and uncertain; there is a risk to their lives if they enter. For instance, the Fukushima nuclear accident requires robots to work in an unstructured and uncertain environment, and humans cannot enter as the radiation and toxic contamination. In (Schwarz et al., 2017), a mobile manipulation robot Momaro has been developed and evaluated in the DARPA robotics challenges. A teleoperation of a rescue robot has been developed with a gamepad and images from a camera mounted on a robot (Asami et al., 2016).

2.6 Challenges and future directions

2.6.1 Manipulation skill modeling

Since the existing encoding methods aim for the structural data modeling, representing the multimodal demonstration data simultaneously is still open. To end this, the deep neural network technique is a potential approach. In addition, the demonstration data is often characterized by varied geometries, such as angular velocity, stiffness and force profiles. It is still difficult to encode these heterogeneous data. One potential approach is to introduce domain knowledge into the corresponding models. The framework of Riemannian geometry may be a promising direction to address this issue (Calinon, 2020). Riemannian manifolds are a powerful tool to represent rigid-body orientations, inertial matrices, manipulability ellipsoids, or controller gain matrices through exploiting the geometry of non-Euclidean spaces.

2.6.2 Skill learning through multimodal teleoperation

The synchronization of multimodality is significant in the multimodal teleoperation. If signals of different modalities are out-of-synchronization, overall spatial and temporal immersion is reduced. Another challenging aspect of utilizing multimodal demonstrations is users' comfort and accessibility. It is not clear how to acquire highly multimodal demonstrations by placing an overwhelming number of sensors without burdening the user. Effectively collecting multimodal demonstrations from remote users also remains challenging (Triantafyllidis et al., 2020b).

The existing methods for teleoperation based LfD are limited to learning from a small number of prespecified modalities. To effectively learn a wide variety of complex skills, we need methods that

reason over demonstrations in multiple modalities, identifying the most relevant demonstrations, and learn from them. The research of how the multimodal information influences the learning performance is still open.

Another challenge is to transmit multimodal signals, which require high bit rate to teleoperate remote robots. For instance, the haptic feedback is significant for the contact tasks.

2.6.3 Skill generalisation

Since the working environment is often different and the range of possible tasks that the robot needs to perform is infinite, it is impossible to teach robots all manipulation skills through LfD. When the robots work in less structured environments, the robots need to react in a smooth and fast manner to various perturbations. In this case, it needs to modulate the movement with respect to the situation, instead of re-planning the whole trajectory. Thus, the robot should own the capabilities to cope with novel situation by online learning and adaptation. In (Chatzilygeroudis et al., 2019), Chatzilygeroudis *et al.* proposed a "micro-data reinforcement learning", where a robot adapts with only a handful of trial and a few minutes.

In addition, the generalisation of movement primitives to different tasks comes from two sources: the individual movement primitive and the combination of movement primitives. The generalisation of each movement primitive arises from integrating the perception into the active planning module. The combination among the movement primitive library generates complex manipulation planning for unseen situations.

2.7 Summary

In this chapter, we reviewed multimodal teleoperation-based LfD to realize the manipulation skill transfer from humans to robots. First, the multimodal teleoperation system for LfD including the human teacher, multimodal interfaces, remote robots, communication module, robotic control module and remote perception module, was introduced. In order to encode the multimodal demonstration data, we summarized the skill modelling methods, including the dynamic system and statistical method. In addition, to achieve the complex manipulation skill transfer from humans to robots, the multimodal interface plays an important role to enhance the telepresence, improve the performance of demonstrators and gather the demonstration data. We further discussed the design of multimodal interface and how to integrate it with LfD. Several typical applications of skill acquisition through the multimodal teleoperation were also presented. Finally, we provided the remaining challenges and future work in terms of skill modelling, multimodal teleoperation and skill generalisation.

3 Multimodal teleoperation system development and performance evaluation

3.1 Introduction

In this chapter, we developed multimodal-based teleoperation interfaces of human-robot interaction and collaboration for human-robot skill transfer, which is the foundation of robot skill learning and generalising study in this project. The teleoperation interface (also named the human-robot interface in this thesis) provides an effective approach to combine human intelligence and the autonomy of robots, which can improve the safety and efficiency of the robot. The intelligent and natural interface is significantly essential for human-robot interaction and even human-robot skill transfer by allocating the whole task into human beings and robots, reducing human workload, especially for dexterous manipulation tasks, such as medical examination (Conti, Park, and Khatib, 2014). Thus, a number of teleoperation interfaces have been developed for telemanipulation, such as (Lin, Krishnan, and Li, 2019; Luo et al., 2019a; Conti, Park, and Khatib, 2014; Gholami et al., 2022; Wu et al., 2019; Enayati, Ferrigno, and De Momi, 2018; Havoutis and Calinon, 2019; Li et al., 2019). However, developing an intuitive and immersive human-robot interface with multimodal feedback for human-robot interaction and collaboration is still challenging, since the different configuration and less transparency between the leader devices and the follower robots. These days multimodal feedback-based teleoperation systems are studied, e.g., visual feedback, haptic feedback and audio feedback etc., to help human operators improve

scenario awareness. However, various teleoperation interfaces make it difficult for system designers to select a suitable teleoperation interface for their tasks. Although the (Gholami et al., 2022) studied the quantitative physical ergonomics assessment for the teleoperation interface of industrial assembly application, the task is a pick-and-place task that is different from the ultrasound scanning. There is a research gap in comprehensive metrics for medical examination and teleoperation interface study for robot-assisted ultrasound scanning. Thus, we developed a multimodal-based teleoperation system and carried out user studies to evaluate the performance of the developed teleoperation interfaces.

3.2 Development of multimodal teleoperation system

This section presents the hardware and software components of the developed teleoperation system for human-robot skill transfer in this project.

3.2.1 Hardware components

Collaborative robot - Franka Emika Panda

There are many commercial collaborative robots (cobots), such as Baxter [1], Universal Robots (UR) [2], Franka Emika Panda [3], etc. The cobots enable humans to work together with robots in a shared space safely. Although there are many cobots platforms, they provide different control interfaces for developer users. For example, Baxter and Franka Emika Panda provide a torque control interface for development users, which is necessary to implement and study robot control algorithms. While the UR robot arm only provides position and velocity control interfaces, which is limited for some control algorithm research, such as impedance control. Thus, to evaluate the control and learning algorithms,

[1] https://robots.ieee.org/robots/baxter/

[2] https://www.universal-robots.com/

[3] https://www.franka.de/

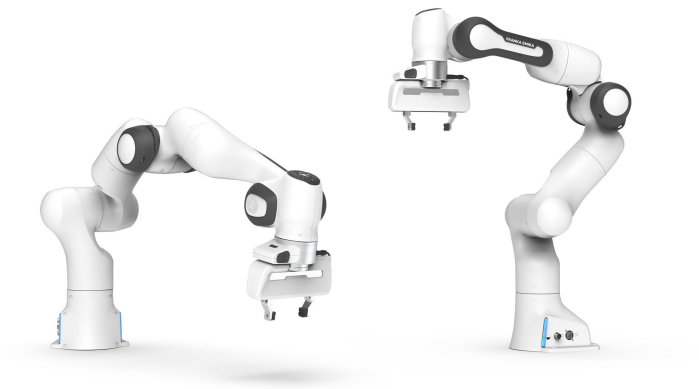

Figure 3.1: The bimanual collaborative robot arms with 7 DoFs, Franka Emika Panda.

the robot arm, providing torque control interfaces, is more flexible for researchers. In addition, the research community of a robot arm is also important because an active research and development community can provide detailed help documents and various open-source libraries.

Franka Emika Panda is a friendly robot for the study of advanced control algorithms and robot skill learning algorithms. Thus, in our project, 7 DoFs cobots manipulator, Franka Emika Panda, as shown in Fig. 3.1, was employed to conduct various experiments, introduced in the following chapters. Detailed parameters and tutorial of Franka Panda can refer to [4]. This cobot provides a wide range of low-level control interfaces, including position, velocity, and torque control. Thus, we can use this robot to study the various control algorithms, including variable impedance control, shared control, and force control, etc. In addition, the Franka Emika Panda also provides a software development kit (SDK) [5], libfranka and Franka Control Interface (FCI) with researchers. The FCI allows the users to access a range of robot states, model parameters, and log data.

Teleoperation device - SpaceMouse 3D mouse

[4] https://www.franka.de/

[5] https://github.com/frankaemika/libfranka

Figure 3.2: The teleoperation device, 3D mouse.

SpaceMouse 3D mouse[6] is a cheap and intuitive device for human-robot interaction (Garate, Gholami, and Ajoudani, 2021), as shown in Fig. 3.2. The compact mouse was originally designed for 3D navigation in CAD design, which has a 6-DoFs motion sensor and two programmable buttons. The 3D mouse can be programmed in both Linux and Windows systems. The 6-DoF sensor is specifically designed to manipulate digital objects in the virtual environment. Simply push, pull, twist or tilt the 3Dconnexion controller cap to intuitively control the translation and orientation of the robot arm.

Teleoperation device - Touch and Touch X

As shown in Fig.3.3, haptic devices, Touch [7] and Touch X [8] were employed for bilateral teleoperation. The Touch X is suitable for haptic research, which provides more-precise positioning input and high-fidelity, force-feedback output. Haptic devices allow a user to feel 3D on-screen objects by applying force feedback on the user's hand, and the Touch X delivers expanded, true-to-life sensations with a more fluid feel and lower friction. Its durability, affordability, and accuracy make the Touch X haptic device ideal for commercial, medical, and research applications, especially when compactness and portability matter. The touch haptic device has been used in medical research, such as medical student training.

Electromyography (EMG) armband

[6] https://www.3dconnexion.com/spacemouse$_compact/en/$

[7] https://www.3dsystems.com/haptics-devices/touch/features

[8] https://www.3dsystems.com/haptics-devices/touch-x

(a) (b)

Figure 3.3: The teleoperation devices, touch and touch X.

Figure 3.4: EMG armband.

We employed Myo gesture armband [9] to estimate the muscle constraction. As shown in Fig.3.4, the commercial EMG armband was used in this project. The Myoarmband has 8 medical grade stainless steel sEMG single differential electrodes. The Myo-armband sampled 8 sEMG sensors at a 200 Hz frequency with a resolution of 8 bit signed and streamed the data through a Bluetooth low energy connection to the computer where data was recorded. The sEMG data from the Myo-armband is already notch filtered at 50 Hz to avoid power grid interference.

6-axis force/torque sensor (F/T sensor)

F/T sensor was employed to measure the interaction force between the end-effector and the en-

[9]https://www.grattify.com/tech/control-armband

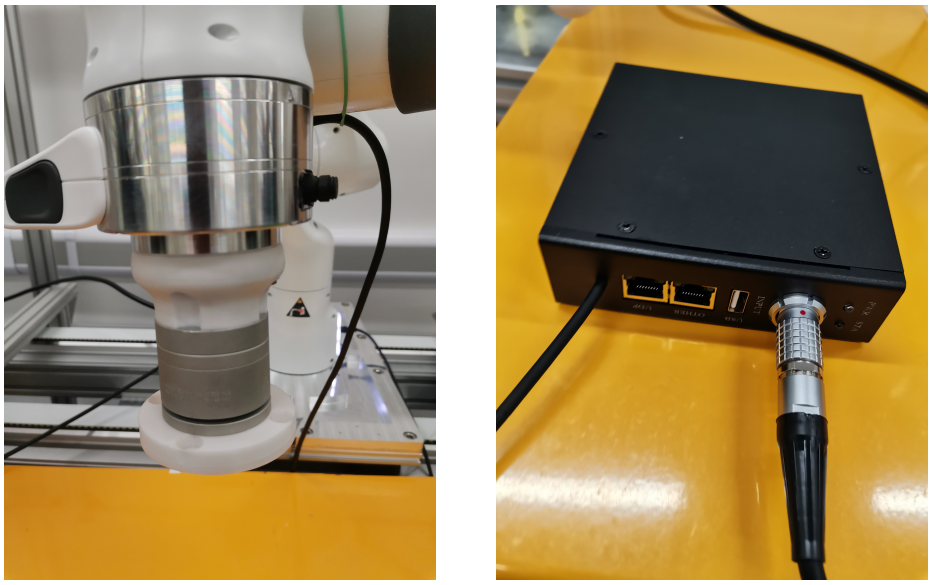

(a) (b)

Figure 3.5: (a) Force sensor equipped on the robot arm and (b) the embedded computer for data collection.

vironment, as shown in Fig.3.5. F/T sensor[10] was employed to sense the contact force during the robot-assisted scanning. The communication between the force sensor and the computer is EtherNet. The measuring range along the XY axis is 100N, and 200N along the Z axis. The range of torque sensing is 8Nm for X-Y-Z. The force measurement accuracy is 0.01N. Haptic feedback, specifically the contact force feedback, is based on the measured interaction force.

Depth Camera

RealSense depth camera [11] has been widely used in the robotic community, such as virtual reality and robot vision, due to the low price and friendly API for researchers. RealSense depth camera was used to capture the experiment scenarios and provide visual feedback for human operators, as shown in Fig.3.6. Its sensing range is from 0.3m to 3m, which is suitable for our project. And the RGB frame

[10] http://www.nbit6d.com/product/656.html

[11] https://www.intelrealsense.com/depth-camera-d435/

Figure 3.6: Realsense Depth camera D435.

resolution is 1920*1080, which is enough for our recognition.

Ultrasound scanning machine

For robot-assisted ultrasound scanning experiment, we use two types of commercial ultrasound machines to conduct experiments on both Phantom and the human body, as shown in Fig.3.7. There are two types of probes, linear and convex probes. The SONON 300L[12] ultrasound probe was used to scan the Phantom and carotid arteries of human beings.

Phantoms for ultrasound scanning

As shown in Fig.3.8, we used two types of Phantoms for robot-assisted ultrasound scanning experiments. The multi-purpose multi-tissue ultrasound phantom[13], from Sun Nuclear company, was used to conduct the user study experiment. This standard phantom is suitable for teleoperation study to evaluate the acquired ultrasound images. The homemade phantom can be customised for different features, and this phantom is cheap for experiments with many times tests. Thus, in the multimodal deep imitation, we adopted this type of phantom.

Various 3D printing components integrating different parts

In this chapter, we will only introduce the general experimental platforms. We will present the details and parameters of these components for different experiments in subsequent Chapters.

[12]http://www.orcamedical.co.uk/product/1/Healcerion-Sonon-300L/

[13]https://www.cirsinc.com/products/ultrasound/zerdine-hydrogel/multi-purpose-multi-tisse-ultrasound-phantom/

Figure 3.7: Two ultrasound machines used in this thesis. (a) is for the convex probe, which is used in the user study. (b) is a wireless ultrasound machine for liner probe, which is used in Chapter 8.

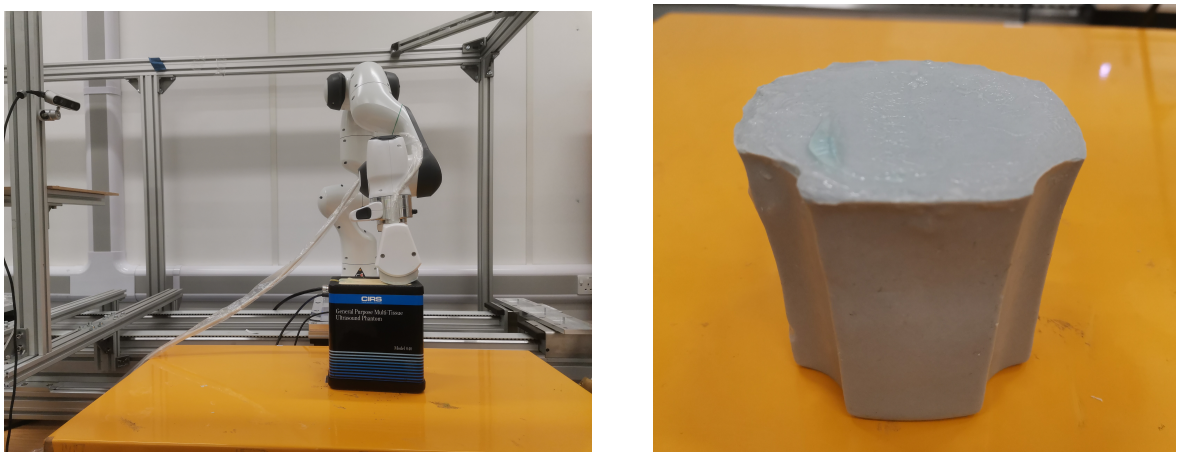

Figure 3.8: Phantoms for ultrasound scanning. (a) Commercial and standard phantom. (b) Homemade phantom.

3.2.2 Software tools

In this chapter, we will only introduce the whole software system for the multimodal teleoperation learning and control system. We will present the details and parameters of different components for

different experiments in subsequent Chapters. The whole software system is run on the Linux system [14]. QT is used for GUI development to visualise the Force/Torque data since the QT is a cross-platform software.

Robot Operating System (ROS). Robot Operating System (ROS) [15] system was used to integrate all the systems for different modules.

OpenCV library. OpenCV library [16], a real-time computer vision library, was used to process the RGB images.

PyTorch. PyTorch [17] library, an open-source machine learning framework, was used to implement the deep neural network model.

Libfranka. Libfranka [18] is a C++ library providing the low-level control interfaces for the Franka Panda arm. Libfranka is used to control the robot arm.

SOLIDWORKS and MATLAB. SOLIDWORKS was used to draw the 3D model of various 3D printing components. MATLAB was used to process the experiment data and plot the figures.

3.3 Control system design

3.3.1 Cartesian impedance controller

The dynamics of the general serial n-DOF manipulator robot in joint space can be modelled as,

$$M(q)\ddot{q} + C(q,\dot{q})\dot{q} + G(q) + \tau_f(\dot{q}) + d_u = \tau_c + J^T(q)F_e \tag{3.1}$$

[14] https://ubuntu.com/

[15] https://www.ros.org/

[16] https://opencv.org/

[17] https://pytorch.org/

[18] https://github.com/frankaemika/libfranka

where $M(q) \in R^{n\times n}$ is the inertial matrix, $q \in R^{n\times 1}$ is the joint angle, $\dot{q} \in R^{n\times 1}$ and $\ddot{q} \in R^{n\times 1}$ are the velocity and acceleration in joint space. $C(q,\dot{q})\dot{q} \in R^{n\times 1}$ represents the Coriolis and centrifugal terms. $\tau_c \in R^{n\times 1}$ is the control torque, and $F_e \in R^{m\times 1}$ is the interaction force between the end-effector and environment, which can be measured by force sensor. $J(q) \in R^{m\times n}$ is the Jacobian matrix. $G(q) \in R^{n\times 1}$ is the gravity term. $\tau_f(\dot{q}) \in R^{n\times 1}$ denotes the friction torque. $d_u \in R^{n\times 1}$ is the modelling uncertainty.

We model the manipulation skill in the task space, and thus, we derive the controller in the Cartesian space. Based on the kinematic equation of the manipulator, we can describe the position, velocity and acceleration of the end-effector as,

$$x(t) = f(q) \tag{3.2}$$

$$\dot{x}(t) = J(q)\dot{q} \tag{3.3}$$

$$\ddot{x} = \dot{J}(q)\dot{q} + J(q)\ddot{q} \tag{3.4}$$

where $f(q)$ is the feedforward kinematics of the robot manipulator, and $x(t) \in R^{m\times 1}$, $\dot{x}(t) \in R^{m\times 1}$ and $\ddot{x}(t) \in R^{m\times 1}$ are the position, velocity and acceleration of the end-effector in Cartesian space, respectively. Considering the above equations and Eq.(3.1), we can attain the robot dynamics in task space,

$$\Lambda_p(q)\ddot{x} + B(q,\dot{q})\dot{x} + G_p(q) + T_f + D_u = T_c + F_e \tag{3.5}$$

$$\Lambda_p(q) = (J(q)M^{-1}(q)J^T(q))^{-1} \tag{3.6}$$

$$B(q,\dot{q}) = \bar{J}(q)^T(C(q,\dot{q}) - M(q)\bar{J}(q)\dot{J}(q))\bar{J}(q) \tag{3.7}$$

where $\Lambda_p(q) \in R^{m\times m}$ is the inertia matrix in Cartesian space, $B(q,\dot{q}) \in R^{m\times m}$ is the Coriolis term in Cartesian space, $G_p(q) \in R^{m\times 1}$ is the gravity in Cartesian space; $D_u \in R^{m\times 1}$ is the modelling uncertainty. $\bar{J} \in R^{m\times n}$ is the dynamically consistent inverse of $J \in R^{m\times n}$, which can be calculated as (Santos and Cortesão, 2018),

$$\bar{J} = M^{-1}(q)J_p^T(q)\Lambda_p(q) \tag{3.8}$$

$$G_p(q) = \bar{J}^T(q)G(q) \tag{3.9}$$

$$T_f = \bar{J}^T(q)\tau_f \tag{3.10}$$

$$T_c = \bar{J}^T(q)\tau_c \tag{3.11}$$

We design the $T_c \in R^{m\times 1}$,

$$T_c = T_{c1} + T_{c2} \tag{3.12}$$

$$T_{c1} = \Lambda_p(q)\ddot{x} + B(q,\dot{q})\dot{x} + G_p(q) + T_f + D_u \tag{3.13}$$

where $T_{c1} \in R^{m\times 1}$ is used to compensate for the dynamic force of the robot manipulator.

An impedance controller can be described as,

$$A_d\ddot{x} + D_d(\dot{x} - \dot{x}_d) + K_d(x - x_d) = F_e \tag{3.14}$$

where $A_d = \Lambda_p(q) = (J(q)M^{-1}(q)J^T(q))^{-1}$,

$$T_{c2} = D_d(\dot{x} - \dot{x}_d) + K_d(x - x_d) \tag{3.15}$$

where T_{c2} is the impedance controller to track the desired position and compliant interaction with the environment.

3.3.2 Bilateral teleoperation control

The structure of the bilateral teleoperation control is shown in Fig.3.9. In the bilateral teleoperation, the dynamics of the leader robot and follower robot in Cartesian space are given,

$$M_m(q_m)\ddot{x}_m + C_m(q_m,\dot{q}_m)\dot{x}_m + G_m(q_m) = u_m + f_h \tag{3.16}$$

$$M_r(q_r)\ddot{x}_r + C_r(q_r,\dot{q}_r)\dot{x}_r + G_r(q_r) = u_r + f_e \tag{3.17}$$

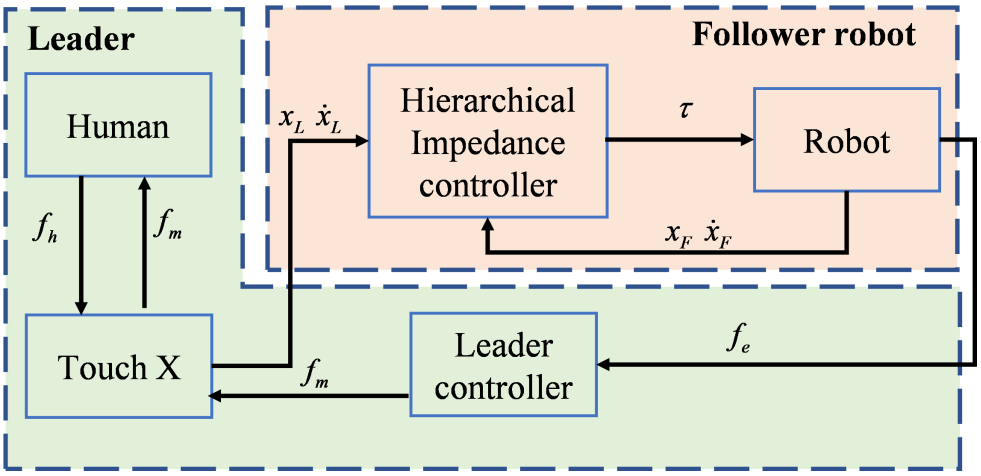

Figure 3.9: The bilateral teleoperation control structure of Touch X.

where $M_m(q_m) \in R^{m\times m}$ and $M_r(q_r) \in R^{m\times m}$ are the inertia matrix, $C_m(q_m, \dot{q}_m) \in R^{m\times m}$ and $C_r(q_r, \dot{q}_r) \in R^{m\times m}$ are the Coriolis and centrifugal terms, and $G_m(q_m) \in R^{m\times 1}$ and $G_r(q_r) \in R^{m\times 1}$ represent the gravity of the leader and follower robots [19] respectively. $u_m \in R^{m\times 1}$ and $f_h \in R^{m\times 1}$ are the control input and operator force of leader robot. $q_m \in R^{n\times 1}$ and $\dot{q}_m \in R^{n\times 1}$ are the joint position and velocity of leader robot. The $\dot{x}_m \in R^{m\times 1}$ and $\ddot{x}_m \in R^{m\times 1}$ are the velocity and acceleration of leader robot in Cartesian space. $u_r \in R^{m\times 1}$ and $f_e \in R^{m\times 1}$ are the control and interaction force of the follower robot. $q_r \in R^{n\times 1}$ and $\dot{q}_r \in R^{n\times 1}$ are the joint position and velocity of follower robot, the $\dot{x}_r \in R^{m\times 1}$ and $\ddot{x}_r \in R^{m\times 1}$ represents the velocity and acceleration of the follower robot. Impedance control models the relationship between robot and the environment as a mass-spring-damper system. We designed the impedance controller in task space for the follower robot,

$$u_r = K_r(x_m - x_r) - D_r\dot{x}_r \tag{3.18}$$

where u_r is the control command of follower robot, K_r is the stiffness matrix, the D_r represents the damping matrix. x_m and x_r are the position of the leader and follower robots, respectively.

[19] Note the leader robot refers to the teleoperation device, Omni Touch, and the follower robot refers to the Franka robot manipulator.

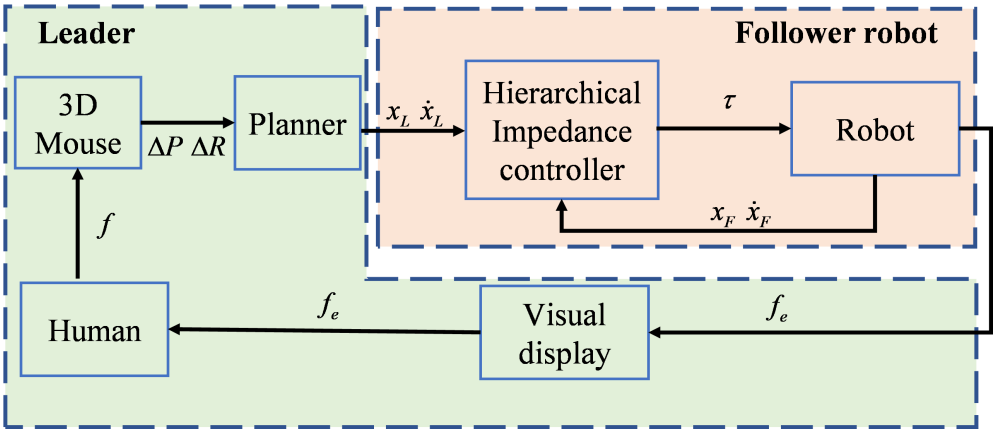

Figure 3.10: The teleoperation control structure by 3D mouse. The contact force is visualised by force bar on computer monitor.

The force feedback is designed to reflect the force of interaction between the follower robot and the environment,

$$u_m = -K_m f_e - D_m \dot{x}_m \tag{3.19}$$

where u_m is the control input of the leader robot, D_m is the damping matrix. f_e is the interaction force between the follower robot and environment, K_m is the scaling parameter. One advantage of bilateral teleoperation is that force feedback for the human operator benefits the human-robot skill transfer.

3.3.3 Coordinate frames of the teleoperation control system

There are several coordinate systems in the robot-assisted ultrasound scanning system. We defined the coordinates used in this work: probe contact frame F_C, probe frame F_P, force sensor frame F_T, end-effector frame F_E, robot base frame F_B, touch tip frame F_{TT} and touch base frame F_{TB}, as shown in Fig. 3.11. For the human demonstration through teleoperation, Touch X was used as the input device. A teleoperation control mapping algorithm was developed to map the relative pose between Touch tip frame F_{TT} and the Touch base frame F_{TB} to the relative pose between robot base frame F_B and the

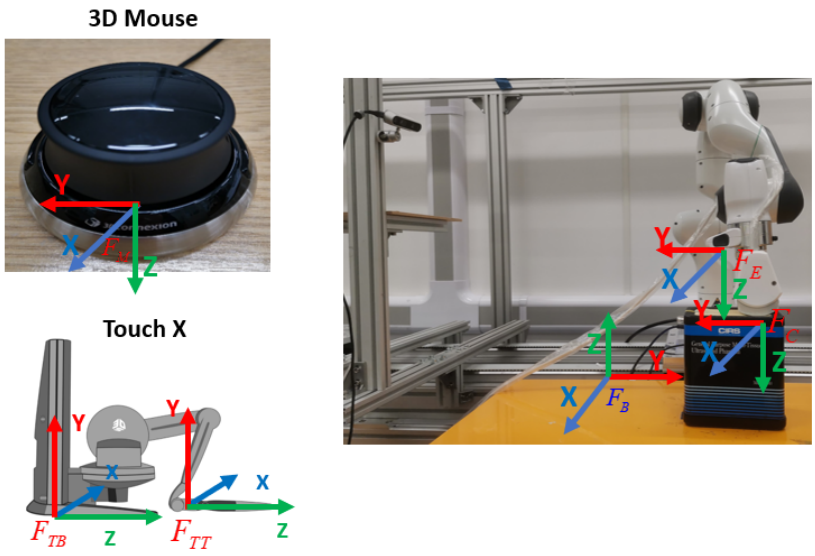

Figure 3.11: The coordinate systems of two teleoperation interfaces.

end-effector frame F_E.

3.4 User study experiment

In this section, we conduct several experiments to evaluate the multimodal teleoperation system and the control system, as shown in Fig.3.12. We evaluate the teleoperation system from two aspects: the feasibility of shared control system and the intuitiveness of different teleoperation interfaces. In this study, seven healthy participants of different ages (26 ± 4 years), heights (177.8 ± 12.2 cm), genders (5 males and 2 females) and majors (5 robotics students and 2 students from other majors) will perform the same task with two different teleoperation interfaces. The whole experimental procedure was conducted in accordance with the Faculty Research Ethics Committee, and the protocol was approved by the UWE Research Ethics Committee (UWE REC REF No: FET-2122-59).

To evaluate the proposed framework, we conducted robot-assisted sonography on the standard Phantom, which is a standard medical examination tool for sonographers. The participants need to

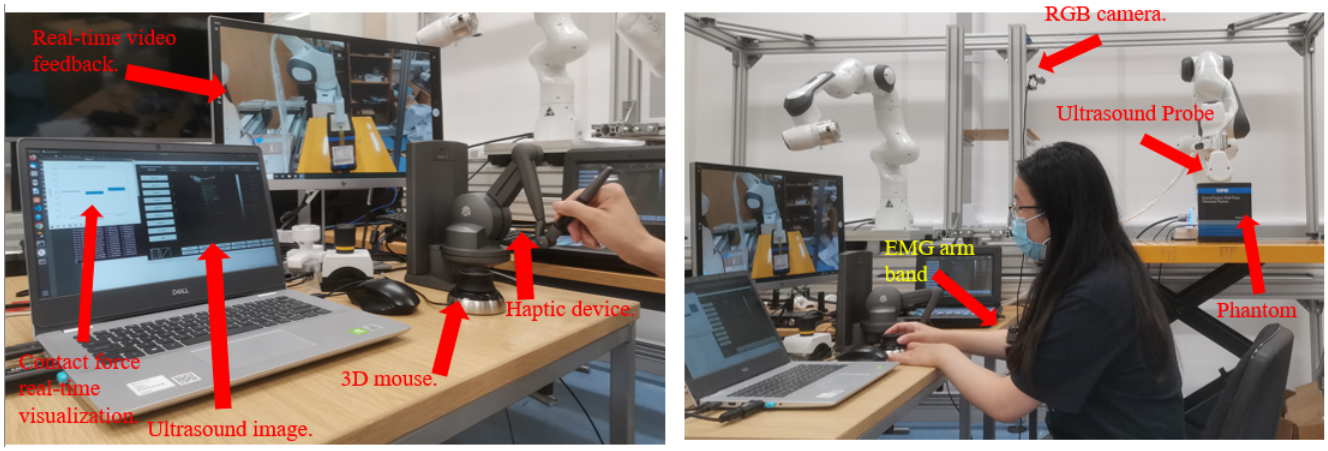

Figure 3.12: The setup of experimental platform. Haptic teleoperation interface and 3D mouse interface are used to teleoperate the robot arm to perform the medical examination.

teleoperate the ultrasound probe to approach the Phantom and then scan the Phantom to acquire high-quality ultrasound images by adjusting the motion and orientation. The teleoperation trajectory is shown in Fig. 3.13.

After participants have completed the task, participants will be asked to complete the NASA-TLX questionnaire (Hart and Staveland, 1988). The NASA-TLX questionnaire assesses workload for both operation modes by giving scores in six areas: Mental Demand (MD), Physical Demand (PD), Temporal Demand (TD), Performance (PE), Effort (EF) and Frustration (FR). All six aspects were divided into 0-21, with higher scores indicating higher levels of participant satisfaction. Additionally, the data during the completion of the experiment is recorded and evaluated at the end. The NASA-TLX questionnaire focuses on assessing the subjective experience of the participants, while the data during the completion is more focused on the objective performance of the task, such as accuracy, and duration of the task. As shown in Figs.3.14 and 3.15, the position tracking and orientation tracking by bilateral teleoperation. The contact force during teleoperation scanning by these two interfaces is presented in Fig. 3.16. Before the experiment, the desired contact force is 10N. From the contact force results, the

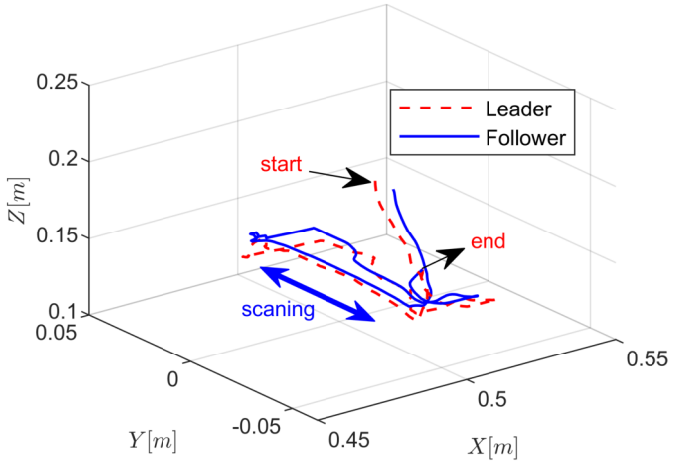

Figure 3.13: 3D trajectories by tele-sonography.

variance of the contact force by Touch X is larger that the 3D Mouse.

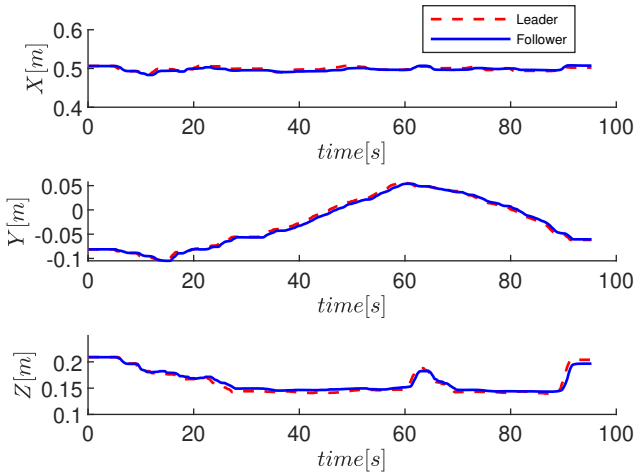

Figure 3.14: Position trajectory by teleoperation.

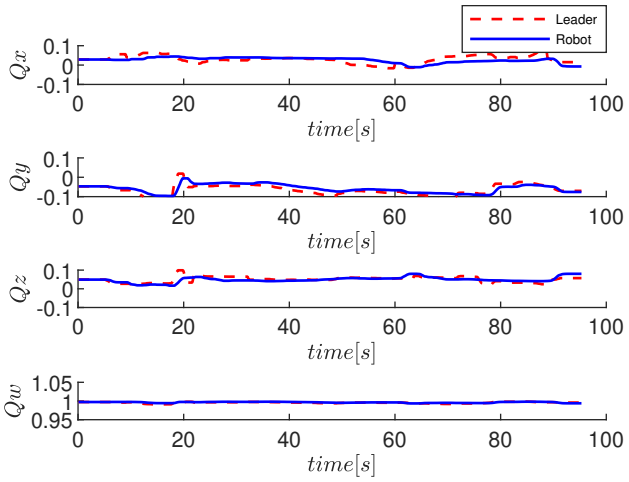

Figure 3.15: Orientation trajectory by teleoperation.

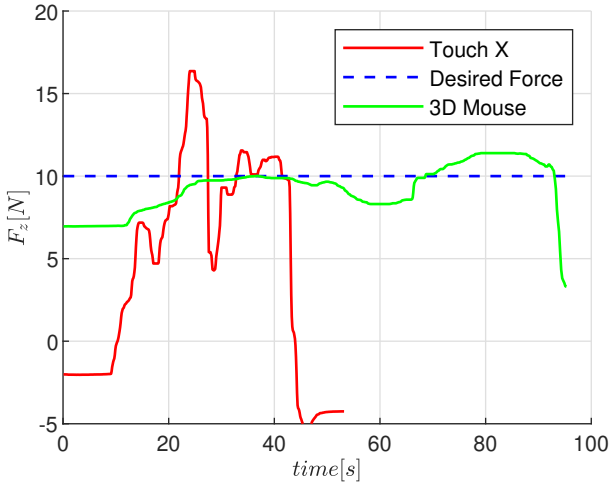

Figure 3.16: Contact force comparison of two interfaces.

3.4.1 The learning and task execution time

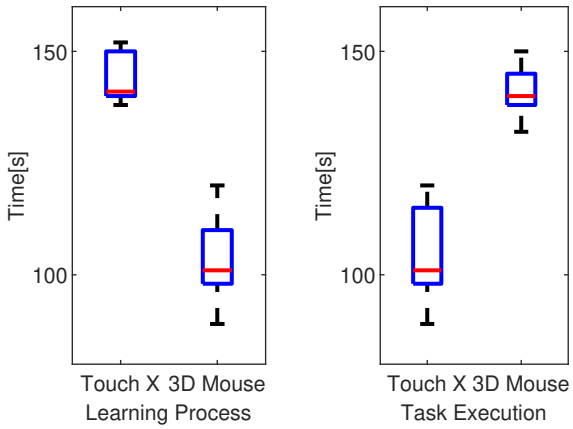

Figure 3.17: The comparison of the learning time and performing time.

We chose the learning time and task execution time as the evaluation metrics. The learning time can describe the intuitive's of the teleoperation interface. The task execution time could represent work efficiency. The performance of the efficiency of different teleoperation interfaces is an important aspect. These objective metrics can be used to describe the performance of the different teleoperation interfaces. As shown in Fig.3.17, the comparison of the learning and execution time by these two different interfaces. The learning time of using the 3D mouse interface is less than the Touch X interface, which means that the 3D mouse is easy to learn for users. In terms of the execution time, the 3D mouse is larger than Touch X, which means that the work efficiency of Touch X is better than 3D mouse.

3.4.2 Performance evaluation based on NASA-TLX

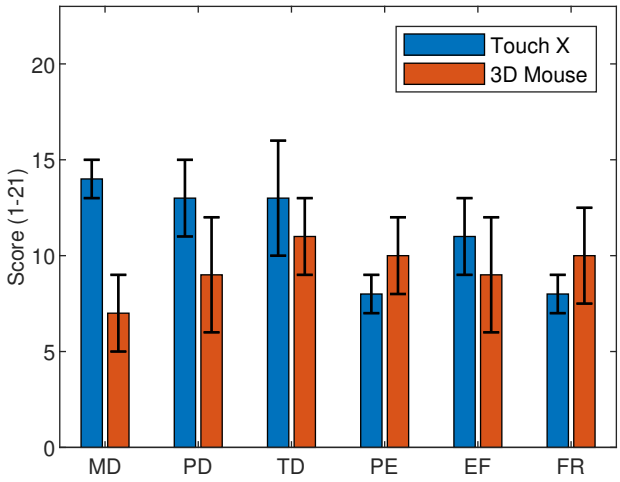

Figure 3.18: The user feedback result.

In the experiment, participants were asked to complete the same task using Touch X and 3D Mouse, after which they completed the NASA-TLX questionnaire to give scores in six aspects, MD, PD, TD, PE, EF and FR. The scores are presented in Fig. 3.18 as a box plot, to graphically demonstrate the maximum, upper quartile, median value, lower quartile, minimum value (shown as horizontal lines from top to bottom respectively) as well as mean value. In general, 3D Mouse users gave lower scores in more aspects, including MD, PD, TD and EF. The difference in scores can be spotted most evidently in MD, where the mean value of Touch X (13.4) is almost twice as high as that of 3D Mouse (6.8). The distinction between Touch X and 3D Mouse in PD and EF is also noticeable, with a difference of 4.2 and 3 correspondingly. On the contrary, participants with Touch X had shown lower scores in PE and FR, indicating that despite the higher demand and effort of the task, the performance was slightly better with lower frustration using Touch X.

3.5 Summary

In this chapter, we introduce the multimodal teleoperation system, encompassing both the hardware and software components. Additionally, we discuss the communication protocols employed between various modules. Furthermore, we conduct experiments to assess the performance of the teleoperation system, including a user study to evaluate the effectiveness of the teleoperation interface. The developed teleoperation system will be utilized for human demonstration and the study of human-in-the-loop mechanisms.

4 Composite and primitive manipulation skill modelling and generalising

4.1 Introduction

In this chapter, composite dynamic movement primitives (DMPs) based on radial basis function neural networks (RBFNNs) are investigated for robots' skill learning from human demonstrations. The composite DMPs could encode the position and orientation manipulation skills simultaneously for human-to-robot skills transfer. As the robot manipulator is expected to perform tasks in unstructured and uncertain environments, it requires the manipulator to own the adaptive ability to adjust its behaviours to new situations and environments. Since the DMPs can adapt to uncertainties and perturbation, and spatial and temporal scaling, it has been successfully employed for various tasks, such as trajectory planning and obstacle avoidance. However, the existing skill model mainly focuses on position or orientation modelling separately; it is a common constraint in terms of position and orientation simultaneously in practice. Besides, the generalisation of the skill learning model based on DMPs is still hard to deal with dynamic tasks, e.g., reaching a moving target and obstacle avoidance. In this chapter, we proposed a composite DMPs-based framework representing position and orientation simultaneously for robot skill acquisition and the neural networks technique is used to train the skill model. The effectiveness of the proposed approach is validated by simulation experiments.

4.2 Preliminaries

4.2.1 Radial basis function neural networks (RBFNNs)

The neural network has been proved to an effective approach to robot applications, and much work on the neural network has been studied, such as the stability of neural network (Peng, Qiao, and Xu, 2002). RBFNNs are a useful tool to approximate nonlinear functions for robot control and robot skills learning. For instance, RBFNNs is combined with the broad learning framework to learn and generalise the basic skills (Huang et al., 2019a). RBFNNs are employed to approximate the nonlinear dynamics of the manipulator robot to improve tracking performance (Yang et al., 2018a; Wang, Chen, and Yang, 2020). Therefore, RBFNNs can approximate the nonlinear forcing term in the DMP framework. Radial basis function networks consist of three layers: an input layer, a hidden layer with a nonlinear RBF activation function and a linear output layer. It is an effective approach to approximate any continuous function $h : R^n \rightarrow R$,

$$h(x) = W^T S(x) + \varepsilon(x) \tag{4.1}$$

where $x \in R^n$ is the input vector, $W = [\omega_1, \omega_2, ..., \omega_N]^T \in R^N$ denotes the weight vector for the N neural network nodes. The approximation error $\varepsilon(x)$ is bound. $S(x) = [s_1(x), s_2(x), ..., s_N(x)]^T$ is a nonlinear vector function, where $s_i(x)$ can be defined as a radial basis function,

$$s_i(x) = \exp(-h_i(x - c_i)^T (x - c_i)) \; i = 1, 2, ..., N \tag{4.2}$$

where $c_i = [c_{i1}, c_{i2}, ..., c_{in}]^T \in R^n$ denotes the centres of the Gaussian function and $h_i = 1/\chi_i^2$, χ_i denotes the variance. The ideal weight vector W is defined as,

$$W = \underset{\hat{W} \in R^N}{\arg\min} \left\{ \sup \left| h(x) - \hat{W}^T S(x) \right| \right\} \tag{4.3}$$

which minimises the approximation error of nonlinear function. The nonlinear functions in DMPs can be learnt by RBFNNs from demonstration data. In this work, RBFNNs will be utilised to parameterise the nonlinear functions in DMPs.

4.2.2 Position and orientation DMP in Cartesian space

DMP is a useful tool to encode the movement profiles via a second-order dynamical system with a nonlinear forcing term. Robots skills learning by DMPs aims to model the forcing term in such a way to be able to generalise the trajectory to a new start and goal position while maintaining the shape of the learnt trajectory. DMPs can be used to model both periodic and discrete motion trajectories. However, in this work, we will focus on the discrete motion trajectories. Currently, the most research on DMPs mainly focuses on the position DMPs and its modifications, which can be used to represent arbitrary movements for robots in Cartesian or joint space by adding a nonlinear term to adjust the shape of trajectory. For one degree of multiple-dimensional dynamical systems, the transformation system of position DMP can be modelled as follows (Ijspeert et al., 2013),

$$\tau_s \dot{v} = \alpha_z(\beta_z(p_g - p) - v) + F_p(x) \tag{4.4}$$

$$\tau_s \dot{p} = v \tag{4.5}$$

where the p_g is the desired position, p is the current position; the v is the scaled velocity, τ_s is the temporal scaling parameter, α_z, β_z are the design parameters, generally, $\alpha_z = 4\beta_z$. $F_p(x)$ is the nonlinear forcing term responsible for tuning the shape of trajectory. The $F_p(x)$ can be approximated by a set of

radial basic functions,

$$F_p(x) = \frac{\sum_{i=1}^{N} \psi_i(x) w_i}{\sum_{i=1}^{N} \psi_i(x)} x(p_g - p_0) \tag{4.6}$$

$$\psi_i(x) = \exp(-h_i(x - c_i)^2) \tag{4.7}$$

where $\psi_i(x)$ is a Gaussian radial basis function with the centre c_i and width h_i; p_0 is the initial position, and w_i is the weight learning from demonstration. The phase variable x is determined by the canonical system, which can be represented as follows,

$$\tau_s \dot{x} = -\alpha_x x, \quad x \in [0,1]; \quad x(0) = 1 \tag{4.8}$$

where α_x is a positive gain coefficient, τ_s is the temporal scaling parameter and the $x_0 = 1$ is the initial value of x, which can converge to 0 exponentially. For the multiple degree-of-freedom (DoF) dynamic system, each dimension can be modelled by a transformation system, but they share a common canonical system to synchronise them.

The orientation DMP has been first proposed by (Ude et al., 2014), which is vital to robot learning and control. The orientation in DMP is often represented by rotation matrix or quaternions. For example in (Koutras and Doulgeri, 2020a), the unit quaternions are used to model the orientation, and the unit quaternion set minus one single point also has been proved to be contractible (Karlsson, Robertsson, and Johansson, 2018). This property of the unit quaternion set could guarantee the convergence of orientation DMPs. In addition, as the quaternion formulation has less variable than the rotation matrix, it has been used widely in the orientation representation for robot learning and control. In (Ude et al., 2014), the unit quaternion-based transformation system can be described as,

$$\tau_s \dot{z} = -\alpha_z(\beta_z 2\log(q_g * \bar{q}) - z) + F_o(x) \tag{4.9}$$

$$\tau_s \dot{q} = \frac{1}{2} \begin{bmatrix} 0 \\ \\ z \end{bmatrix} * q \tag{4.10}$$

where $q \in S^3$ denotes the orientation as a unit quaternion, $q_g \in S^3$ represent the final orientation, ω denotes the angular velocity, $z = \tau_s \omega \in R^3$ is the scaled angular velocity, '*' denotes the quaternion product, $\bar{q}$ represents the quaternion conjugate which is equal to the inverse quaternion for unit quaternions and $2\log(q_2 * \bar{q}_1) \in R^3$ denotes the rotation of q_1 around a fixed axis to reach q_2. The forcing term $F_o(x) \in R^3$ for each DMP will learn the desired orientation skills from the demonstration data.

4.3 Composite position and orientation dynamic movement primitives

Currently, the separate position or orientation DMP has been studied widely (Liu et al., 2020b); however, research on the composite DMPs, modelling the position and orientation simultaneously, is not common. In real practice, most manipulation skills often mix the position and orientation skills, which requires robots to satisfy the specific position constraints as well the orientation for many tasks, such as polishing, spraying, assembly (Wen and Chen, 2020; Huang et al., 2020). In addition, for human-robot interaction tasks, such as two partners collaborating an object handover interaction, the target position is always changing. It is still open to guarantee various orientation requirements. Inspired by the improvement in the orientation DMP, the proposed framework has great generalisation and adaptability to novel tasks and situations. Studying on the DMPs to handle the moving goals is also vital to the practical application. Therefore, we propose the composite DMPs, coupling the position and orientation modelling in a framework, and the RBFNNs are used to learn the nonlinear term in models.

4.3.1 The composite DMP formulation

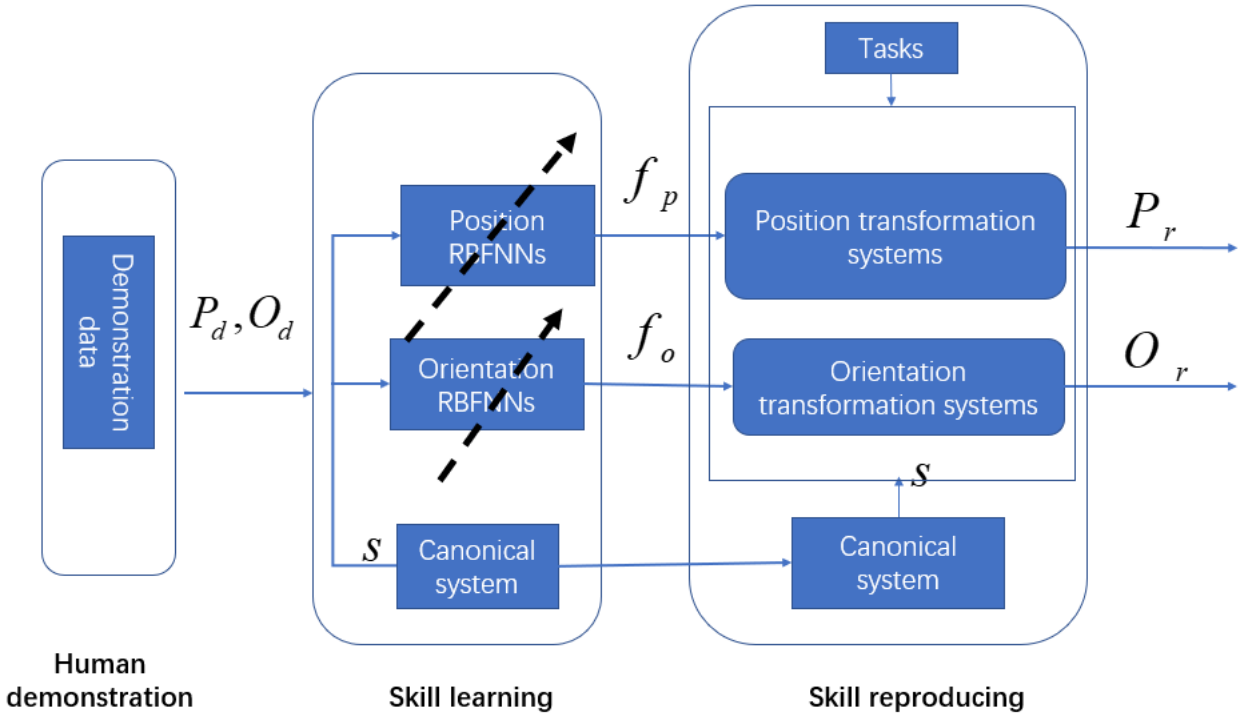

Figure 4.1: The structure of human-robot skill transfer using the composite DMP model.

As shown in Fig. 4.1, the manipulation skill modelled by position and orientation DMPs consisted of recoding the demonstration data, training the RBFNNs and reproducing the skills. The demonstration data include the position and orientation trajectories, and the output of skills reproducing is the reference of position and orientation trajectories associated with specific tasks. The canonical system is used to coordinate the position and orientation constrains in the composite DMPs. The nonlinear forcing terms associated with each DMP are trained by using RBFNNs from the position and orientation demonstration data. Six RBFNNs are used to parameterise the nonlinear functions for position and orientation DMPs, respectively. After the DMPs have learned the demonstration, the dynamic and multiple constraints can be guaranteed: (1) the goal and initial position and orientation can be changed; (2) the targets can be moved, the velocity profiles of DMP output will keep in a safe bound; and (3) the re-

quirements of position and orientation can be achieved simultaneously. The position DMP formulation can be described as,

$$\tau_s \dot{v} = -\alpha_z(\beta_z e_p + v) + diag(p_g - p_0) f_p(x) \tag{4.11}$$

$$\tau_s \dot{e}_p = v \tag{4.12}$$

where $e_p = p_g - p \in R^3$ is the position error and $v \in R^3$ is the scaled velocity error. The α_z, β_z are positive gains, and $f_p(x)$ is trained by RBFNNs for each orientation coordinate. The system is trained using a demonstration from the initial position $p_{0,d}$ to the stationary goal $p_{g,d}$ with temporal scaling τ_d. The orientation DMP formulation can be described as (Koutras and Doulgeri, 2020a),

$$\tau_s \dot{z} = -\alpha_z(\beta_z e_o + z) + diag(q_g * \bar{q}_0) f_o(x) \tag{4.13}$$

$$\tau_s \dot{e}_o = z \tag{4.14}$$

$$e_o = 2\log(q_g * \bar{q}) \tag{4.15}$$

where the e_o is the quaternion error, z is the scaled quaternion error velocity. $*$ denotes the quaternion product. To obtain the orientation, we solve equation (15),

$$q = \overline{\exp(\frac{1}{2} e_o)} * q_g \tag{4.16}$$

The angular velocity is,

$$\omega = 2vec(\dot{q} * \bar{q}) \tag{4.17}$$

where the $\dot{q}$ can be obtained by the following equations,

$$\dot{q} = -\frac{1}{2} q * \bar{q}_g * J_{\log q}(q_g * \bar{q}) \dot{e}_o * q \tag{4.18}$$

$$\dot{e}_o = -2J_q(q_g * \bar{q})(q_g * \bar{q} * \dot{q} * \bar{q}) \tag{4.19}$$

Inspired by the work (Dahlin and Karayiannidis, 2019), the temporal scaling can be adjusted based on the task and the velocity constraints. The target position and velocity update the shared temporal parameter in the position and orientation DMPs, and it may be described as (Koutras and Doulgeri, 2020b),

$$\dot{\tau}_s = -\gamma(\tau_s - \tau_a) + \dot{\tau}_a \tag{4.20}$$

where the γ is a design parameter, τ_a is determined by

$$\tau_a = \frac{\|e\|}{\|e_d\|} * \tau_d \tag{4.21}$$

$$\begin{aligned} e &= \left[e_p^T,\ e_o^T\right]^T \\ e_d &= \left[e_{p,d}^T,\ e_{o,d}^T\right]^T \end{aligned} \tag{4.22}$$

where the e_p is the position error between the goal and the initial point, e_o is the orientation error between goal and start. The $e_{p,d}$ is the position error between the goal and the initial point in the demonstration, $e_{o,d}$ is the orientation error between the goal and start in the demonstration. τ_d is the temporal scaling coefficient in the demonstration. The temporal parameter update law has been proved to converge to the moving goals in (Koutras and Doulgeri, 2020b).

4.3.2 The training of DMPs by RBFNNs

Take one dimension for position and orientation DMP as examples. The nonlinear forcing terms of position and orientation DMP can be approximated by RBFNNs respectively,

$$f_p(s) = \sum_i w_p^i \psi^i(s) \tag{4.23}$$

$$f_o(s) = \sum_j w_o^j \psi^j(s) \tag{4.24}$$

w_p^i, w_o^j are the weight coefficients, $\psi^i(s)$ and $\psi^j(s)$ are the Gaussian activation functions, defined as,

$$\psi^i(s) = \exp(-h^i(s-c^i)^2) \tag{4.25}$$

$$\psi^j(s) = \exp(-h^j(s-c^j)^2) \tag{4.26}$$

In the demonstration phase, one position trajectory $p_d, \dot{p}_d, \ddot{p}_d$ is recorded, from starting position $p_{0,d}$, to the target position $p_{g,d}$. According to the position DMP transformation system and the demonstration data, the desired force function is,

$$f_p^d(s) = \frac{1}{p_{g,d} - p_{0,d}}(\tau_d^2 \ddot{p}_d - \alpha_z(\beta_z(p_{g,d} - p_d) - \tau_d \dot{p}_d)) \tag{4.27}$$

where the τ_d is the temporal scaling during demonstration. Similarly, the force term in the orientation DMPs can be described as,

$$\begin{aligned} f_o^d(s) = &(diag(2\log(q_{g,d} * \bar{q}_{0,d})))^{-1} \\ &*(\tau_d^2 \dot{\omega}_d - \alpha_z(\beta_z(2\log(q_{g,d} * \bar{q}_d) - \tau_d \omega_d))) \end{aligned} \tag{4.28}$$

The following error function between the desired force term and the approximated value is the objective function of the optimisation problem, which will be minimised for learning the parameters of RBFNNs in the DMPs.

$$E = \frac{1}{2}((f_p^d(s^t) - f_p(s^t))^2 + (f_o^d(s^t) - f_o(s^t))^2) \tag{4.29}$$

s^t is the value of s. A gradient descent approach is used to derive the weight update law as (Sharma et al., 2019),

$$w_p^i(t+1) = w_x^i(t) - \lambda_1 \frac{\partial E}{\partial w_p^i} \tag{4.30}$$

$$w_o^j(t+1) = w_o^j(t) - \lambda_2 \frac{\partial E}{\partial w_o^j} \tag{4.31}$$

$$\begin{aligned} \frac{\partial E}{\partial w_p^i} &= (f_p^d(s^t) - f_p(s^t)) \frac{\partial}{\partial w_p^i}(-\sum_i w_p^i \psi^i(s)) \\ &= (f_p^d(s^t) - f_p(s^t))(-\psi^i(s^t)) \end{aligned} \tag{4.32}$$

The weight update law of w_p^i is given as,

$$w_p^i(t+1) = w_p^i(t) + \lambda_1 (f_p^d(s^t) - f_p(s^t)) \psi^i(s^t) \tag{4.33}$$

Similarly, the weight w_o^i is updated by,

$$w_o^j(t+1) = w_o^j(t) + \lambda_2 (f_o^d(s^t) - f_o(s^t)) \psi^j(s^t) \tag{4.34}$$

The weights in the RBFNNs can be attained through the gradient descent approach and demonstration data.

4.4 Experimental results

As a complex task can be hierarchically decomposed into different subtasks involving multiple primitive actions and manipulated objects, several basic motion skills could be synthesised to complex tasks.

Thus, in the chapter, we will conduct several typical motion skills through simulation and experiments. Omni Phantom is an input device for human-robot skill transfer, which has been used in the teleoperation applications. This haptic device could provide the operator force feedback when interacting with the objects or the environments. In this chapter, the Omni Phantom is used to acquire training data of human demonstration in 3D Cartesian space for training the DMP model.

We use Omni Phantom to demonstrate trajectories, including the position and orientation in Cartesian space. The Omni is connected through Simulink of MATLAB to collect the demonstration trajectories. Wthen used the demonstrated data to train all DMPs and executed the DMPs with new start and goal position and orientation. Omni Phantom can record the position and pose of the end. During the demonstration, both the position and orientation trajectories are recorded, used to train the skill model. In the execution, we modify the desired task to test the generalisation performance. All the algorithms and experiments are conducted in MATLAB. The parameters in DMP are shown in Table 1.

Figure 4.2: Six-DoF Omni Phantom.

4.4.1 Spatial scaling of composite DMP

To demonstrate the spatial generalisation ability, we carried out simulation experiments to test the composite DMPs. When the DMP reproduces trajectory, we set a new goal position; the proposed DMPs could converge to the desired position. We test the spatial generalisation of DMPs through

Table 4.1: Parameters in DMP

Parameter	**Descriptions**	**Value**
N	Number of RBFNNs	10
α_z	Coefficient of DMP	60
β_z	Coefficient of DMP	15
λ_1	Learning rate for position	0.1
λ_2	Learning rate for orientation	0.15
γ	Coefficient for tracking target	2

the task shown in Fig. 4.3, simulating the picking and placing skill in the industrial case. First, we demonstrate an obstacle-free trajectory from point A to point B for robots. However, when the robot performs the task, the target moves from Point B to Point C. Our experiment assumes the target moves from B to C at a constant velocity, which is known. The position DMP could generate one trajectory online to adapt the dynamic tasks.

In Fig. 4.4, the trajectory generated by DMPs could reach the desired position of the moving goal even when we learn the DMP using a static goal. (a) shows the human demonstration trajectory and trajectory reproduced by DMP. Although the goal is moving, the trajectory generated by DMP maintains the shape of the demonstration. The red dash line in (c) represents the target velocity, and the green line is the velocity trajectory generated by DMP. From the (d), it can be seen that the temporal scaling parameter τ_s is increasing. In the beginning, since the target velocity is relatively high, the rate of change of τ_s is also relatively large, until it decreases to zero. When the target does not move, the τ_s does not change. Since the temporal scaling coefficient is tuned based on the goal's position and velocity, it could achieve the target and maintain the demonstrated shape. In original DMP, the

(a) (b)

Figure 4.3: (a) Represents the human demonstration from Point A to Point B; (b) represents the target goal moving from Point B to Point C.

temporal scaling parameter is fixed; hence, it is hard to deal with the dynamic perturbance, such as the moving target and the stopping by an obstacle. Therefore, the composite DMP could adapt to a dynamic environment and tasks based on the position and velocity of the goal.

4.4.2 The temporal scaling of orientation DMP

It often requires robots to satisfy the orientation requirements when the robot coordinates with humans or other robots in the industrial application. To demonstrate the temporal scaling ability in the orientation of composite DMP, we modify the execution duration when DMP is reproducing the trajectory. As shown in Fig. 4.5, a human demonstrates how to change Omni's orientation from (a) to (b) and the demonstration data are recorded for training the orientation DMP. In reproduced period, we set the duration time as twice, and the result is shown in Fig. 4.6.

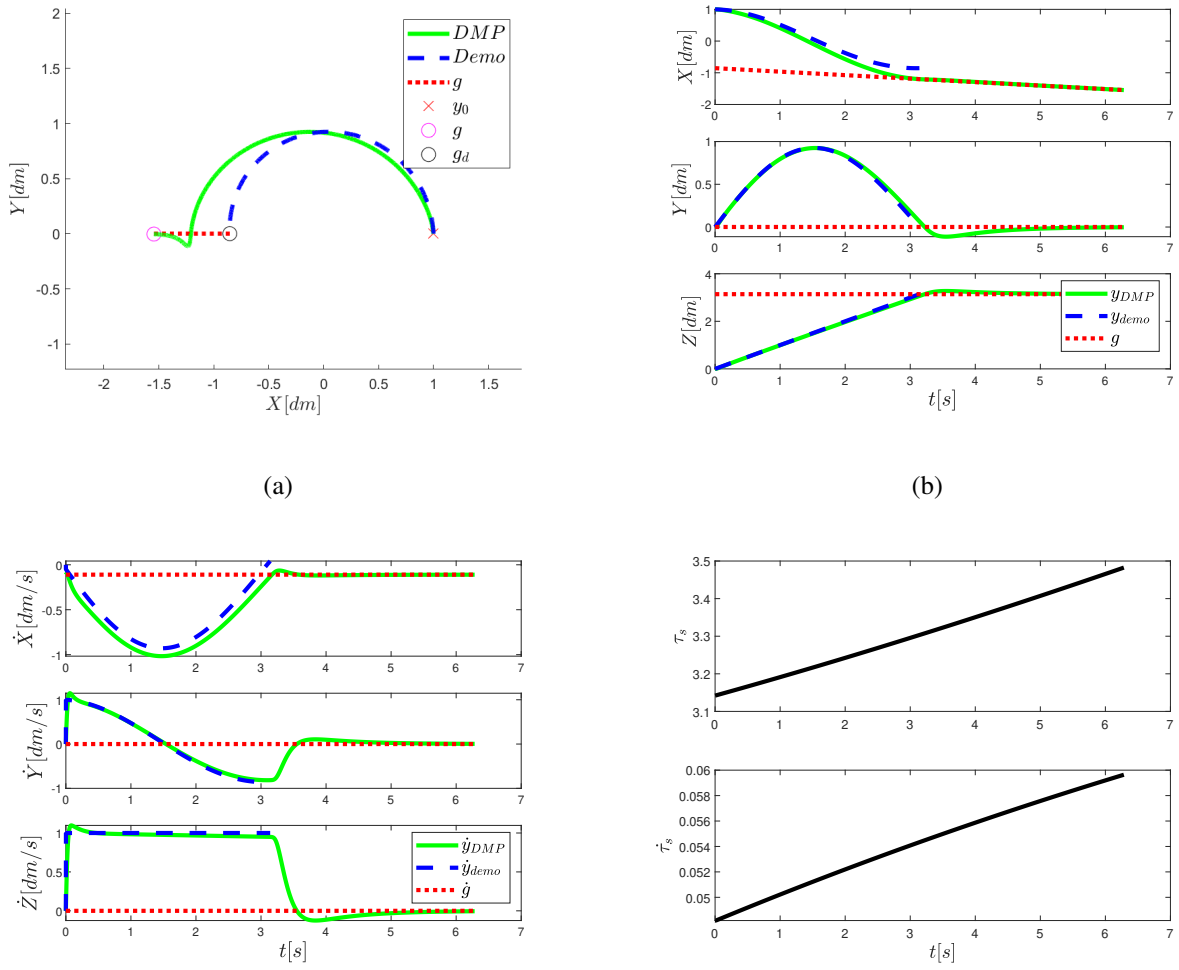

(a) (b)

(c) (d)

Figure 4.4: In (a), the blue line is the human demonstration trajectory; the green line is the reproduced trajectory by DMPs; the red dash line represents the moving target. (b) The position trajectory generated by demonstration and DMP; the red dash line is the goal's position trajectory. (c) The velocity trajectory generated by demonstration and DMP; the red dash line is the goal's velocity trajectory. (d) Provides the evolution of the temporal coefficient and its derivative.

From the (a) in Fig. 4.6, we can find the orientation DMPs can be scaled temporally, and since the execution time is longer, the angular velocity is slower than the demonstration one. The orientation scaling could be achieved by adjusting the temporal parameter. When the temporal coefficient τ_s is

(a) (b)

Figure 4.5: Human demonstrating to changing the pose of the Omni from (a) to (b) through the three orientation joints (red arrow).

twice, the execution time is double, and the trajectory shape is maintained. Also, from the (b), the angular velocity trajectory has the same pattern with the demonstrated one, when modifying the execution time. The trajectory is also smooth and can be adjusted temporally based on the task requirement and perception information on the external environment. This property could be used to adjust the orientation dynamically and satisfy the orientation requirement. When the DMP couples the position and orientation, the temporal coefficient is adjusted based on the position and orientation tasks, and the external environment.

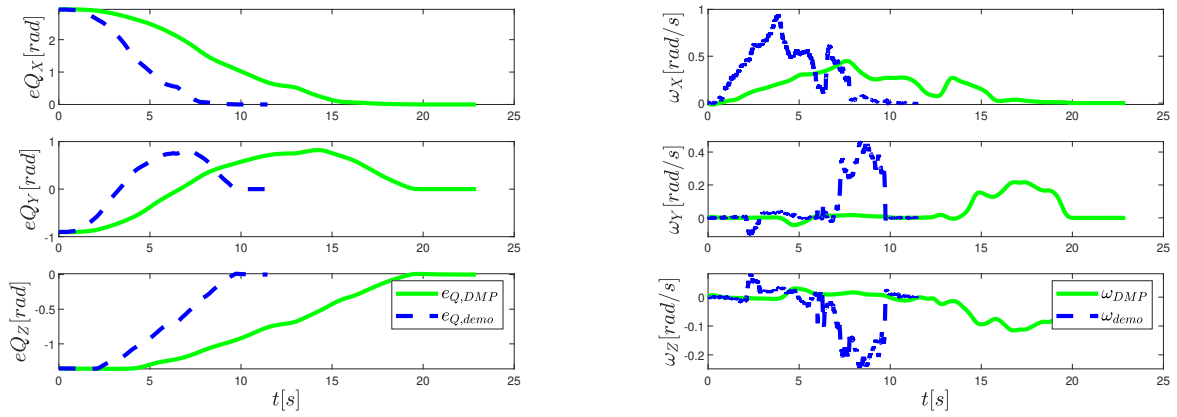

(a) (b)

Figure 4.6: (a) Pose of Omni: the blue line is the demonstration trajectory; the green one is the output of DMP when the execution time is set twice the demonstration one; (b) provides the angular velocity generated by demonstration and DMP

4.4.3 The performance of composite DMP for a moving goal

For the tasks with position and orientation constraints, the composite DMPs between the position and orientation are necessary. Test the performance of composite DMPs to the tasks requiring the position and orientation simultaneously. For this case, we first demonstrate a trajectory involving the position and orientation and then train the composite DMPs using the demonstration data. During the reproducing stage, the DMPs need to generate position and orientation trajectory for the moving goal and satisfy the orientation constrains. The performance of reaching a moving target with orientation constraint can be found in Fig. 4.7.

Through (a) and (b) in Fig. 4.7, the trajectory generated by DMPs could reach the moving goal with the desired orientation. Due to the moving goal, the temporal scaling τ_s is increasing. Although the target has a constant velocity, the shape of position and orientation is consistent with the demonstra-

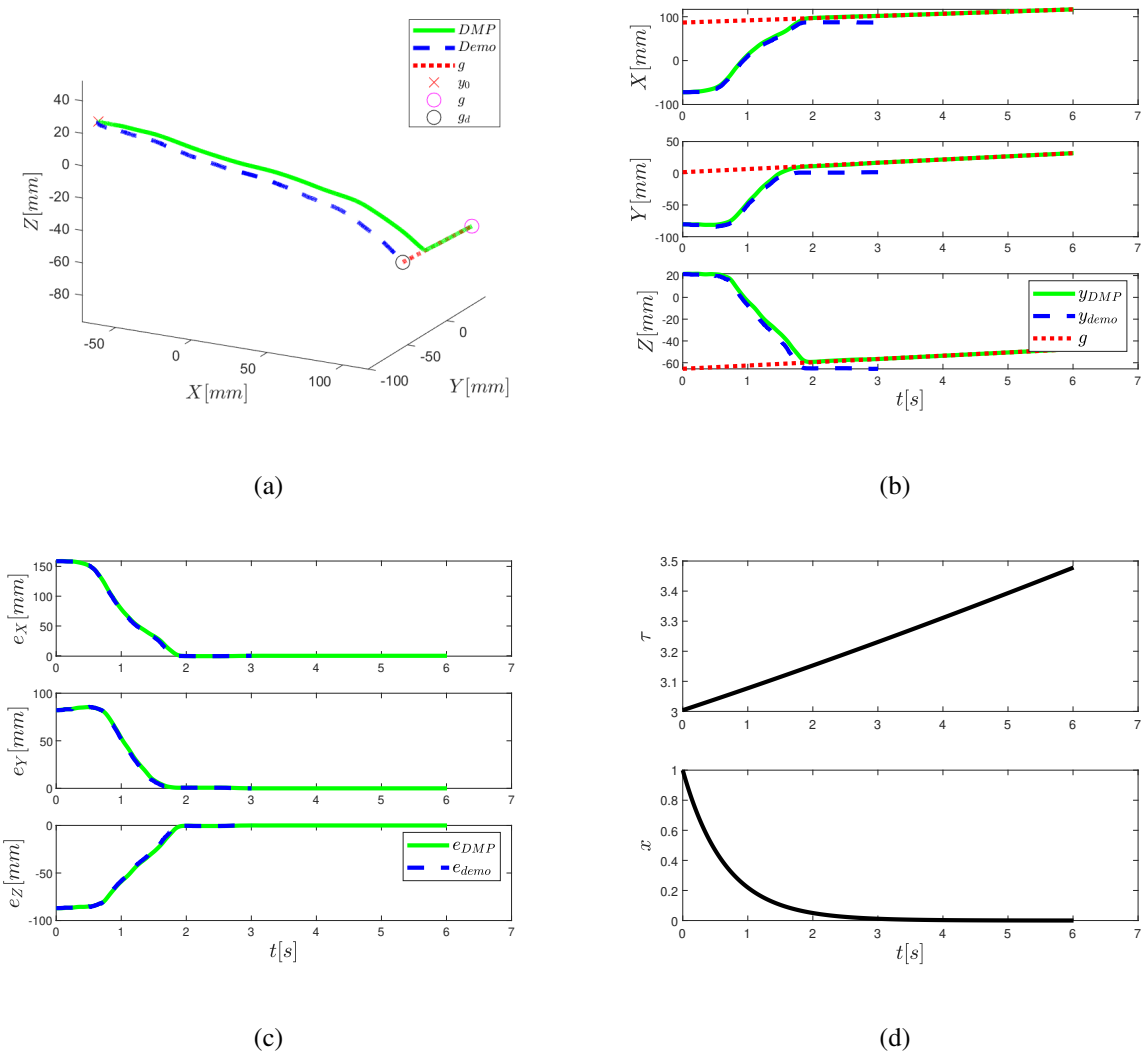

Figure 4.7: (a) 3D trajectory. The blue and green lines in (b) show the demonstration and DMP trajectory in each direction; the red dash line is the goal trajectory in XYZ directions. (c) The orientation error between the current orientation and the goal orientation. (d) provides the evolution of the temporal coefficient and the phase variable x with time.

tion. Due to the goal's velocity, the temporal scaling is increasing, which guarantees the velocity shape is similar to the learned pattern. The position and orientation constraints are satisfied simultaneously. For the composite DMP, because the goal's motion information could influence the temporal scaling and phase variable, it could influence the trajectory shape. The position and orientation could be cou-

pled and adjusted based on the task and the external environments through the temporal scaling. The proposed composite DMP considers the moving goal and the orientation requirements simultaneously.

4.5 Summary

This chapter proposed composite DMPs, coupling the position and orientation representation simultaneously and using the RBFNNs to approximate the nonlinear forcing term in DMPs. The composite DMPs can track moving goals and guarantee the velocity stays in a safe range. The generalisation performance of temporal and spatial scaling is validated through several primitive skills. Additionally, this approach can be applied in cooperation manipulation tasks involving bimanual manipulators.

5 Human-in-the-loop method for compliant skill learning and generalising

5.1 Abstract

Adapting to unexpected events and dynamic environments is essential for the robot manipulator while executing physical contact-rich manipulation tasks, such as rolling pizza dough and medical examination. In this chapter, we proposed a novel framework combining learning from demonstration (LfD) and human experience to enhance the safety and adaptability of robot manipulation. Dynamic movement primitives (DMPs) are employed for manipulation skills learning from demonstrations, and human correction is studied to update the pre-trained DMPs skills model. We conducted experiments on the Franka Emika Panda Robot with pizza dough rolling tasks, as shown in Fig. 5.1. The dough's varying hardness demands the roller to interact with different forces. Humans can naturally adjust force and motion during this task. The robot manipulator also needs to adjust its force and motion to achieve successful manipulation simultaneously. The results demonstrate that the proposed framework could effectively improve the performance of physical contact-rich tasks, and the human correction through the teleoperation method provides a potential solution for advanced interaction tasks with complex and dynamic physical properties.

The main contributions of this chapter can be summarized as follows.

- We developed a hybrid control architecture for a bilateral teleoperation system that includes

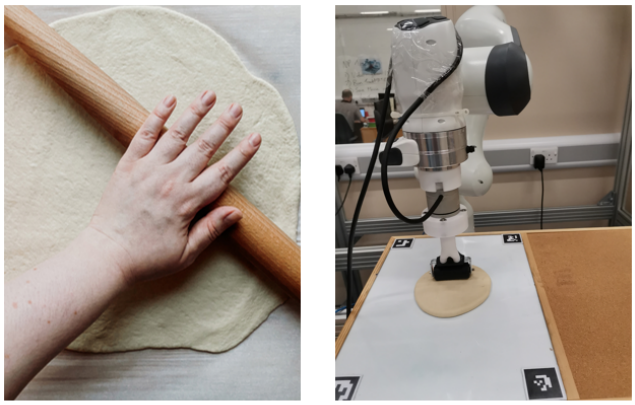

Figure 5.1: Rolling the pizza dough.

hybrid force and position control as well as impedance control to achieve compliant skill transfer from humans to robots.

- The teleoperation-based system allows human operators to correct the behaviour of the autonomous robot. The updated behaviour is employed to update the pre-learned compliant skills model.

- The proposed solution, as shown in Fig. 5.2, is evaluated on the pizza dough rolling of different hardness. The updated skill model can increase the performance of the dough rolling, including the success rate and uniform force on the dough. This solution also has the potential to extend to other contact-rich tasks, such as medical scanning.

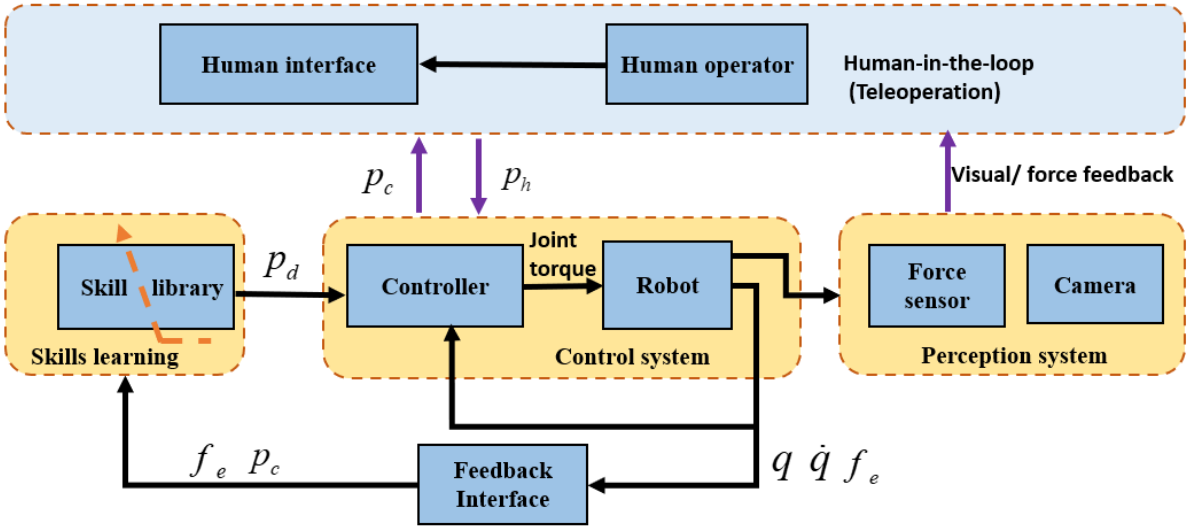

Figure 5.2: The overview of the proposed framework. The visual and force feedback provided perceptual information to the human operator. The control system consists of impedance control and hybrid force and position control to generate the joint torque. More details of the control system can be found in Fig.5.3. The skills learning module encodes the manipulation profile f_e, p_c in Cartesian space and generates desired pose p_d. The teleoperation module monitors the process and provides human correction p_h when necessary.

5.2 Preliminary of robot control

5.2.1 Robotic dynamics and control

The dynamics of the general serial n-DOF manipulator robot in Cartesian space can be modelled as (Zeng et al., 2021),

$$M(q)\ddot{x} + C(q,\dot{q})\dot{x} + G(q) = f_c + f_{ext} \tag{5.1}$$

where the $M(q) \in R^{m\times m}$ is the inertia matrix in Cartesian space, the $C(q,\dot{q}) \in R^{m\times m}$ is the Coriolis term and $G(q) \in R^{m\times 1}$ represents gravitational force. $f_c \in R^{m\times 1}$ is the control force and $f_{ext} \in R^{m\times 1}$ is the

interaction force with the environment. $q \in R^{n\times 1}$ and $\dot{q} \in R^{n\times 1}$ represent the joint position and velocity, respectively, and the $\dot{x} \in R^{m\times 1}$ and $\ddot{x} \in R^{m\times 1}$ are the velocity and acceleration of the robot end-effector in Cartesian space.

For the bilateral teleoperation system, the dynamics of the leader robot can be described as (Michel et al., 2021),

$$M_m(q_m)\ddot{x}_m + C_m(q_m,\dot{q}_m)\dot{x}_m + G_m(q_m) = f_m + f_h \tag{5.2}$$

where $M_m(q_m) \in R^{m\times m}$ is the inertia matrix of leader robot, $C_m(q_m,\dot{q}_m) \in R^{m\times m}$ is the Coriolis and centrifugal terms and $G_m(q_m) \in R^{m\times 1}$ represents the gravitational force. $f_m \in R^{m\times 1}$ and $f_h \in R^{m\times 1}$ are the control and operator force, respectively. $q_m \in R^{n\times 1}$ and $\dot{q}_m \in R^{n\times 1}$ are the joint position and velocity in the joint space, respectively, the $\dot{x}_m$ and $\ddot{x}_m$ represents the velocity and acceleration of end-effector in Cartesian space. Similarly, on the remote manipulator side, the dynamics of the follower robot can be described as,

$$M_r(q_r)\ddot{x}_r + C_r(q_r,\dot{q}_r)\dot{x}_r + G_r(q_r) = f_r + f_e \tag{5.3}$$

where the $M_r(q_r) \in R^{m\times m}$ is the inertia matrix of the follower robot, $C_r(q_r,\dot{q}_r) \in R^{m\times m}$ is the Coriolis and centrifugal term and $G_r(q_r) \in R^{m\times 1}$ represents the gravitational force. $f_r \in R^{m\times 1}$ and $f_e \in R^{m\times 1}$ are the control and interaction force executed on the robot, respectively. $q_r \in R^{n\times 1}$ and $\dot{q}_r \in R^{n\times 1}$ are the joint position and velocity in the joint space, respectively, the $\dot{x}_r \in R^{m\times 1}$ and $\ddot{x}_r \in R^{m\times 1}$ represents the velocity and acceleration of end-effector in Cartesian space. For both the leader and follower robots, $(\dot{M}_i - 2C_i)$ for $i = \{r,m\}$ are skew symmetry, which represents that the remote manipulator and the leader device are passive respectively. The control command for the remote follower manipulator is generated by an impedance controller,

$$f_r = K_r(x_m - x_r) - D_r\dot{x}_r \tag{5.4}$$

where K_r is the stiffness matrix, the D_r represents the damping matrix. x_m and x_r are the position of the

leader and follower robots, respectively. For the leader robot, the force feedback is designed to reflect the interaction force between the follower robot and the environment,

$$f_m = K_m(-f_e - D_m\dot{x}_m) \tag{5.5}$$

where D_m is the damping matrix. K_m is the scaling parameter. The stability of the bilateral teleoperation system can be proved by passivity analysis (Michel et al., 2021). The bilateral teleoperation could provide force feedback for the human operator.

5.3 Framework of human-in-the-loop for robot learning

5.3.1 Dynamic movement primitives (DMPs)

DMPs was proposed by Ijspeert to study motor control of humans, which was inspired by the dynamic systems and human motor control. The essential of DMPs was to encode the manipulation skills by a dynamic system. For the complex and multi-step tasks, merging the separate DMPs into a complex manipulation was also investigated (Saveriano, Franzel, and Lee, 2019). DMPs can also be employed to model multiple DoFs system, each DoF can be modelled separately, and a canonical system achieves the coupling among these DoFs. For readability, we introduce the DMPs for one degree of multiple dynamic systems,

$$\begin{aligned} \tau_s\dot{v} &= \alpha_z(\beta_z(p_g - p) - v) + F(x) \\ \tau_s\dot{p} &= v \end{aligned} \tag{5.6}$$

where the p_g represents the goal position, p represents the current position; τ_s is the scaling parameter, the v is the velocity, α_z, β_z need to be designed, however, these parameters satisfying $\alpha_z = 4\beta_z$. $F(x)$ is the nonlinear forcing term, which is used to affect the trajectory. Generally, the $F(x)$ can be composed

of the Gaussian functions,

$$F(x) = \frac{\sum_{i=1}^{N} \psi_i(x) w_i}{\sum_{i=1}^{N} \psi_i(x)} x(p_g - p_0) \tag{5.7}$$

$$\psi_i(x) = \exp(-h_i(x - c_i)^2) \tag{5.8}$$

A canonical system was used to determine the phase variable x, and the canonical system can coordinate different DoFs, which can be described as,

$$\tau_s \dot{x} = -\alpha_x x, \quad x \in [0,1]; \quad x(0) = 1 \tag{5.9}$$

where τ_s represents the scaling parameter, α_x is a positive coefficient, and the initial value of x is $x(0) = 1$, which can converge to zero exponentially.

The original DMPs model is used to encode the manipulation skill offline, and it is not suitable for online skill update. Recently, a sensory-based coupling term was proposed to achieve reactive planning and control. In addition, the coupling term could be used to avoid obstacles based on the real-time perception feedback. Inspired by the work (Rai et al., 2017), we proposed a novel formation of DMPs for robot skill update online through human-in-the-loop,

$$\begin{aligned} \tau_s \dot{v} &= \alpha_z(\beta_z(p_g - p) - v) + F(x) + H(\cdot) \\ \tau_s \dot{p} &= v \end{aligned} \tag{5.10}$$

where $H(\cdot)$ is the human interaction terms, which provides a human interface to update the pre-defined skill online. This human interaction term is activated only in the shared control mode when humans interact with the execution process since the pre-trained skill cannot generalise to new cases. The $H(\cdot)$ is approximated by a set of radial basis functions as same as $F(x)$, and the locally weighted projection regression (LWPR) technique is used to calculate the weights of this term $H(\cdot)$. Moreover, this term is modified only in the specific DoF, and this interaction term could be updated iteratively.

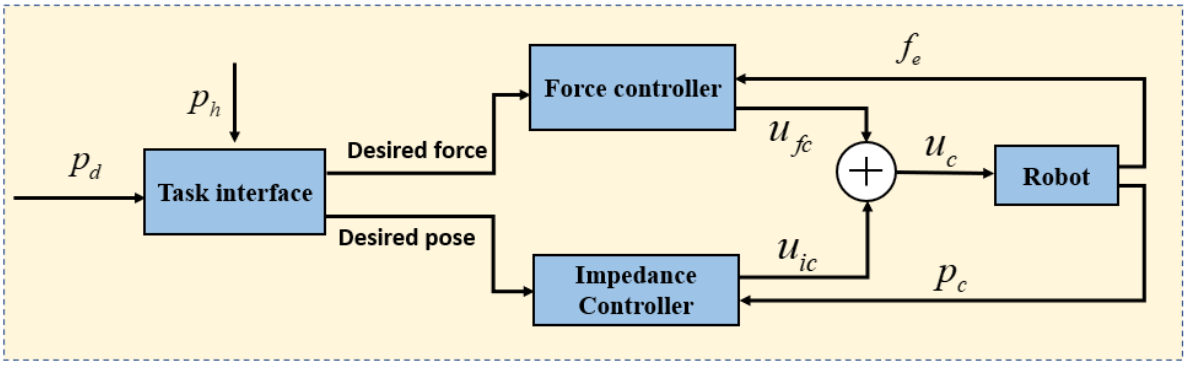

Figure 5.3: The architecture of the control system. The required poses and forces are derived from the skill model and teleoperation. The task interface decouples the tasks to each DoF, and the desired commands are fed to the corresponding controllers. The computed torques from the force and impedance controllers are combined and provided to the robot.

$$H(\cdot) = \begin{cases} h(s) & \gamma = 1 \\ 0 & \gamma = 0 \end{cases} \tag{5.11}$$

where $h(s)$ is the output of interaction term trained based on the human correction. $\gamma = 0$ and $\gamma = 1$ represent autonomous mode and human correction mode, respectively.

For the multi-step tasks, it often needs to merge several DMPs. In this work, we adopt the first method described in (Saveriano, Franzel, and Lee, 2019), which could guarantee position and orientation to be smooth. This method requires fewer parameters than other methods, e.g., smooth acceleration transition, and it is feasible for multi-step merging without high requirement on efficiency.

$$p_{ne} = p_{pr} \qquad v_{ne} = v_{pr} \tag{5.12}$$

$$q_{ne} = q_{pr} \qquad \omega_{ne} = \omega_{pr} \tag{5.13}$$

where the p_{ne}, v_{ne}, q_{ne}, ω_{ne} are the initial position, velocity, angular and angular rate of next DMP respectively; the p_{pr}, v_{pr}, q_{pr}, ω_{pr} are for the last DMP. For the orientation control, we adopt the

unit quaternion based DMPs (Saveriano, Franzel, and Lee, 2019) to model the orientation skills. The generalisation of orientation skill was not considered in this work; the details of orientation DMPs can refer to (Saveriano, Franzel, and Lee, 2019).

5.3.2 Hybrid force and position control

Impedance control, proposed by Hogan in 1985 (Hogan, 1985), has been investigated widely for robot manipulator control, such as compliant control and human-robot interaction etc. The impedance controller is similar to a spring-damper dynamic system, which is used to model the dynamic interaction between the robot and its environment. This control of dynamic behaviour allows human-robot and robot-environment safety interaction. In addition, adaptive impedance control has proven an effective approach to improve control performance during the interaction between robots and the environment (Zeng, Yang, and Chen, 2020; Michel et al., 2021; Li et al., 2018). The impedance controller can be implemented in the joint space and Cartesian space. For the tasks of end-effector interaction with the environment, the impedance controller in Cartesian space is more suitable. We implemented the impedance control in the task space, and the control law can be described as,

$$u_{ic} = -J^T(q)(K\Delta x_t + D\Delta \dot{x}_t + k_t) \tag{5.14}$$

where the u_{ic} is the command in joint space generated by the impedance controller, the $J(q)$ is the Jacobian matrix associated with robot configuration, K and D are the stiffness and damping matrix, which is used to determine the characteristic of impedance. Δx_t is the position error between the current position and the desired position; $\Delta \dot{x}_t$ is the velocity error between the current velocity and the desired velocity. k_t is the feedforward compensation calculated by the dynamic model of manipulator.

The hybrid force-position approach investigates the two reciprocal subspaces: twists and wrenches, regulating the contact force and simultaneously tracking the desired motion. For the force controller

part, a proportional-integral method can be stable for a high-stiffness control process. The force controller can be described as (Marin and Weitschat, 2016),

$$\Delta f = \Im_{ee}(t) - \Im_d(t) \tag{5.15}$$

$$u_{fc} = J^T(q)[K_{fp}\Delta f + K_{fi}\int \Delta f dt] \tag{5.16}$$

where the $\Im_{ee} = (f_{ee}^T, m_{ee}^T)$ is measured wrench of end-effector generated by interacting with the environment. K_{fp} and K_{fi} are the proportional and integral gains respectively. The f_{ee} and m_{ee} are the current force and torque measured from torque/force sensor in this work. $\Im_d = (f_d^T, m_d^T)$ is the desired wrench, f_d and m_d are the desired force and torque. The command to the robot is the combination of force controller and the impedance controller. The combined command in joint space u_c of the robot to execute a given task can be,

$$u_c = u_{ic} + u_{fc} \tag{5.17}$$

where the u_{ic} is the command generated by the impedance controller, and the u_{fc} is the command generated by the force controller.

Based on the hybrid force-position controller, the control allocation for motion tracking by the impedance controller and force control is realized by a task matrix. We defined the task matrix as the control allocation matrix for the n-DOF to realize the switch among different tasks. We introduce the position control matrix M_p; hence the force control matrix M_f can be described as,

$$M_f = I_6 - M_p \tag{5.18}$$

$$M_p = diag(s_i) \tag{5.19}$$

where the task matrix, M_f and M_p, are diagonal matrix, with the $s_i \in \{0,1\}$, $s_i = 1$ represents position control in this direction, and $s_i = 0$ represents force control in this direction. For example, $M_p \in R^{6\times 6}$

is a identity matrix. which represents only position control.

Different controllers are usually used for a multi-step task in different stages, for example, impedance control in the approaching stage and hybrid force and position control in the rolling stage. It is important to design the transition strategy when switching between different controllers to ensure smooth transitions and reduce jitter. The transition of two mode, u_1 and u_2, is realized through the linear interpolation during the transition windows,

$$u = (1-\beta)u_1 + \beta u_2 \tag{5.20}$$

where u is the control command during the transition. u_1 and u_2 are the joint torque in two control modes, respectively. $\beta = t/T$ and $t \in [0,T]$. T is the transition window. The linear interpolation allows for a smooth transition between two different controllers.

5.3.3 Human correction interface

In (Hagenow et al., 2021), the authors proposed a shared control interface to mix human input and autonomous commands. The modification strategy by human operators can be described as,

$$x = x_n + \delta y \tag{5.21}$$

where $x_n \in R^m$ is the nominal robot state, and $\delta y \in S(R^m)$ is the modification to the robot state variable. $S(R^m)$ is the correction interface, the input is the modification command, and the output of the correction interface is the modified task variables. A nominal task model can be learned through demonstration offline. A corrective command is generated by the human operator based on the observations of any errors of the robot state or the environment state.

The human-in-the-loop allows humans to intervene autonomous execution of the robot through the teleoperation input device. The human correction command can be modelled an ordinary differential

equation about the input of teleoperation device (Hagenow et al., 2021),

$$\ddot{\delta}y + b_c\dot{\delta}y + k_c\delta y = u \tag{5.22}$$

where δy represents the human command, k_c and b_c are the stiffness and damping parameter of the human correction dynamics, u represents the output of the haptic device.

The force/torque sensor has noise; therefore, it is necessary to filter the measurement data. In this work, we adopted the Kalman filter to reduce the noise, and the Kalman filter's update equations can refer to (Sidhik, Sridharan, and Ruiken, 2021). Other robot state variables, e.g., position and velocity, are used directly from the data provided by the Franka Control Interface (FCI), without additional filtering processing.

5.4 Experiments

We evaluated the proposed framework through a typical task in life, rolling pizza dough. This task consists of the interaction of the robot with its environment, a task that requires both appropriate contact force control and trajectory control simultaneously. In addition, it requires the robot to adapt its behaviour to the shape and hardness of the dough. However, the exact hardness of the dough is practically difficult for robots to attain in advance. The experimental setup is shown in Fig.5.4.

5.4.1 Rolling dough skill transfer through bilateral teleoperation

In terms of the demonstration through teleoperation, we decoupled into two steps, motion skills in the X-Y plane and force skills along the Z-axis, as shown in Fig. 5.6. First, we teleoperate the robot to roll the dough through the Touch input device. The translation mapping between the Touch and the end-effector is direct mapping with a scaling parameter in Cartesian space. And the demonstrated

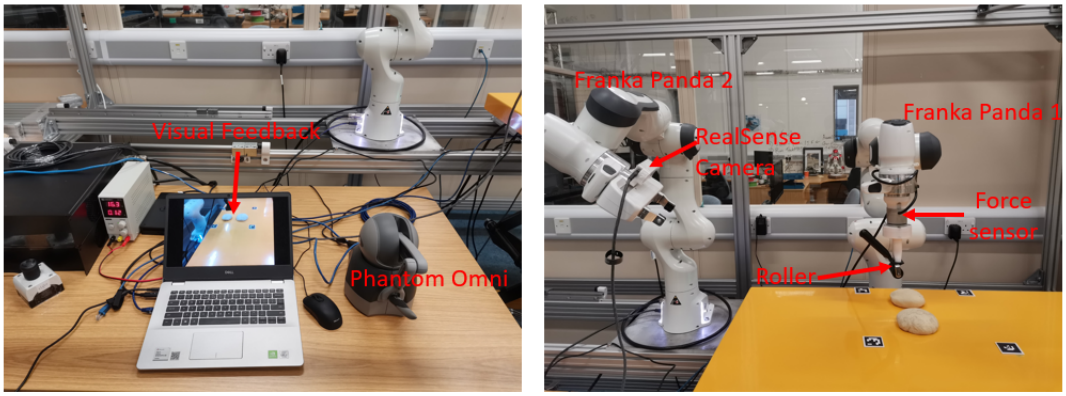

Figure 5.4: The setup of experimental platform.

Figure 5.5: (a) The robot rolls the pizza dough with proper force and motion. (b) The robot interacts with the soft dough with a large force, so the roller gets stuck. In this case, the forces along the X and Y axes are too large, which means that the task has failed.

trajectory of the end-effector in the X-Y plane is recorded. The demonstration trajectory is used to encode the nominal skills in X-Y plane motion by the DMPs model. The learned skill can generate motion trajectories in the X-Y plane for the robot; hence the motion of the robot on the X-Y plane can be autonomous execution. The autonomous execution in the X-Y plane requires only the current coordinates and goal coordinates in the X-Y plane.

In the following demonstration, the Touch is used to demonstrate the force control along the Z-axis alone, while the motion in the X-Y plane is generated by the learned DMPs. In this shared control mode, the human operator only teleoperates the contact force control, which could reduce the cognitive

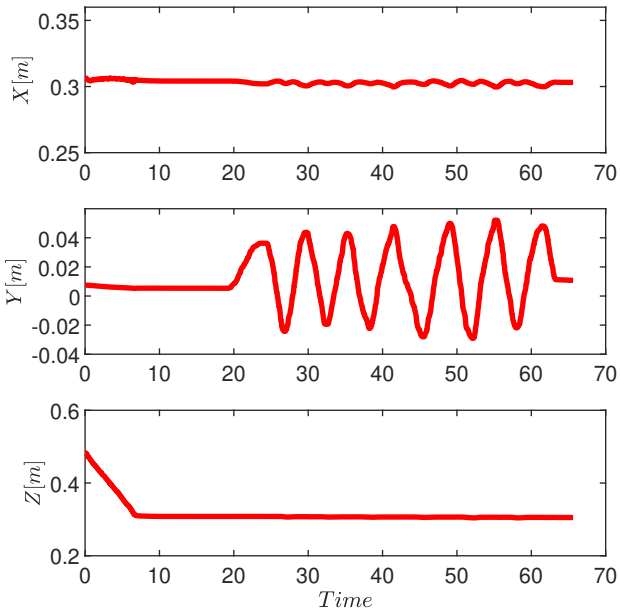

Figure 5.6: The trajectories along the X, Y, Z axes in teleoperation demonstration.

work and improve the accuracy of teleoperation. In addition, this also reduces communication traffic, which is helpful to reduce the time delay in the human-robot skill transfer, especially for the bilateral teleoperation in a long distance. The human could demonstrate to the robot the human-like manipulation skill, how to roll the dough only based on the force and visual feedback. To reproduce the learned skill, we let the robot roll the pizza dough with the same hardness autonomously. The interaction forces along the X, Y and Z-axis are shown in Fig.5.7.

5.4.2 Robot rolling soft dough

When the robot rolls soft pizza dough, it needs to adjust the contact force according to the hardness of the dough. It cannot accomplish the task only relying on the learned force skill offline, for example, the large contact force causing the roller stuck, as shown in Fig. 5.8 and Fig.5.5. Although adaptive force control may deal with the uncertainty of hardness, it is hard to design a controller to deal with all kinds

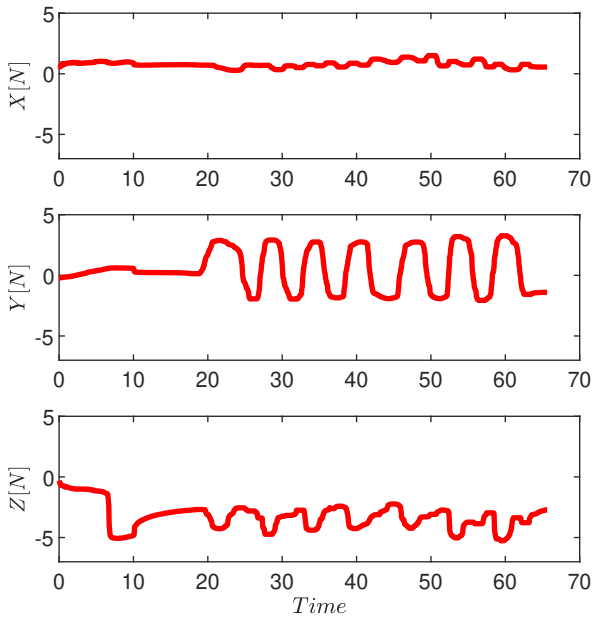

Figure 5.7: The interaction forces along the X, Y and Z axes during the demonstration stage.

of hardness, especially since the properties of the dough are hard to model and attain in advance. In this case, the human could correct the contact force on top of the learned force skill through a shared control mechanism. For example, humans can reduce the contact force to generate an appropriate contact force for soft doughs. The human corrects the contact force based on the interaction force between the roller and the dough (force feedback via the Touch) and the deformation of the dough shape (visual feedback via the camera).

We evaluated the learned force skill on a novel dough that is softer than the one used in the demonstration phase to evaluate the generalization capability to the different hardness of the dough. As shown in Fig. 5.8, this is a failed case where the roller is stuck because the contact force is too large. Because the roller only moves along the Y-axis, we provide the motion along Y-axis and contact forces along Y-axis and Z-axis. The force along the Y-axis is too large, which means the task fails, and the roller is stuck. In addition, we tested on a novel dough, which is stiffer than the one used in the demonstration. However, the robot could not accomplish the task in the given time, and it needed more time to roll

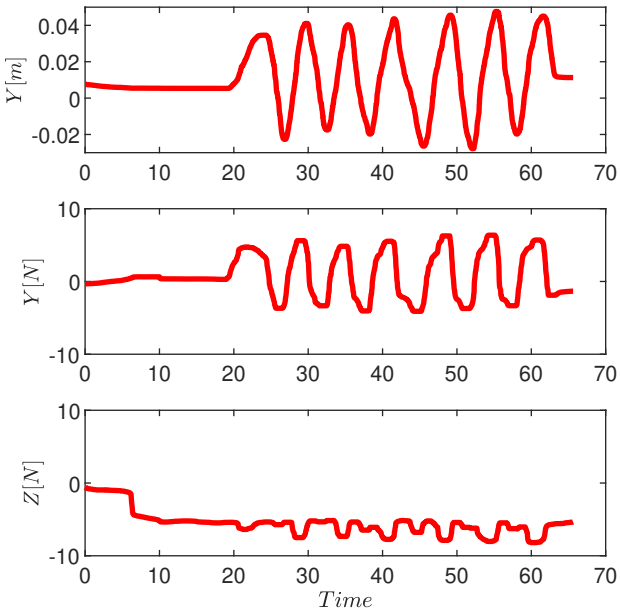

Figure 5.8: The robot fails on the soft dough with learned force skill. The trajectory along Y-axis and the interaction forces along the Y-axis and Z-axis. The force along the Y-axis (direction of motion) is larger than 6N (normally, the force should be within 3N), which means that the roller is stuck.

because the contact force was too small. In these cases, human correction is very useful to update the force skills. Compared to previous work, the human-guided method to update the skills model is more efficient. In addition, the human-guided method can also ensure safety.

For the above case, the human corrects the contact force on top of the autonomous commands (normal force) to generate an appropriate contact force for the soft dough. The contact force perceived by the force sensor is recorded to update the force skill model. The difference between the corrected contact force and the nominal force skill is used to train the human interaction term $H(\cdot)$ in the DMPs. As shown in Fig.5.9, for the soft dough, the force along the Y-axis is less than 1N, and the corrected contact force along the Z-axis is around 2N. In this work, although we showed the human operator correct the contact force alone through the human-in-the-loop mechanism, this method can also be employed to update other variables, such as the orientation and motion, to meet some specific requirements in

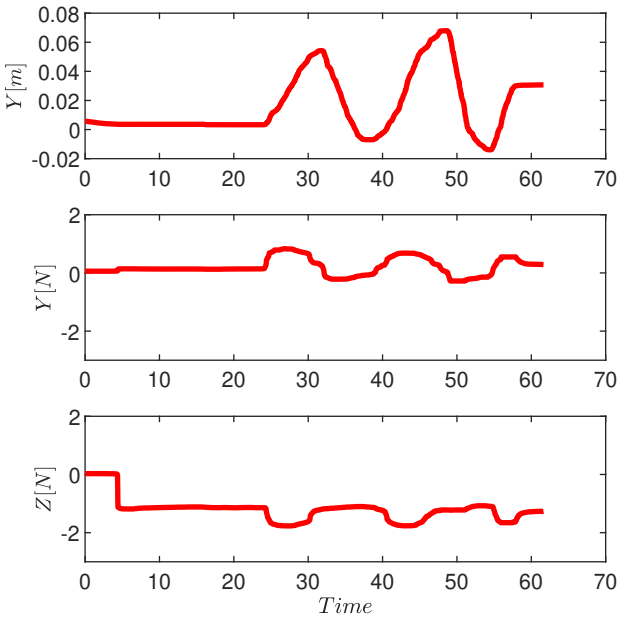

Figure 5.9: The human corrects the contact force along the Z-axis through teleoperation online for the soft dough. The contact force along the Y-axis is less than 1 N, and the contact force along the Z-axis is less than the contact force for stiff dough (around 5N).

contact-rich applications.

We test the updated skill model with another soft dough. As shown in Fig. 5.10, the robot can roll the new soft dough autonomously. The contact force along the Y-axis is less than 2N, which means that the task is successful. Moreover, the motion pattern along the Y-axis is reproduced, which is similar to the learned pattern in the demonstration. Hence, the updated force skill can succeed in the novel doughs with soft hardness. In addition, the novel skills for soft dough can be put into the skill library as a new skill. This online correction and learning mechanism can expand the skill library built offline. This framework provides a solution to correct the robot's behaviour online through the developed interface, and the modified behaviour can be learned to update the skill library.

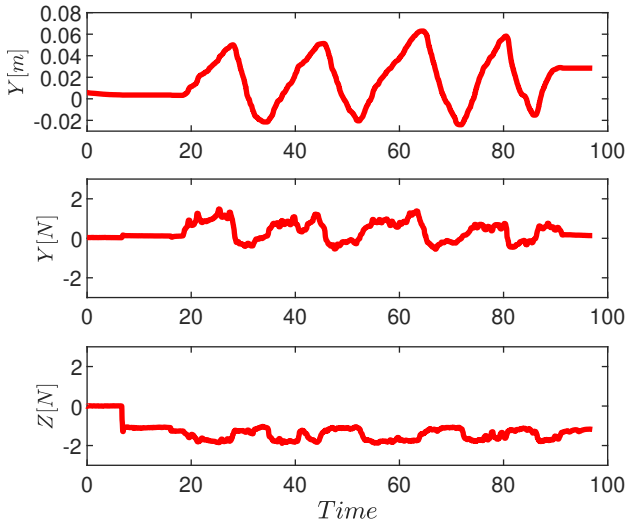

Figure 5.10: Success on the soft object. The trajectory along Y axis and the contact force along Y and Z axis. The contact force is reduced to roll on the soft dough.

5.5 Summary

In this chapter, we developed a bilateral teleoperation system that includes a haptic device, collaborative manipulators, and force sensors etc. This system can be used to transfer contact-rich skills from humans to robots in a remotely feasible manner. It can also provide a human interaction interface for the human operator to interact and correct the robot's behaviour on top of the autonomous commands. Manipulating deformable objects by robots such as dough and medical scanning is challenging, especially since the interaction process is hard to model in advance. These tasks often include dynamic skills learning, such as force and stiffness, as well as kinematic skills. Therefore force feedback is essential for these tasks. In addition, in some cases, humans cannot enter hazardous environments. The teleoperation-based human-robot skill transfer provides the solution to deal with this problem. We adopted rolling dough as a task to evaluate the performance of this solution, and the results show that the solution can deal with the uncertainty of the soft object.

In the beginning, the human could teach the robot to roll pizza dough through the shared control framework. To deal with the soft pizza dough, the human could correct the force command on top of the nominal skill output. And the correction profiles are used to update the pre-learned skill. The updated skills are put into the skill library. Compared with work (Hagenow et al., 2021), we exploited the correction behaviour and provided the skill updated mechanism based on the improved DMPs model. In addition, unlike the DRL method, the human-guided skill learning and updating approach is more efficient. Especially in some cases, it is not feasible to try and update the skill model, such as medical scanning. The human-in-the-loop mechanism involving the human ensures safety, and the human interaction will benefit the robot skill learning.

6 Perception enhanced contact-rich manipulation skills learning and generalising

6.1 Abstract

This chapter studied a vision-based reactive adaptation method for contact-rich manipulation tasks. For contact-rich tasks that involve deformable objects with unknown properties, such as pizza dough, compliant interaction is essential. However, the generalization capabilities of learning from demonstration (LfD) for such tasks remain challenging, particularly for unknown and dynamic tasks. Therefore, this chapter investigates the use of vision and force-based perception feedback to enhance the generalization of the LfD. To this end, a computer vision algorithm was developed to recognize the object's shape and calculate the deviation between the desired shape and the current shape. The deviation of shape adjusts the parameters of learned primitive skills encoded by dynamic movement primitives (DMPs). The proposed method's performance was evaluated by rolling the pizza dough as the typical case, wherein the shape and thickness of the dough can be made to the desired shape and thickness. The contributions of this chapter can be summarized as follows:

- Vision-based deformation-aware method was investigated for deformable object manipulation to achieve the target shape. Comparing our previous work (Si, Guan, and Wang, 2022), we investigated subgoal decision strategy based on shape recognition and deviation from the target shape.

- In addition, to manipulate the deformable dough, a compliant controller was designed to track the trajectories generated from LfD. We integrated the learning from demonstration and compliant control for deformable objects in a unified framework.

- We adopted pizza dough stretching tasks as an evaluation case on a real robot, and the pizza dough's shape and thickness are the evaluation criteria.

6.2 Introduction

Collaborative robots have attracted significant attention in both academic and industrial communities. Various cobots, such as the Baxter robot and Franka Emika Panda, have been employed in numerous fields, including manufacturing, medical examinations, and home service (Si, Wang, and Yang, 2021a). Despite their widespread use in industry, interacting with deformable objects such as textile cloth, soft and deformable food in the kitchen, and human tissue remains challenging (Matas, James, and Davison, 2018; Hu, Sun, and Pan, 2018; Si, Guan, and Wang, 2022). This difficulty arises due to the lack of an accurate model of the object and the unknown properties of the deformable objects. However, deformable objects, including cloth, fruits, and even human bodies, are ubiquitous in daily life, and interacting with such objects is commonplace (Racca et al., 2016). Therefore, robotic manipulation of deformable objects has gained substantial attention from both academic and industrial communities.

Deformable object modelling and control have been studied extensively in the literature, with a particular focus on pizza dough manipulation (Kim et al., 2022; Gutiérrez-Giles et al., 2019; Petit et al., 2017; Satici et al., 2016). Siciliano et al. provided a comprehensive investigation of pizza dough manipulation, encompassing perception, trajectory planning, and controller design for the deformable object (Kim et al., 2022). Specifically, they studied deformable object modeling and optimized trajectory

generation for real-time robot control. Robotic manipulation of pizza dough has attracted considerable attention due to its relevance in the food industry. Stretching dough with a rolling pin is a classic example of nonprehensile manipulation, involving manipulation without grasping, such as pushing, flipping, throwing, and squeezing[1]. This type of manipulation has also been studied in detail in the context of pizza dough (Kim et al., 2022).

Vision-based trajectory planning and control methods, such as visual servoing, have been well studied in the industry (Espiau, Chaumette, and Rives, 1992). However, pure vision-based planning and control method is hard to manipulate deformable objects autonomously. Due to the complex property of deformable objects, it is impossible to plan the trajectories of robots in complex tasks manually in advance. Visual and haptic information provides real-time feedback for online planning and decision-making of robots working on complex tasks under unknown conditions (Pairet et al., 2019). On the other hand, with developments in the field of machine learning, deep convolutional networks have better performance than traditional computer vision methods for visual recognition tasks. Some new neural network architectures, such as U-net (Oktay et al., 2018; Ronneberger, Fischer, and Brox, 2015), are capable of accurate segmentation of complex medical images, including cardiac MR segmentation (Oktay et al., 2018) and lung cancer nodule detection (Ronneberger, Fischer, and Brox, 2015), that can reach near radiologist level performance.

To tackle with the challenging issue of autonomous manipulation of deformable objects, we proposed a learning and adaptive framework for compliant manipulation of deformable objects, as shown in Fig. 6.1.

[1]Note that nonprehensile manipulation refers to manipulation without grasping, such as pushing, flipping, throwing, and squeezing.

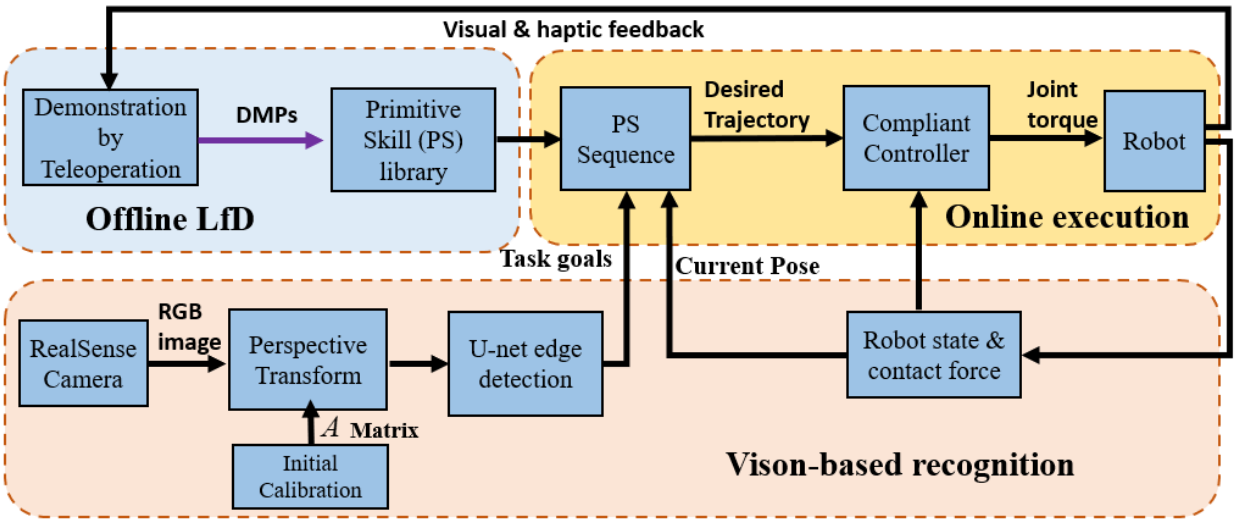

Figure 6.1: The overall structure of the proposed framework.

6.3 Framework of perception enhanced skills generalising

6.3.1 Vision-based deformation recognition

The vision-based recognition is to detect the outline of the dough on the table and to attain the position of the dough edge in the robot's base coordinate system. The camera calibration work is required to record the robot's working space in advance. As shown in Fig.6.2, four ArUco markers [2] are placed on the table at a certain distance from each other. The object needs to be placed within this area, and the dough also needs to stay in this workspace. With these markers, the camera's view plane (the camera's frame) can be mapped onto the table using a perspective transformation method. The camera frame can be used to obtain an image of the dough within the working area. Once the image is obtained, the dough can be distinguished from the background using U-net and the final positions of the dough edges can be obtained using canny edge detection.

[2] https://docs.opencv.org/4.x/d5/dae/tutorial$_{a}ruco_{d}etection.html$

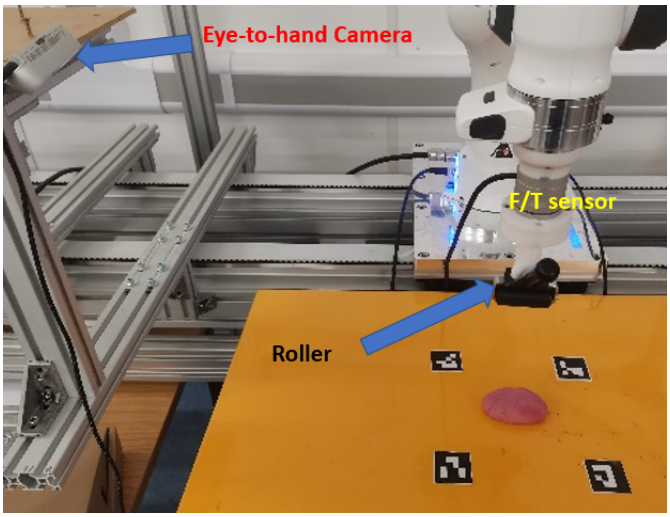

Figure 6.2: The setup of deformation-aware stretching a pizza dough with a rolling pin. RealSense camera and F/T sensor were used to capture the deformation of shape and the contact force. A customised roller was used to stretch the pizza dough.

Perspective transformation

Perspective transformation is the projection of an image onto a new viewing plane, also known as projective mapping (Mezirow, 1978). The transformation matrix required in the affine transformation of an image is a 2×3 two-dimensional plane transformation matrix, whereas the perspective transformation is essentially a three-dimensional transformation of space, where the three dimensional coordinates are projected onto a different viewing plane according to their sub-coordinate variance.

For a perspective transformation, it can be thought of as a projection from a point on a quadrilateral onto the target quadrilateral after a linear transformation, where the shape of the target quadrilateral is a known condition. A general formula for a perspective transformation is as follows (Hartley and

Zisserman, 2003),

$$\begin{bmatrix} X' \\ Y' \\ \omega' \end{bmatrix} = \begin{bmatrix} a_{11} & a_{12} & a_{13} \\ a_{21} & a_{22} & a_{23} \\ a_{31} & a_{32} & a_{33} \end{bmatrix} \begin{bmatrix} u \\ v \\ 1 \end{bmatrix} \tag{6.1}$$

$$\omega' = a_{31}u + a_{32}v + a_{33} \tag{6.2}$$

$$A = \begin{bmatrix} a_{11} & a_{12} & a_{13} \\ a_{21} & a_{22} & a_{23} \\ a_{31} & a_{32} & a_{33} \end{bmatrix} \tag{6.3}$$

where u and v are the pixels of the original image. X', Y' and ω' are the temp coordinates in transformation space; New coordinates x, y after transformation by perspective are $x = \frac{X'}{\omega'}$ and $y = \frac{Y'}{\omega'}$.

The above equation shows that the coordinates under the new view plane can be expressed as (Hartley and Zisserman, 2003):

$$x = \frac{X'}{\omega'} = \frac{a_{11}u + a_{12}v + a_{13}}{a_{31}u + a_{32}v + a_{33}} = \frac{k_1u + k_2v + k_3}{k_7u + k_8v + 1} \tag{6.4}$$

$$y = \frac{Y'}{\omega'} = \frac{a_{21}u + a_{22}v + a_{23}}{a_{31}u + a_{32}v + a_{33}} = \frac{k_4u + k_5v + k_6}{k_7u + k_8v + 1} \tag{6.5}$$

To solve for the eight unknown factors in Matrix A, it requires eight sets of equations. Four known coordinate points are the pixel positions read from ArUco markers in the original image and four coordinate points of the target image are set to $(0,0),(0,500),(500,500),(500,0)$. This is due to the fact that the corresponding work area captured by the camera is a $12.5 * 12.5cm$ square on the table plane, which corresponds to $1/500 * 12.5cm$ per pixel on the image. The transformation matrix A is calculated for each pixel point in the original image. The new image is projected to give a top view of the dough on the table.

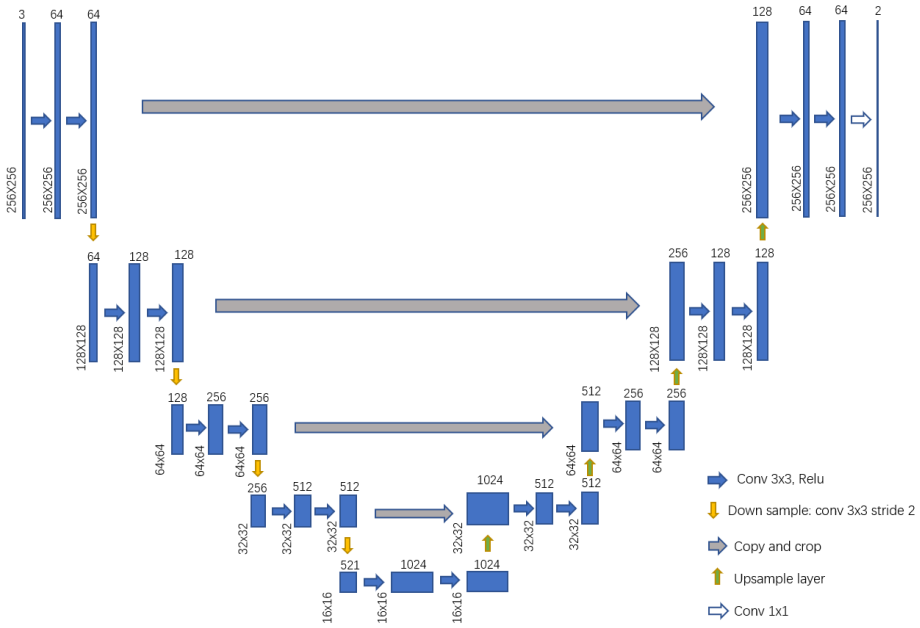

Figure 6.3: U-net architecture. Each blue box corresponds to a multi-channel feature map. The number of channels is indicated at the top of the box. The dimensions of the feature map are in the lower left corner of the blue box. The arrows indicate the different operations.

Image segmentation

Once the perspective-transformed image is obtained, the exact position of the dough needs to be obtained from the image. A deep learning approach with higher accuracy was chosen over traditional vision algorithms. The architecture of the U-net is shown in Fig.6.3, which was used to segment the background from the dough in this work. It consists of a systolic path (left side) and an extended path (right side). The systolic path follows the typical structure of a convolutional network like VGG19. It consists of two 3×3 convolution (padded convolutions) layers, and each layer is followed by a rectified linear unit (ReLU) and a 3x3 convolution layer with stride 2 for downsampling. At each downsampling step, we keep the number of feature channels. Each step in the expansion path includes an upsampling of the feature map, followed by a 2×2 convolution ("up-convolution") that halves the number of fea-

ture channels, concatenates with the correspondingly cropped feature map in the contraction path, and performs two 3×3 convolutions, each followed by a ReLU. In the final layer, a 1×1 convolution is used to map each 64-component feature vector to the desired number of categories. 1×1 convolution classifies each pixel in the image thereby distinguishing the dough from the background. The output of the network is shown in Fig.6.6 (c) and (f).

The network is trained by a stochastic gradient descent using the input photos and their accompanying segmentation maps. Before being fed into the network, the input pictures and segmentation maps are downsized to 256×256 to match the network's input. By performing canny edge detection on the generated dough mask image, the positions corresponding to edge pixels are transformed into positions in the robot coordinate system, thus completing the recognition of dough contours.

6.3.2 Primitive skills modelling

Dynamic movement primitives

We model the primitive skills by position and orientation in a unified formulation in Cartesian space,

$$\tau \dot{z} = \alpha_z(\beta_z(g^p - p) - z) + f_p(x) \tag{6.6}$$

$$\tau \dot{p} = z \tag{6.7}$$

$$\tau \dot{x} = -\alpha x \tag{6.8}$$

where g^p and p are target position and current position respectively, z is the velocity of dynamic system, β_z and α_z are designed parameters. $f_p(x)$ is the nonlinear term, which is used to modify the behaviour of the second-order system. The definition of $f_p(x)$ will be given later and the weight of this term can be learned through human demonstration data. The evolution of the dynamic system is determined by the canonical system, Eq.6.8, where the τ can tune the duration of the dynamic system, and the α is a

positive parameter. The canonical system is shared by the position and orientation dynamic system to coordinate the translation and rotation simultaneously.

The orientation skill can also be encoded by the DMPs, however, the skill model is adopted by the quaternion-based form (Ude et al., 2014). In our previous work, we encoded the translation and orientation simultaneously by DMPs (Si, Wang, and Yang, 2021b). The details of the model can refer(Si, Wang, and Yang, 2021b), we define the model here to facilitate understanding,

$$\tau\dot{\eta} = \alpha_z(\beta_z 2\log(g^o * \bar{q}) - \eta) + f_o(x) \tag{6.9}$$

$$\tau\dot{q} = \frac{1}{2}\eta * q \tag{6.10}$$

where η is the angular velocity, g^o and q are the target angle and current angle encoded by quaternion, respectively. $\bar{q}$ represents the quaternion conjugation, and $*$ denotes the quaternino product, details can refer to (Ude et al., 2014). β_z and α_z are designed parameters, which can be consistent with the position DMPs, $f_o(x)$ is the nonlinear term, which is used to modify the behaviour of the second-order system.

The nonlinear force term is used to define the transient behavior of the dynamic system. This term usually consists of a set of nonlinear basis function (RBFs), which can be given by,

$$f_p = \frac{\sum_{k=1}^{N} w_k^p \Phi_k(x)}{\sum_{k=1}^{N} \Phi_k(x)} x \tag{6.11}$$

$$f_o = \frac{\sum_{k=1}^{N} w_k^o \Phi_k(x)}{\sum_{k=1}^{N} \Phi_k(x)} x \tag{6.12}$$

$$\Phi_k(x) = \exp(-h_k(x-c_k)^2) \tag{6.13}$$

where N is the number of the RBFs, and the x is the phase variable determined by the canonical system. w_k^p and w_k^o are the weights of the i^{th} RBFs, $i \in [1,N]$ and h_k and c_k are the centres and widths of the RBFs, respectively.

We generate the complex trajectory by merging the individual primitive skill (PS), encoded by DMPs for the complex and contact-rich task with multiple-step, as shown in Algorithm 1. The multiple primitive skill are encoded by behavior tree (Saveriano and Piater, 2020), the DMP-based primitive skill was modelled as execution nodes. The target position and orientation of each primitive skills are calculated by shape recognition and desired shape and thickness. In this work, we only consider circular desired shape, four position and four orientation skills are needed. The four primitive skills are approaching, rolling forward, rolling back and back origin. For the circular shape, the primitive skill library with four primitive skills can generate trajectory for the roller. However, the vision-based trajectory generation algorithm can also be employed to different shapes. Different shape only needs to modify the control flow nodes in behavior tree.

Algorithm 1 Vision-based Trajectory Generation

while (!achieve desired shape and thickness) **do**
  starting point P_{st}, direction dir = vision feedback()
  while (current position != end point) **do**
    PS1.run(current position, P_{st}), PS2.run(current direction, dir)
  end while
  while (current position != end point) **do**
    PS3.run(current position, P_{st}), PS4.run(current direction, dir)
  end while
  while (current position != end point) **do**
    PS5.run(current position, P_{st}), PS6.run(current direction, dir)
  end while
  while (current position != end point) **do**
    PS7.run(current position, P_{st}), PS8.run(current direction, dir)
  end while
end while

6.3.3 Compliant control

In terms of the compliant control system, we used the controller designed in Chapter 3. The impedance controller is designed in Cartesian space, which is suitable for skill reproduction and generalisation.

6.4 Experiments of pizza dough rolling

We carry out pizza dough stretching with a rolling pin to evaluate the performance of the proposed framework on a 7 DoFs cobot. A RGBD camera was used to capture the deformation of the object and a computer vision algorithm was used to calculate the difference between the real shape and the desired shape. A customised roller was used to stretch the pizza dough [3]. The setup of the experiment can be seen in Fig. 6.2. We defined evaluation metrics for dough rolling, as shown in Fig. 6.4. The red outline is the desired shape, and we defined two axes (the yellow lines) to judge whether the desired shape is achieved. During the dough rolling, we adjust the orientation of the roller based on the error along these two axes.

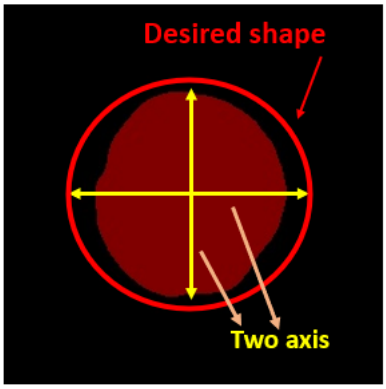

Figure 6.4: The evaluated metric of dough rolling. The red outline is the desired shape, and we defined two axes (the yellow lines) to judge whether the desired shape is achieved. During the dough rolling, we adjust the orientation of the roller based on the error along these two axes.

[3]Note the pizza dough is not as large as the real pizza dough, because the roller is not large enough. The proposed method can be employed for big dough if we adopt a large roller.

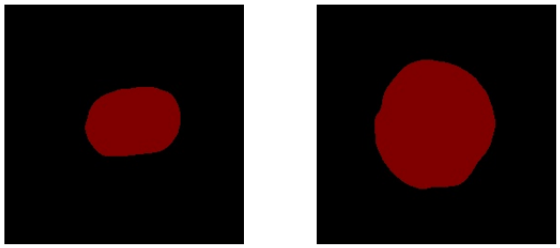

Figure 6.5: The result of deformation recognisation and segmentation. The left one is the original shape of dough, and the right one is the final shape of dough.

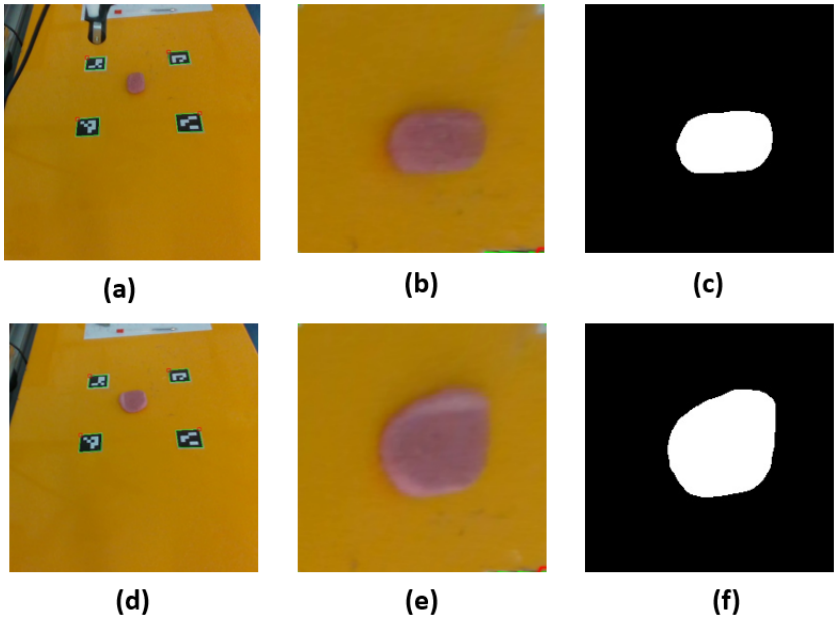

Figure 6.6: Snapshot of dough stretching. (a)-(c) are the initial shape of the dough. (d)-(f) are the shape after stretching. (a) is the original image from camera. (b) is the middle image after neural networks processing. (c) is the segmentation of the dough. The machine vision algorithm can detect and calculate the deformation of dough in real time.

6.4.1 The result of deformation segmentation

As shown in Figs. 6.5 and 6.6, the changing of the shape of the dough is shown during the rolling process. We test the image recognition and segmentation accuracy by U-net. We collected 20 real

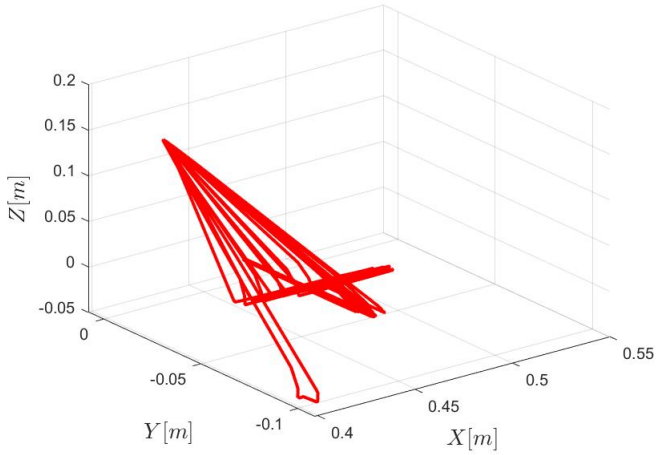

Figure 6.7: The trajectory in 3D dimention.

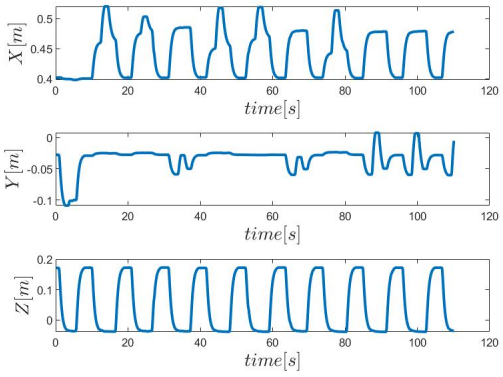

Figure 6.8: The position trajectory along X,Y and Z.

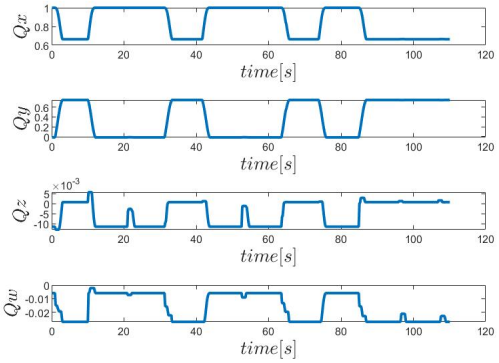

Figure 6.9: The orientation trajectory represented by quaternion.

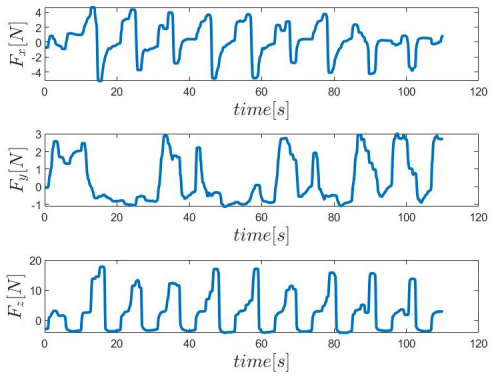

Figure 6.10: The contact force along X,Y and Z.

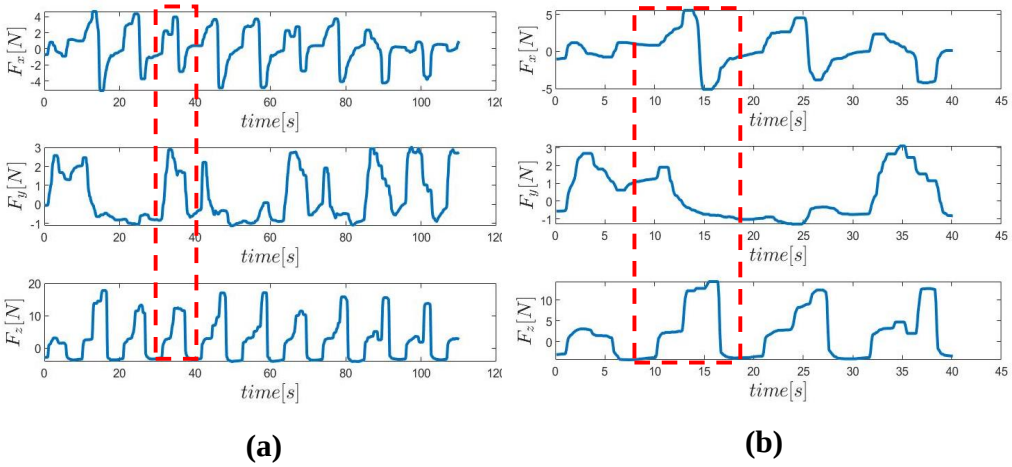

Figure 6.11: (a) the contact force during rolling dough by robot, (b) the contact force during rolling dough by human beings. The red box shows the force change in one cycle. The contact force regulation by robot (a) conforms to the pattern of human operation during demonstration (b).

images during the dough rolling, and humans labelled the real outline of the dough. The segmentation error is less than 1% pixel, meaning that the dough is accurately segmented from the image by the model.

6.4.2 The position, orientation and contact force

Fig. 6.7 is the trajectories in 3D during the rolling. The robot approaches the dough and then rolls the dough based on the visual feedback to adjust the start point and rolling orientation. The rolling process is iteractively changing until the desired shape is achieved.

In Fig. 6.8, position trajectories along X,Y, and Z during the rolling is presented. The robot's range of motion in the X-Y direction changes as the dough is deforming and stretching.

Fig. 6.9 is the orientation trajectories along X,Y, and Z during the rolling. In this experiment, we can see the robot keep changing between two directions, which are based on the direction of movement of the dough stretched in different axes. Fig. 6.10 shows the contact force along X,Y, and Z during the rolling. Due to the complex and unknown properties of the dough, the change of contact force along X-Y-Z is complex in a period. Therefore, it is hard to control the contact force accurately. LfD through bilateral teleoperation provides a promising approach to transferring the contact-rich skill from humans to robots.

We compare the contact force pattern. The red box, in Fig.6.11, shows the force change in one rolling cycle. We found the force change in one cycle by the robot is similar to the force change by our human demonstration, which means that the robot has learned the human-like rolling skills. In addition, as shown in Table 6.1, the error in X is less than 2.3 mm, and the error in Y is less than 2.1mm. The ratio of X length to Y length is 0.98, and the area ratio is 0.94, which means that the final shape is close to a circle.

Table 6.1: Performance evaluation - shape similarity

	X error	Y error	X/Y	Actual/Desired area
Value	2.3mm	2.1mm	0.98	0.94

Table 6.2: Flatness quality performance.

Category	**Variance of height**
Human teleoperation	$3mm \pm 0.3mm$
Robot autonomous	$3.3mm \pm 0.2mm$

6.4.3 The result of thickness

The thickness of the final dough is one metric for dough rolling by robots. We adopt the hybrid force/ position controller to detect the height of the final dough. The F_z along the Z-axis is controlled to 0, and the X-Y motion trajectory is controlled by teleoperation. The height along the Z-axis was recorded, and the variance of thickness can be measured.

We compare the performance of human rolling by teleoperation and autonomous rolling by the robot, and the results are shown in Table 6.2.

6.5 Summary

In this chapter, we investigated a deformation-aware method for the manipulation of deformable objects. The perspective transformation and U-net method were used to recognise the object and segment the object from the background. Based on the target shape and size of the object, we calculate the desired task variables (desired position and orientation). The realtime trajectory was generated from the learned skill based on human demonstration. And compliant controller was designed to track the desired trajectory. Finally, we evaluate the shape of the final dough by calculating the error along the two axes of the dough. And the variance of the dough in the Z axis reflects the thickness quality. The result shows that the shape error is bellow 5% and the variance of the thickness is 0.3mm.

7 Manufacturing application: composite layup skill learning and generalising

7.1 Abstract

In this chapter, an impedance control-based robot-assisted composite layup system was developed, and the teleoperation was investigated to achieve human-robot collaboration and human-robot skill transfer. We developed an impedance control based architecture of telemanipulation in task space for the human demonstration. This framework not only achieves human-robot skill transfer but also provides a solution to human-robot collaboration through teleoperation. The impedance control system enables the compliant interaction between the robot and the environment and a smooth transition between different stages. Dynamic movement primitives based learning from demonstration is employed to model the human manipulation skills, and the learnt skill can be generalised to different tasks and environments, including the different shapes of components and different orientations of components. The performance of the proposed approach is evaluated on a 7 DoF Franka Panda through the robot-assisted composite layup on different shapes and orientations of the components. The main contributions of this work can be summarised as follows:

- We developed a human-robot skill transfer system for composite layup tasks, which consists of a 3D mouse device as the teleoperation interface, a 7 DoF Franka Emika robot manipulator, and a Realsense camera for visual feedback.

- Dynamic movement primitives (DMPs) were used to model the primitive motion skills as high-level "bricks" of the complex task. A complex task is parameterised into several motion primitives represented by the parameters of primitive motion skill; hence combining and re-organising the motion primitives can generate a complex trajectory, which allows generalising the learnt skill to new tasks and environments.

- The human-robot skill transfer based on the proposed system provides a solution for robot skill learning through teleoperation or human-robot collaboration. The proposed method is more suitable for human-robot skill transfer in hazardous environments or situations that humans cannot access, such as nuclear waste disposal, or lockdown during the pandemic.

7.2 Introduction

Collaborative robots have been increasingly important in manufacturing, such as assembly, robot-assisted polishing and drilling etc. Especially for flexible manufacturing, small-batch and variance among the components put forward new requirements for traditional industrial robots in the smart factory. The main challenge is the flexibility of the manufacturing system, which allows the system to react to the changes of the new products. The human-robot skill transfer has proved a potential solution for flexible manufacturing systems (Ochoa and Cortesao, 2021; Yang, Zeng, and Zhang, 2021). To realize lightweight structures with high performance, composites have been widely used in several industries, such as aerospace, automotive and construction etc. Carbon fiber is the main raw material of composite material production. Currently, for low-volume production and complex parts, a hand layup is still the main method, which laminates plies of carbon fiber prepreg (Malhan et al., 2021). The hand layup process is ergonomically challenging and skill-intensive. Human operators must apply various

levels of pressure to the plies. In addition, sometimes several people need to collaborate to conform larger plies to complex contours. However, the hand layup process is labor-intensive and can exhibit inconsistency due to variability in human operation. Sheet layup automation can reduce ergonomic challenges, increase production efficiency and ensure processing quality (Malhan et al., 2020).

Currently, industrial robots have been widely used in manufacturing, however, robots are expected to perform more challenging tasks, such as composite layup. These tasks often feature contact-rich manipulation and significant uncertainty of the different tasks, such as variance among the products in flexible manufacturing. Although our human beings do not understand the principle behind manipulation, humans have the amazing capability to deal with the uncertainty and complexity in these tasks (Zeng et al., 2021). Therefore, roboticists proposed to make the robot learn manipulation skills from humans. One of the main problems is how to learn complex and human-like manipulation skills. This work aims to develop a human-robot skill transfer system based teleoperation, and propose an approach to transfer human skills to robots. Fig.7.1. illustrates the composite layup process through teleoperation and human-robot collaboration. A camera in Figure (A) provides visual feedback for the human operator sitting in Figure (B), who can teleoperate the robot manipulator to execute composite layup based on the visual feedback. Figure (B) presents the teleoperation scenario, in which the human operator commands the robot based on the visual feedback and the teleoperated device. The two people can collaborate to perform the composite layup as well as transfer the composite layup skills to the robot manipulator. It is challenging to transfer the manipulation skill to robots through teleoperation efficiently and intuitively (Si, Wang, and Yang, 2021a).

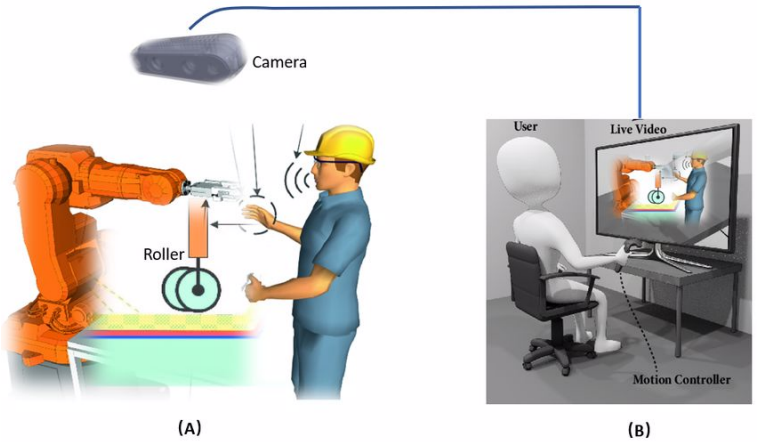

Figure 7.1: The figure (A) shows a robot-assisted composite layup, and an in-site assisted person can collaborate with the robot and a demonstration expert in figure (B).

7.3 Preliminary

7.3.1 Robot dynamics

The general form of dynamics of the n-DOF serial manipulator robot can be modelled as (Santos and Cortesão, 2018),

$$D(q)\ddot{q} + C(q,\dot{q})\dot{q} + G(q) + \tau^{ext} = \tau_c \tag{7.1}$$

where the $D(q) \in R^{n\times n}$ is the inertia matrix, the $C(q,\dot{q}) \in R^{n\times n}$ and $G(q) \in R^{n\times 1}$ represent the Coriolis and centrifugal respectively. $q \in R^{n\times 1}$ and $\dot{q} \in R^{n\times 1}$ are the joint position and velocity in the joint space, respectively. $\tau_c \in R^{n\times 1}$ is the actuator torque and $\tau^{ext} \in R^{n\times 1}$ represents torque generated by the end-effector interacting with environments.

$$\tau_c = \tau^{ext} + C(q,\dot{q})\dot{q} + G(q) + \tau_{cmp} \tag{7.2}$$

Based on Eqs.7.1 and 7.2, the designed control variable can be described as the following,

$$\tau_{cmp} = D(q)\ddot{q} \tag{7.3}$$

where τ_{cmp} represent a new control variable in the joint space. In order to facilitate the following analysis, we design the controller in Cartesian space; hence, the Eq.7.3 is rewritten in Cartesian space as the following,

$$m_p(q)\ddot{x}_p - m_p(q)\dot{J}(q)\dot{q} = f_{tol} \tag{7.4}$$

$$m_p(q) = (J(q)D^{-1}(q)J^T(q))^{-1} \tag{7.5}$$

where $m_p(q)$ represent the inertial matrix in Cartesian space, f_{tol} is the control force in Cartesian space, and $J(q) \in R^{m\times n}$ is the Jacobian matrix. The task space velocity can be described as,

$$\dot{x}_p = J(q)\dot{q} \tag{7.6}$$

The $\dot{x}_p$ is the velocity in Cartesian space. And the control torque τ_{cmp} can be described as,

$$\tau_{cmp} = J^T(q)f_{tol} \tag{7.7}$$

7.3.2 Null-space optimisation

For the redundant manipulator, the null space can be used to execute second priority tasks, such as obstacle avoidance, tracking orientation, and pose optimisation. The property of the null space has a lot of benefits, such as the control torque will not influence the main task. In this work, we optimise the robot pose to keep the joint close to the middle of the range of the joint. The total torque employed in the joint can be described as,

$$\tau_{cmp} = \tau_m + \tau_{null} \tag{7.8}$$

where τ_{null} is the optimization torque in the null space, and τ_m is the torque for the main task. The τ_{null} can be represented as,

$$\tau_{null} = N_{pro}^T(q)\tau_n \tag{7.9}$$

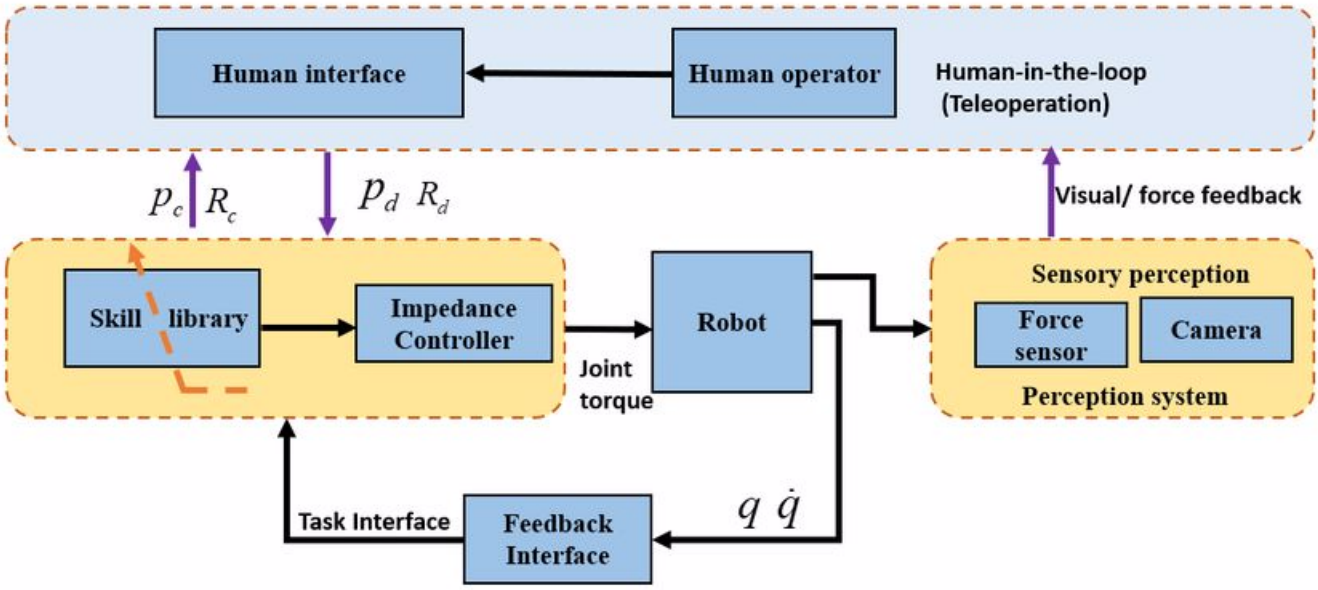

Figure 7.2: The diagram of the proposed framework for human-robot skill transfer through human-in-the-loop. The human-in-the-loop module is the teleoperation based subsystem, which could command the robot through the teleoperation interface, a 3D mouse, and receive visual and force feedback from the perception subsystem. The impedance controller can generate joint torque command for the robot either through the teleoperation or autonomous mode (through skill library) .

where τ_n represents the optimisation torque, and $N^T_{pro}(q)$ is the null space projector. Because the τ_{null} is executed in the null-space, the optimisation task will not affect the main task. The null space projector $N^T_{pro}(q)$ can be described as,

$$N^T_{pro}(q) = [I - J^T(q)J^+(q)^T] \tag{7.10}$$

where I is a identity matrix, and the $J^+(q)$ is the inverse of $J(q)$, which can be described as,

$$J^+(q) = D^{-1}(q)J^T(q)m_p(q) \tag{7.11}$$

where $m_p(q)$ represent the inertial matrix in Cartesian space, $J(q)$ is the Jacobian matrix. $D(q)$ is the inertia matrix. The optimisation torque can be computed as,

$$\tau_n = D(q)K_o\frac{\partial Q(q)}{\partial q} \tag{7.12}$$

K_o is a gain matrix, which needs to be designed based on the requirement on the pose optimization and main tasks. $Q(q)$ is the cost function, which tries to control the joint as close as the middle of the joint angle range.

$$Q(q) = -\frac{1}{2}\sum_{i=1}^{n}\left(\frac{q_i - q_{id}}{q_{imax} - q_{imin}}\right)^2 \tag{7.13}$$

where q_i is the current angle of i^{th} joint, q_{id} is the middle angle of ith joint. q_{imax} and q_{imin} are the maximum and the minimum angle of i^{th} joint.

7.3.3 Dynamic movement primitives (DMPs)

As introduced in Chapter 3, the DMP is an effective model for encoding translation and orientation skills via a second-order dynamical system with a nonlinear forcing term. To improve readability, we present the DMP in brief. The core idea of robot skills based on DMPs is to model the forcing term in such a way allowing to generalise the learned skills to a new start and goal position while maintaining the shape of the learnt trajectory. DMPs can be used to represent arbitrary movements for robots in Cartesian or joint space by adding a nonlinear term to adjust the shape of the trajectory. For one degree of multiple dimensional dynamical systems, the transformation system of position DMP can be modelled as follows (Ijspeert et al., 2013),

$$\tau_s\dot{v} = \alpha_z(\beta_z(p_g - p) - v) + F_p(x) \tag{7.14}$$

$$\tau_s\dot{p} = v \tag{7.15}$$

where the p_g is the desired position, p is the current position; the v is the scaled velocity, τ_s is the temporal scaling parameter, which can be used to modify the velocity. α_z, β_z are the design parameters, generally, $\alpha_z = 4\beta_z$. $F_p(x)$ is the nonlinear forcing term responsible for tuning the shape of the trajectory. The $F_p(x)$ can be approximated by a set of radial basic functions,

$$F_p(x) = \frac{\sum_{i=1}^{N} \psi_i(x) w_i}{\sum_{i=1}^{N} \psi_i(x)} x(p_g - p_0) \tag{7.16}$$

$$\psi_i(x) = \exp(-h_i(x - c_i)^2) \tag{7.17}$$

where $\psi_i(x)$ is a Gaussian radial basis function with the centre c_i and width h_i; p_0 is the initial position, w_i is the weight learning from demonstration. The phase variable x is determined by the canonical system, which can be represented as follows,

$$\tau_s \dot{x} = -\alpha_x x, \quad x \in [0,1]; \quad x(0) = 1 \tag{7.18}$$

where α_x is a positive gain coefficient, τ_s is the temporal scaling parameter, and the $x_0 = 1$ is the initial value of x, which can converge to zero exponentially. For the multiple DoFs dynamic system, each dimension can be modelled by a transformation system, but they share a common canonical system to synchronise them.

7.4 Control system design

7.4.1 Task-space formulation

This section derives the controller in Cartesian space, and the whole control structure can be found in Fig.7.3. It will be convenient to design the controller in the task space because the teleoperation control

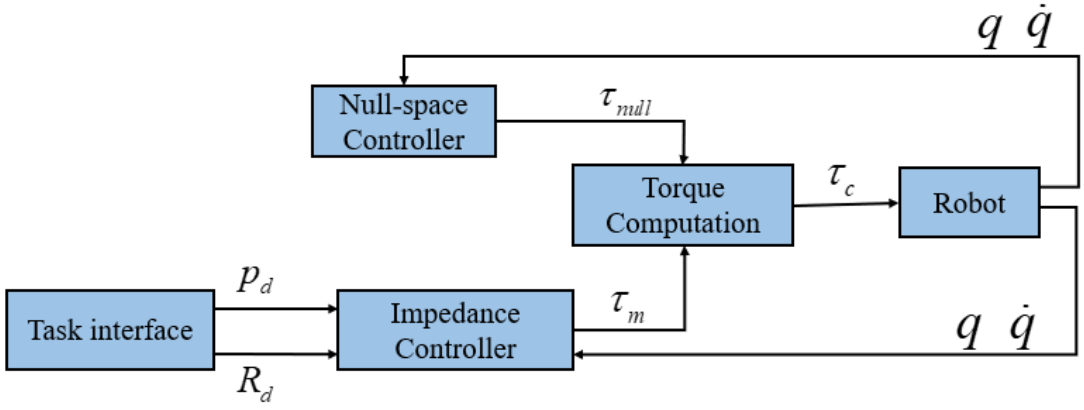

Figure 7.3: The diagram of the impedance-based control system. The task interface module generates the desired position and orientation through teleoperation or learned skill model. The impedance controller is used to track the desired position and orientation. The null-space controller is used to optimise the joint pose by using redundancy to keep the joint angle close to the middle value.

would be intuitive and straightforward in the task space. For the human-robot collaboration task, the safety of the human is significant; hence, compliant control has been employed for the collaborative robots. In 1985, impedance control was first proposed by Hogan (Hogan, 1985), and since then, a lot of exciting work has been done. A number of work on the impedance control was done for the manipulator control. The core idea of impedance control models the dynamic behaviour of robots under disturbance from the environment. In (Ochoa and Cortesao, 2021), the authors proposed a similar impedance controller for the polishing task. The impedance controller can be described as the following,

$$f_{imp} = A\ddot{x}_p + D(\dot{x}_p - \dot{x}_d) + K(x_p - x_d) \tag{7.19}$$

where A is the mass matrix, D is the damping matrix and K is the stiffness matrix. x_d represents the equilibrium point and x_p is the current position of robot end-effector. f_{imp} is the interaction force between the robot end-effector and the environment. For the dynamic equation of the manipulator in

the task space, the total force f_{tol}, exerting on the robot, can be calculated as follows:

$$f_{tol} = f_c + f_{imp} \tag{7.20}$$

We define a new control variable f^*_{tol} , and the f_c is represented as follows,

$$f_c = -m_p(q)\dot{J}(q)\dot{q} + f^*_{tol} \tag{7.21}$$

The Eq.7.4 can be represented as follows,

$$m_p(q)\ddot{x}_p = f^*_{tol} + f_{imp} \tag{7.22}$$

Therefore, the control law of f^*_{tol} is,

$$f^*_{tol} = m_p(q)\ddot{x}_p - [A\ddot{x}_p + D(\dot{x}_p - \dot{x}_d) + K(x_p - x_d)] \tag{7.23}$$

The mass matrix is approximated by (Ochoa and Cortesao, 2021),

$$A = m_p(q) = (J(q)D^{-1}(q)J^T(q))^{-1} \tag{7.24}$$

So, the control law becomes,

$$f^*_{tol} = D(\dot{x}_d - \dot{x}_p) + K(x_d - x_p) \tag{7.25}$$

The joint torque for the main task can be given by,

$$\tau_m = J^T(q)f_{tol} = J^T(-m_p(q)\dot{J}(q)\dot{q} + f^*_{tol}) \tag{7.26}$$

Because the $\dot{J}(q)$ has small influence to the system, the $-m_p(q)\dot{J}(q)\dot{q}$ can be ignored. Therefore, the control law for the main task in the Cartesian space can be written as follows,

$$\tau_m = J^T f^*_{tol} \tag{7.27}$$

where f^*_{tol} can be rewritten as,

$$f^*_{tol} = \begin{bmatrix} f \\ u \end{bmatrix} \tag{7.28}$$

where f is the force vector for translation control in Cartesian space, and the u is the torque vector for orientation control. The translation controller in discrete form can be described as the following,

$$f = -D_p \dot{p}_c + K_p(p_d[t] - p_c[t]) + I_p(i_p[t-1] + (p_d[t] - p_c[t])) \tag{7.29}$$

where D_p is the damping matrix, K_p is the stiffness matrix, and I_p is the integral matrix. $i_p[t-1]$ is the integral error in the position at time $[t-1]$. $p_d[t]$ and $p_c[t]$ are the desired position and current position at time t, respectively. Similarly, the orientation controller in discrete form can be represented as,

$$u = -D_o w_c + K_o \Delta o_{cd} + I_o i_o \tag{7.30}$$

where D_o is the damping matrix, K_o is the stiffness matrix and I_o is the integral matrix. w_c is the angular velocity, Δo_{cd} is the orientation error, and i_o is the integral error in orientation. Finally, based on the Eqs.7.2, 7.8 and 7.28, the total torque command can be described as the following,

$$\tau_c = J^T f^*_{tol} + \tau^{ext} + N^T_{pro}(q)\tau_{null} + C(q,\dot{q})\dot{q} + G(q) \tag{7.31}$$

7.4.2 Task interface design

The desired trajectories, including the translation and orientation, are generated from the input device based on displacement commands in the teleoperation mode. The human operator is provided with a graphical user interface (GUI) and a 3D mouse to monitor and control the system. The 3D mouse has two buttons and a six-DoF motion sensor. The two buttons are used to switch control modes, such as teleoperation, autonomous, and collaboration. The six-DoF motion axis of the 3D mouse is employed to generate the reference trajectory for the impedance controller in Cartesian space.

$$\Delta Z = \begin{bmatrix} \Delta P & \Delta R \end{bmatrix}^T \tag{7.32}$$

where ΔP and ΔR represent the translational and rotational displacements, respectively. ΔZ is then converted to the desired motion in the robot's base frame.

In the autonomous mode, the desired trajectory in the robot's base frame, including the translation and orientation, is generated based on the learned DMPs.

$$Z_d = \begin{bmatrix} P_d & R_d \end{bmatrix}^T \tag{7.33}$$

where P_d and R_d represent the desired trajectory in translational and rotational directions, respectively. Z_d is then converted to the desired motion in the robot's base frame.

7.5 Experiment on real robot

This section aims at evaluating the proposed solution, human-robot skill transfer through teleoperation, by performing composite layup for different components.

7.5.1 The setup of robot-assisted layup

The cobot, Franka Emika Panda, was used to conduct experiments, as shown in Fig.7.4 . An external force/torque sensor is equipped in the wrist to sense the interaction force and torque between the end-effector tool and the environment. We designed the fixtures by 3D printing to connect the layup tool (roller), force/torque sensor and the robot end-effector. A RealSense depth camera D435 is used to observe the working scenario of the robot, and the visual feedback is transmitted to the computer on the leader side for the human operator to monitor the remote scenario.

A 3D mouse from 3DConnexion company is more suitable for teleoperation, which can output linear and angular component of the joystick's position, and its button states as well. The twist command of the 3D mouse, consisting of the linear and angular components, is used to map the translation and orientation of the end-effector. The buttons states as an event-trigger signal were employed to switch control modes. There is a control interface of the robot manipulator provided by the Franka control

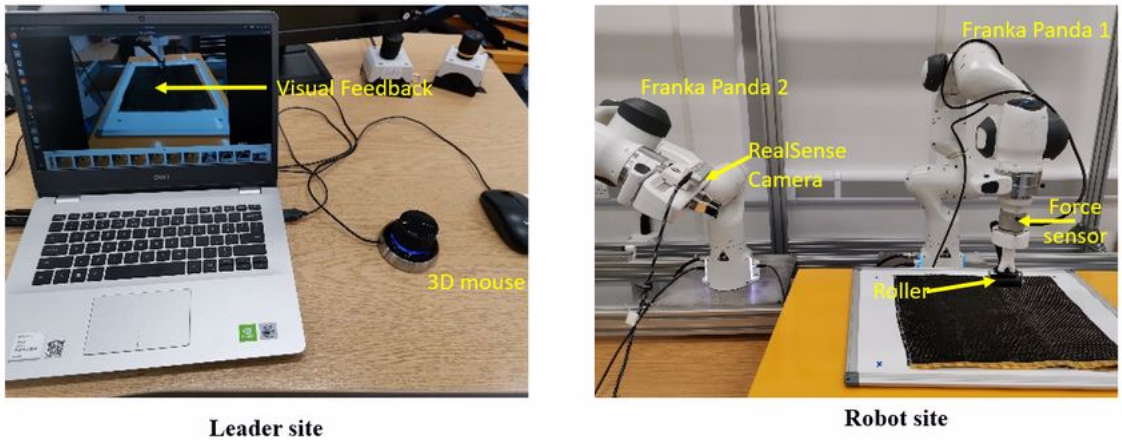

Figure 7.4: The experiment setup for composite layup. In the leader site, the human operators teleoperate the robot to perform the composite layup.

interface (FCI) on the robot side, which provides the control interface and a fast and direct low-level bidirectional connection to the robot arm. In the leader side, there is a computer performing the control and learning algorithm. The generated command is transferred to the Franka control board. Linux Operating system is run on the computer, and Robot Operating System (ROS) is used to communicate among the different modules.

7.5.2 User interface of the control system

As shown in Fig.7.5, the control system parameters can be displayed and modified by the human operators online. The human operators can change the control modes (switching between teleoperation mode and collaboration mode) via adjusting these parameters, including stiffness K_p and K_o, damping D_p and D_o, integral I_p and I_o, and the null-space optimization gain matrix K_n. These parameters can be modified online based on the different task requirements, such as more stiff in one DoF or more compliant in another DoF. The interaction force/torque between the end-effector and the environment can also be displayed on a monitor, which provides more knowledge on the interaction process.

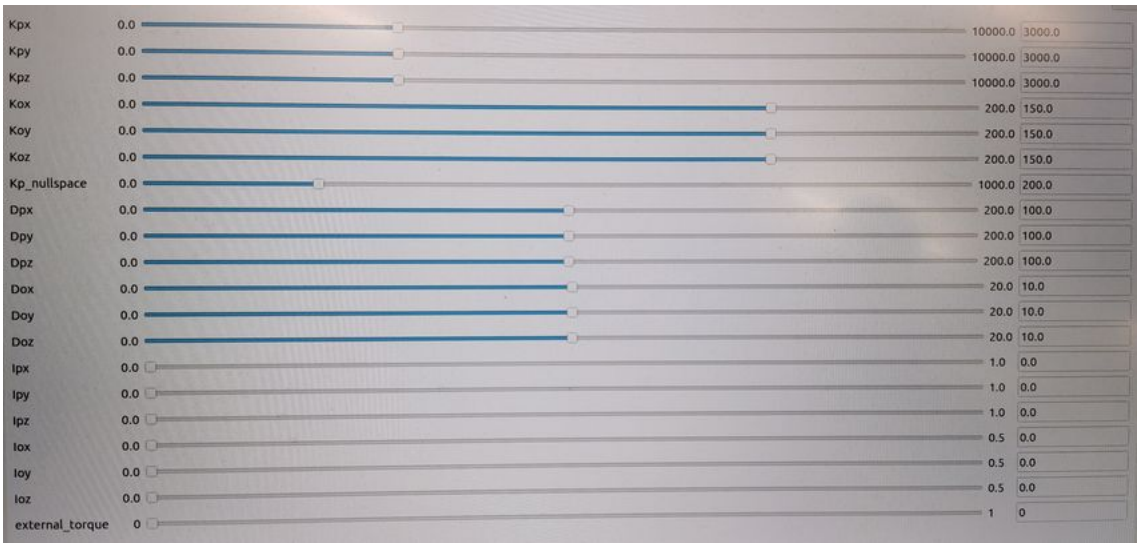

Figure 7.5: The GUI for the control system. The human operator can modify the parameters of the controller online to adjust the compliant behaviour, such as the stiffness and damping of the impedance controller etc.

In terms of the controller design and the human-robot skill transfer, defining the proper coordinate frame is necessary. The proper frame could reduce the cognitive workload during the teleoperation and human-in-the-loop interaction and collaboration. In this work, we defined three frames on the robot sides, as shown in Fig.7.6. The impedance controller is defined in the cartesian space, and the desired command is based on the based frame of the robot. The task description is based on the component frame, and the transformation from the based frame of the robot to component frame is fixed. The impedance gain defined by the user is based on the end-effector frame, therefore, the parameters of the controller need to be transformed into the based frame.

7.5.3 Human demonstration through teleoperation

To enable the human-robot composite layup skill transfer, the human operator needs to composite layup through teleoperation. The motion primitives of composite layup were recorded, as shown in Fig.7.7.

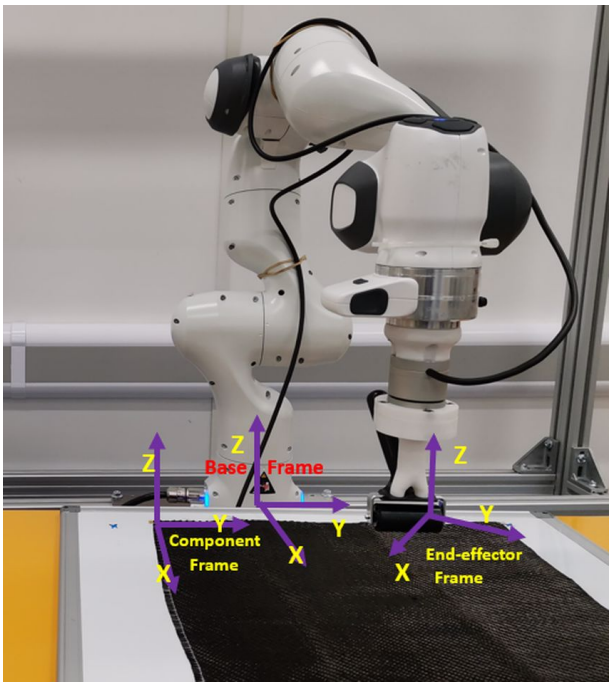

Figure 7.6: The three coordinate frames: the base frame of the robot, the end-effector frame and the component frame.

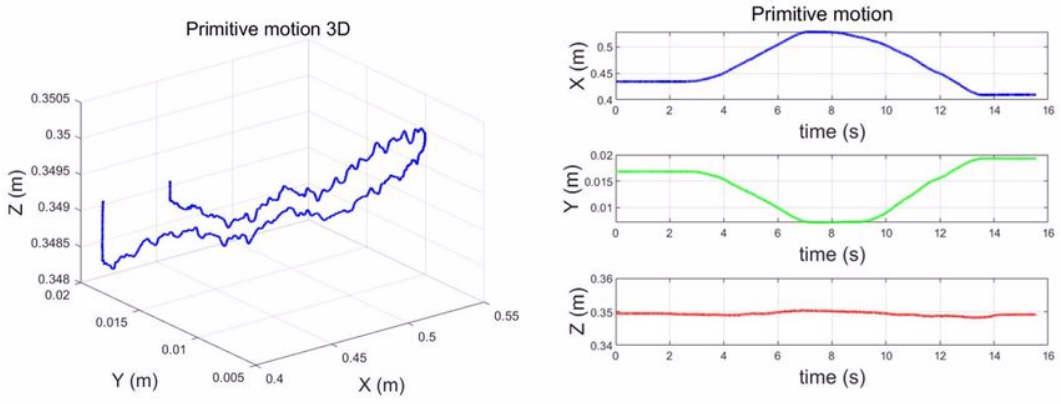

Figure 7.7: Modelling the motion primitive by dynamic movement primitive (DMP).

During the demonstration, the human operator demonstrated the layup for a flat component. From the results, the roller moves forward and back in the X-Y plane, which is the primitive motion skill for the composite layup. We modelled this motion primitive by dynamic movement primitives, which can be

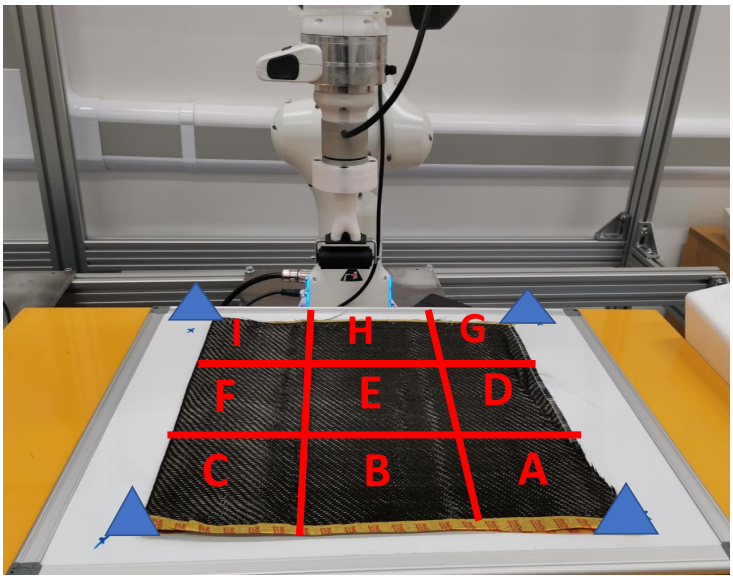

Figure 7.8: Composite layup task illustration.

generalised to different locations. For the Z-axis, there is a small motion, which can be used to generate the contact force along Z-axis in the end-effector frame. The stiffness parameters for the X and Y are the same, K=3000, while for the Z-axis is large, K=6000, which can be guaranteed to generate contact force along Z-axis. The small impedance along X and Y, can feature a compliant manner.

7.5.4 Generalise to a novel and big plane

In this case, we would like to evaluate the generalisation to a novel and large component, which is necessary for the composite layup in the real industry plant. The automation of composite layup only relies on the motion primitive and less information on the component. For example, it is straightforward to attain the geometry of the component based on the CAD model of the part. In this case, we assumed that the vertex coordinates of the part are known. For example, given the four vertex coordinates, we can get the region where the parts need to be manufactured for a plane. For the area that needs to be processed, we divided several sub-areas (including A, B, C, D, E, F, G, H, I), as shown in Fig.7.8.

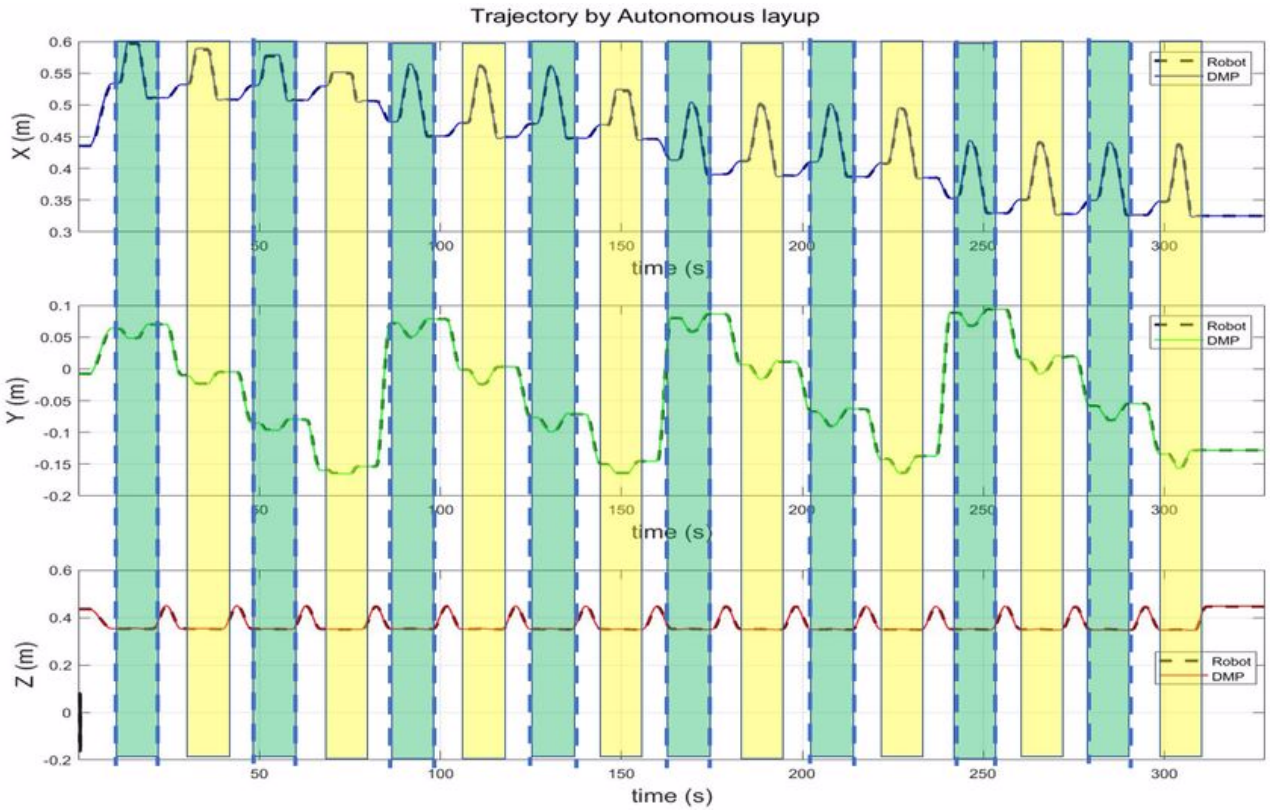

Figure 7.9: The trajectory of the roller in the autonomous mode. The green bar and the yellow bar represent the motion primitive. In this work, the motion primitive is the same, but the start and end of each motion primitive are different.

Each sub-area can be modelled with task variables, including the start and end coordinates. For the DMPs-based skill model, only the task variable is needed to reproduce the motion skills.

The number of motion primitives is dependent on the size of the component. For the X direction, as the generalisation of DMP, the number can be random. In the Y direction, the number is the length of the workpiece divided by the width of the roller, which can be guaranteed roller can cover the whole workpiece. As shown in Fig.7.9., there are 16 motion primitives for the big plane. Each motion primitive is similar to the human demonstration motion. Between two motion primitives, we used a motion planning algorithm to generate a transition trajectory. The first row, along X-axis, shows that

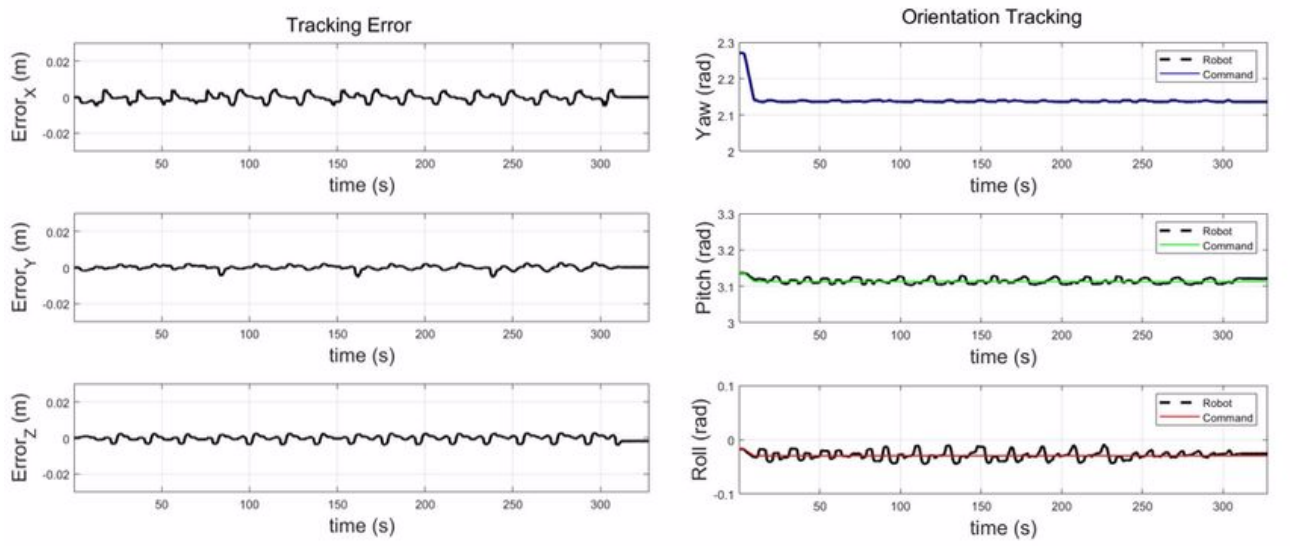

Figure 7.10: The tracking error along X, Y, and Z axis; and the orientation tracking in yaw, pitch and roll.

the coordinates of the roller decrease from 0.6m to 0.34m. The middle row, along the Y-axis, shows that the coordinates of the roller change between -0.17m and 0.1m. The real trajectory of robots can cover the whole workpiece.

The Fig.7.10. shows the tracking error between the command from the DMP model and the actual trajectory of the roller. The tracking error is less than 0.005m in the X, Y and Z axis. During the composite layup, the orientation of the end-effector is fixed, and the tracking error is less than 0.02 rad. The control accuracy is enough for the composite layup, which proves the performance of the impedance controller for the composite layup.

7.5.5 Generalise to a sloping plane

This experiment case aims at evaluating the generalisation to an inclined plane. As shown in Fig.7.11, when the board is rotated, the learned skill can generalise to the rotated component. In this case,

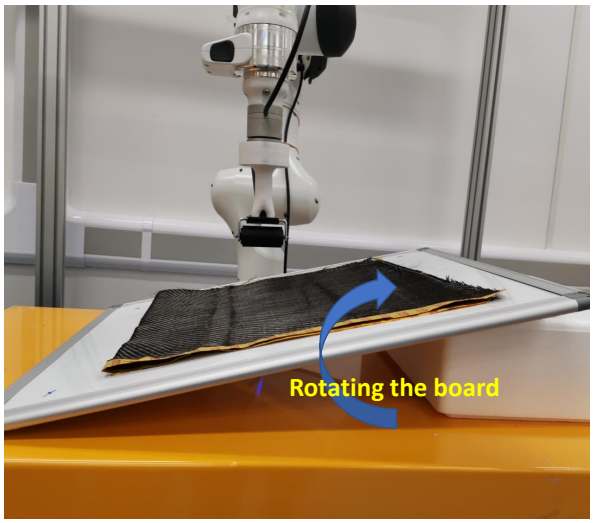

Figure 7.11: Component rotation case study.

the key points for this task are $P_1(0.36,-0.14,0.38)$, $P_2(0.37,0.01,0.42)$, $P_3(0.50,0,0.42)$, and $P_4(0.50,-0.18,0.38)$. We assume that we know the CAD model of the component or the orientation of the model can be measured based on sensing technology, such as machine vision.

From Fig.7.12., there are eight motion primitives to cover the whole inclined plane. The main differences between the inclined plane and the horizontal plane are the motion along the Z axis and the orientation. From the third row, the motion range along the Z-axis is from 0.41m to 0.38 in Fig.7.13. And the orientation is different, which needs to keep the roller perpendicular to the plane. The tracking errors are less than 0.005m, and the orientation tracking errors are less than 0.02 rad, which demonstrates the generalisation of the learnt skill and the performance of the impedance-based controller for a composite layup in the inclined plane.

7.5.6 Collaboration through teleoperation

This experiment aims at evaluating the collaboration performance of the impedance control-based teleoperation system. Most of the existing work studied physical human-robot collaboration, and less

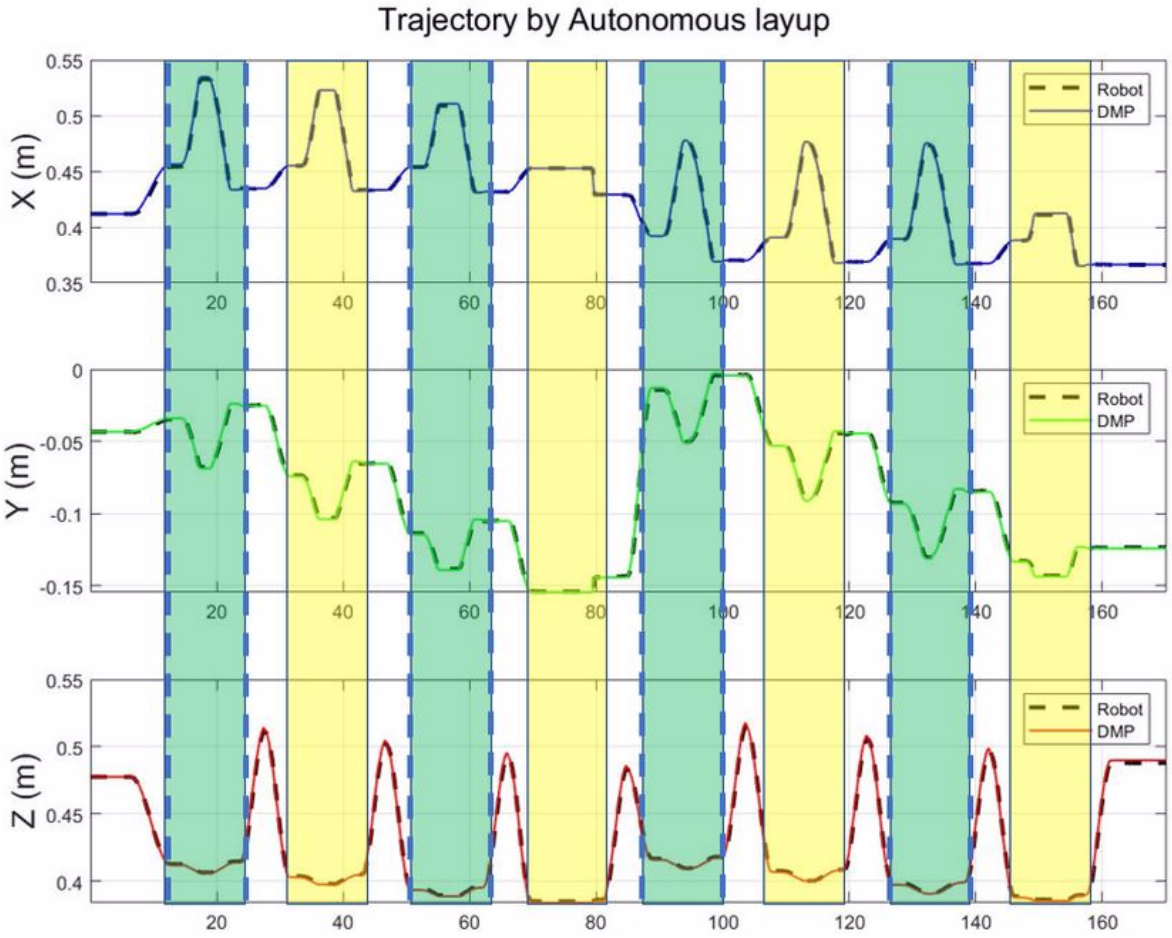

Figure 7.12: The trajectory of end-effector in the base frame of robot in autonomous mode for the sloping plane.

research work on the collaboration between teleoperation, in-site humans and robots. In this experiment, we evaluated that teleoperation and in-site human can collaborate smoothly by modifying the parameters of the impedance controller. We make use of the character of the torque-computed control based on impedance control. For example, we set the stiffness of the impedance controller to zero in a specific DoF; the control along this DoF becomes a free-motion mode, which can be kinesthetic teaching or adjusting the robots by an in-site human.

From Fig. 7.14, (A) is the control command from the teleoperation, and (B) is the command by

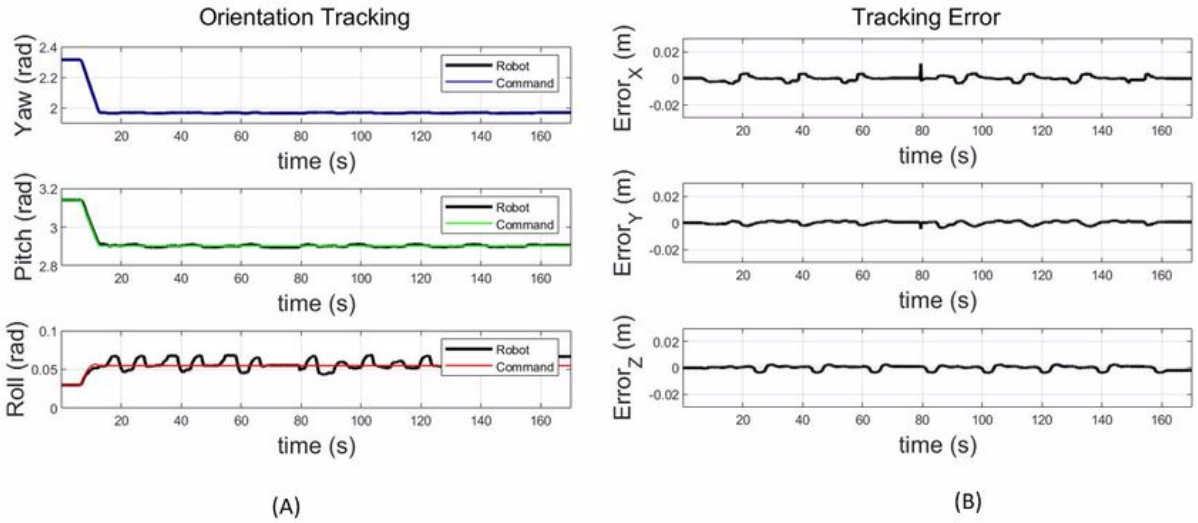

Figure 7.13: The tracking error along X,Y, and Z axis; and the orientation tracking in yaw, pitch and roll for the sloping plane.

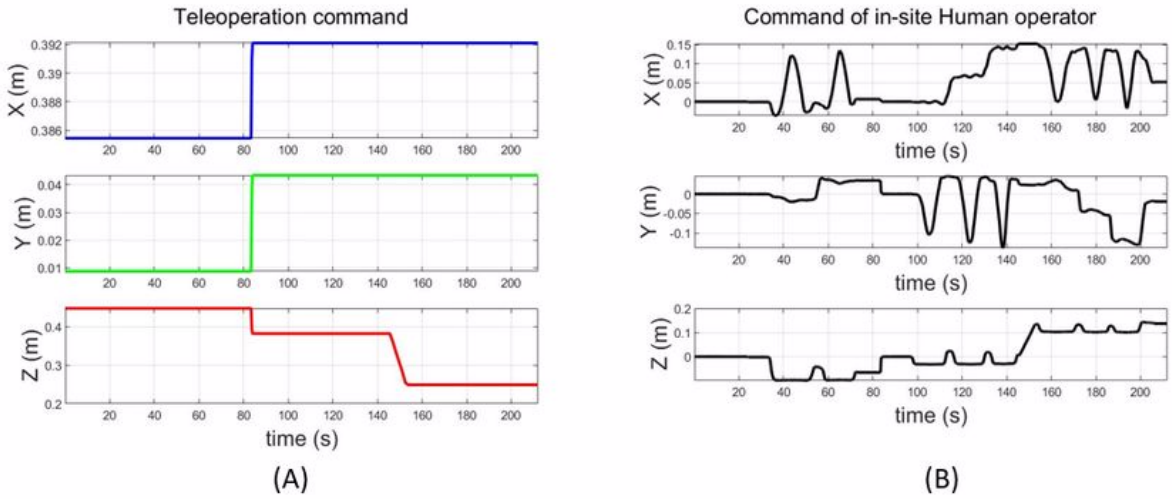

Figure 7.14: The trajectory of end-effector in the collaboration mode through teleoperation. Figure (A) is the teleoperation command, and figure (B) is the input command from the in-site human operator.

in-site human operation. The orientation control is autonomous by the robot. Fig.7.15. is the trajectory of the end-effector in the hybrid control mode. The results show that the control system can integrate teleoperation and kinesthetic demonstration and autonomous. The transition between the three modes

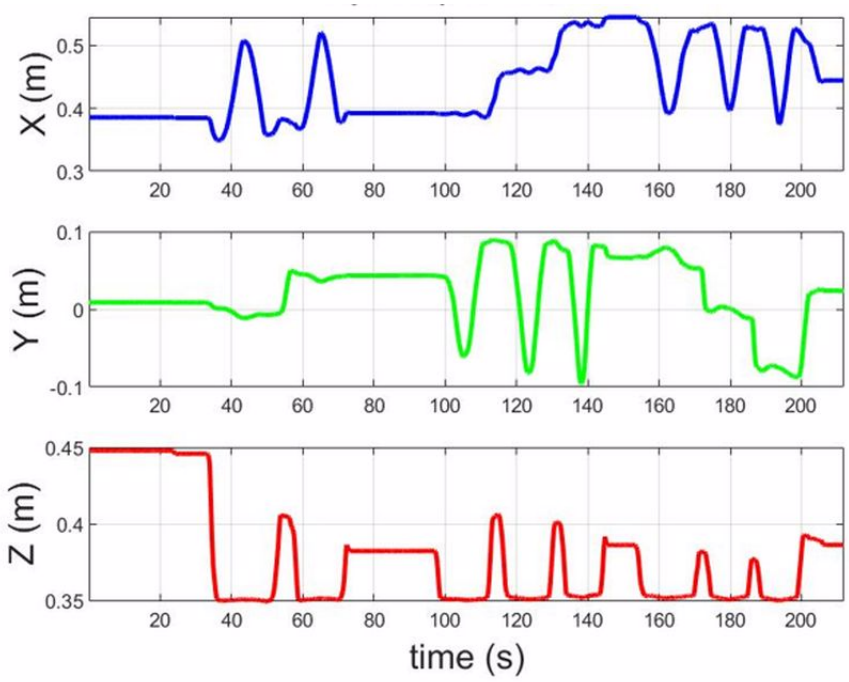

Figure 7.15: The trajectory of end-effector in the base frame of robot in the collaboration mode.

is smooth.

7.6 Summary

In this chapter, a torque-computed framework based on impedance control was proposed to enable the human-robot skill transfer through teleoperation. The human user interface was developed to display the parameters of the controller and the contact force, and the human operator could modify the parameters of the control system. The 3D mouse has been used as the input device for teleoperation. For the robot-assisted composite layup, the layup skills are modelled by DMPs and transferred to the robot through teleoperation. The generalisation of the proposed framework has been demonstrated through different components with various sizes and orientations. And the tracking error of the impedance-based controller is less than 0.005m, which is feasible for the composite layup.

8 Medical examination application: robot-assisted sonography

8.1 Abstract

Medical ultrasound scanning is a challenging dexterous manipulation task for robots, even for experienced sonographers, since it involves decision-making, motion control and force regulation based on real-time ultrasound images and patient feedback. We proposed a robot-assisted ultrasound scanning framework, integrating deep multimodal imitation learning and compliant control. We employed deep neural networks to encode multimodal information, including RGB images, force data, ultrasound images, and proprioceptive information (e.g., pose of the end-effector) for robot-assisted ultrasound scanning. The deep imitation learning model predicts reference motion and desired force. We designed a compliant controller in Cartesian space to track the reference trajectory and desired force. In addition, we smooth the reference trajectories generated by the deep imitation learning module, and the smoothy trajectory is sent to the low-level compliant controller. Lastly, the generalisation capability, control performance and quality of acquired ultrasound images were evaluated. The results show that the proposed approach is able to improve the success rate of procedure completion, and the complete time is shorter compared to a pure deep neural network model. The main contributions can be summarized as follows.

- We investigated a deep multimodal imitation learning framework, including the RGB image,

force profile, ultrasound image, and proprioceptive information, for robot-assisted ultrasound scanning artery on the Phantom[1] and human subject. Compared with the conventional imitation learning method, the deep multimodal imitation learning module owns better generalisation capability for the generation of reference motion and force commands for different patients.

- The proposed deep multimodal imitation approach is able to significantly improve the success rate of procedure completion from 75% to 90%. We evaluated the generalisation capability of the deep multimodal imitation learning module and control performance, as well as the quality of the acquired ultrasound image through Phantom and the human subject.

8.2 Introduction

Sonography is an easily available assessment tool for screening and assessment of a wide variety of pathologies and has the benefit of not using ionizing radiation. Consequently, sonography is often considered the first line of investigation for assessing the solid organs of the abdomen, vessels with blood flow such as the aorta and the deep veins of the distal limbs, small soft tissue structures and collections of fluid. However, there is an urgent challenge of shortage of medical resources or imbalance of medical resources, especially for the poor areas during the pandemic. For example, the UK's healthcare system is unable to meet the increasing demand for radiologists due to a tremendous shortfall (27- 37%) in qualified staff. The NHS radiologist workforce is short-staffed by 33% and needs at least another 1,939 consultants to meet the demand for scans and surgery.

On the other hand, medical ultrasound examination is a challenging dexterous manipulation task even for experienced sonographers since it involves motion control and force regulation based on the real-time ultrasound (US) image and patient feedback, as shown in Fig.8.1. The medical examination

[1]The Phantom is made to simulate artery, which is introduced in Chapter3

Figure 8.1: Sonographers scan the vein and artery.

results by sonographers depend heavily on the sonographers' skills, where poor skills may cause inconsistency and even false detection. One of the limitations of scanning by sonographers in US scanning is the variation among different users, such as the contact force and scanning orientation etc., which have significant impact on US image quality. Hence it is still challenging to acquire consistent and high-quality US images (Gilbertson and Anthony, 2015). In addition, repeated and physical work may cause work-related musculoskeletal disorders for sonographers. Therefore, fully autonomous ultrasound scanning by robots can be a promising solution, enabling consistent and accurate operation and reducing the workload of sonographers. Robot-assisted ultrasound scanning has gained much attention from the robot community in the past, and the tele-echography system was developed to assist medical experts to acquire high-quality images (Conti, Park, and Khatib, 2014). However, its development is limited to structured and controlled conditions, lacking generalisation on different patients and reactively dealing with unexpected disturbances, such as the motion of patients during the examination.

Nowadays, autonomous robotic ultrasound scanning has been conducted towards autonomous medical examination. For example, Ma et al. proposed an automatic robotic lung ultrasound system based on the vision and human pose estimation (Ma, Zhang, and Zhang, 2021). In (Huang et al., 2021), Huang et al. employed the learning from demonstration techniques and visual servoing to achieve autonomous ultrasound scanning. In addition, the ultrasound confidence map (Chatelain, Krupa, and Navab, 2017),

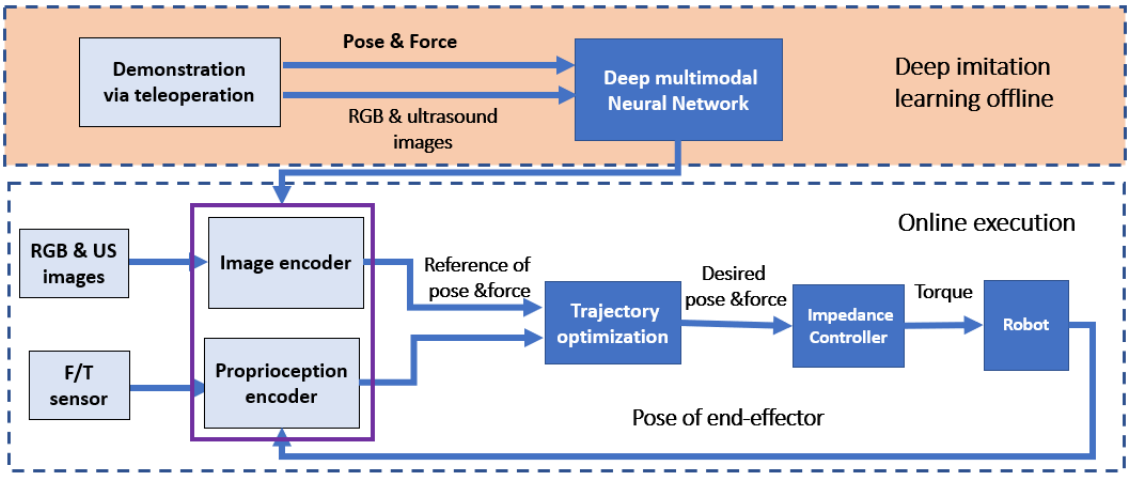

Figure 8.2: The framework of the unified deep multimodal imitation learning and control method.

as an ultrasound image quality criterion, was proposed to guide the robot arm to acquire high-quality ultrasound images. The authors proposed the visual servoing method based on the ultrasound confidence map to optimise the ultrasound image quality (Chatelain, Krupa, and Navab, 2017). Recently, Jiang et al. developed a vision-based ultrasound system to precisely reposition the robotic ultrasound arm, and a confidence-based optimisation algorithm was investigated to avoid the gap between the probe and contact surface (Jiang et al., 2022). And the confidence map was also used to optimise the orientation of the ultrasound probe to automatic normal positioning (Jiang et al., 2020).

Deep multimodal learning has been investigated for contact-rich manipulation tasks in unstructured environments (Lee et al., 2020). To address the abovementioned problems in robot-assisted ultrasound scanning tasks, we proposed a unified deep imitation learning and compliant control framework for robot-assisted sonography, as shown in Fig. 8.2.

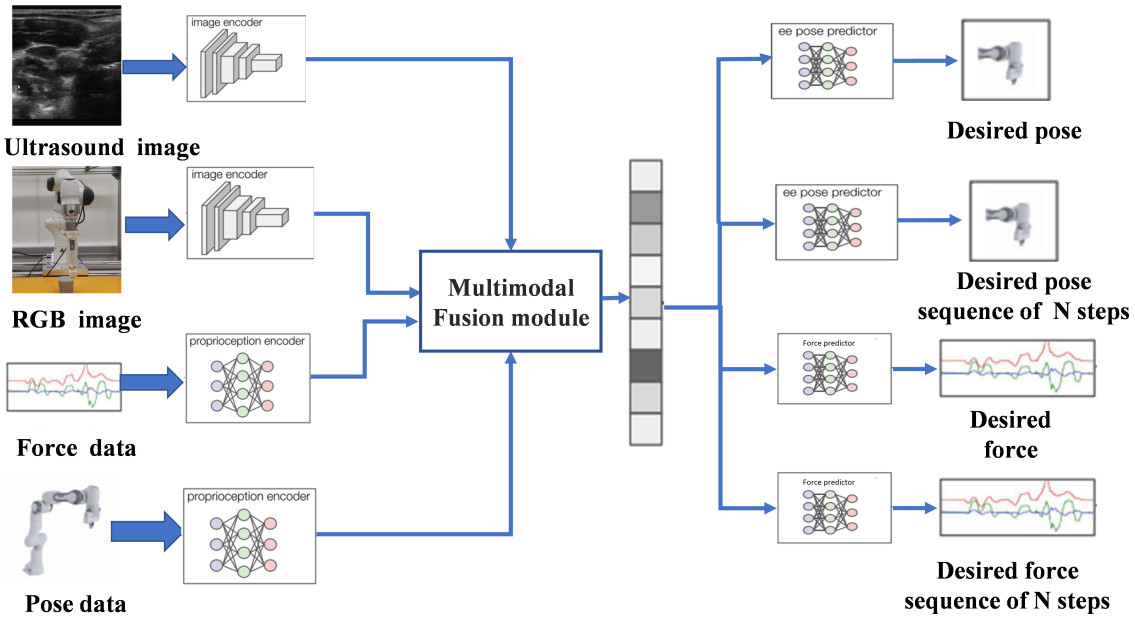

Figure 8.3: The neural network (NN) architecture for multimodal representation learning.

8.3 Deep imitation learning and compliant control

8.3.1 Multimodal imitation learning

In this work, we studied a deep multimodal imitation learning algorithm for robot-assisted ultrasound scanning tasks, as shown in Fig. 8.3. The NN takes data from four different sensors as input: RGB image, ultrasound image, force data, and the position and orientation of the end-effector. It encodes and fuses this data into a multimodal representation module using a variational Bayesian method, on which a policy for ultrasound scanning is trained in an end-to-end style. The policy of robot-assisted ultrasound scanning is learned by combining multiple sensor data. Compared to conventional control, end-to-end imitation learning owns better generalization. The detailed structure of deep multimodal imitation learning model is presented in Fig.8.4.

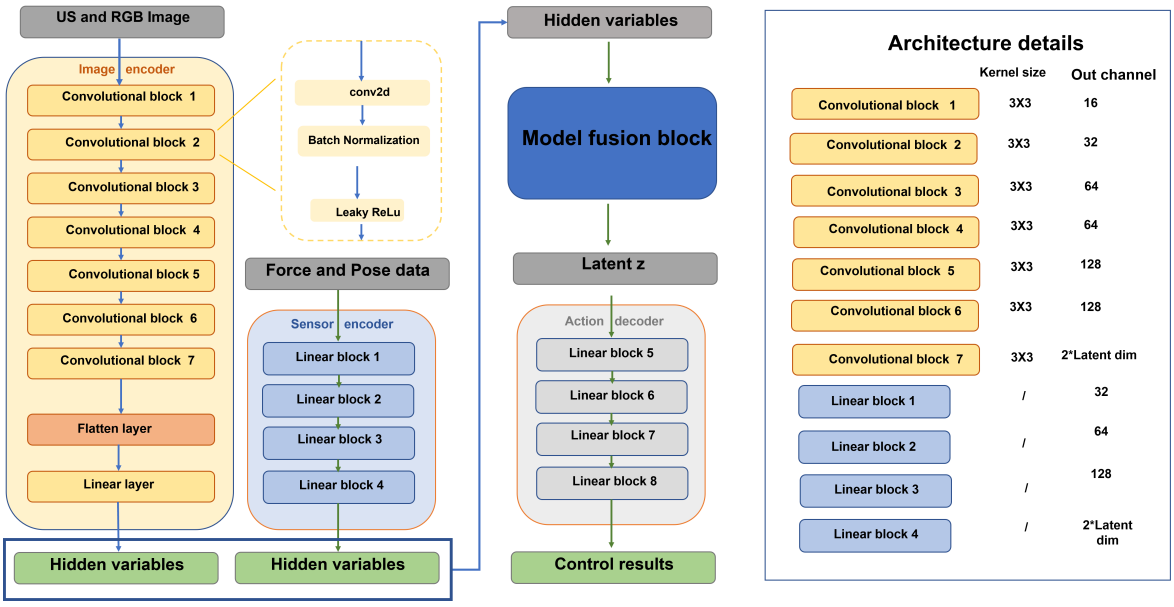

Figure 8.4: The architecture details of deep multimodal imitation learning model.

Encode layer

The encoders of the models need to process different multimodal data, including RGB and ultrasound images, force profiles and the pose of end-effector. The heterogeneity of these data require different encoders to capture the embedded information features. For the image information (ultrasound and RGB images), the model scales the images uniformly to 256×256 and normalises the pixels, then passes them through a VGG-like convolutional neural network structure and finally outputs the required hidden variable through a fully connected layer. The contact force and the pose of the end-effector are passed through four layers of a fully connected neural network, each layer of which is followed by a Leaky ReLu activation layer, and then the required hidden variable is outputted.

Multimodal fusion

Because the data from different sensors describe different aspects of the task, in the same hidden state, it can be assumed that these patterns are conditionally independent of the potential representation. The

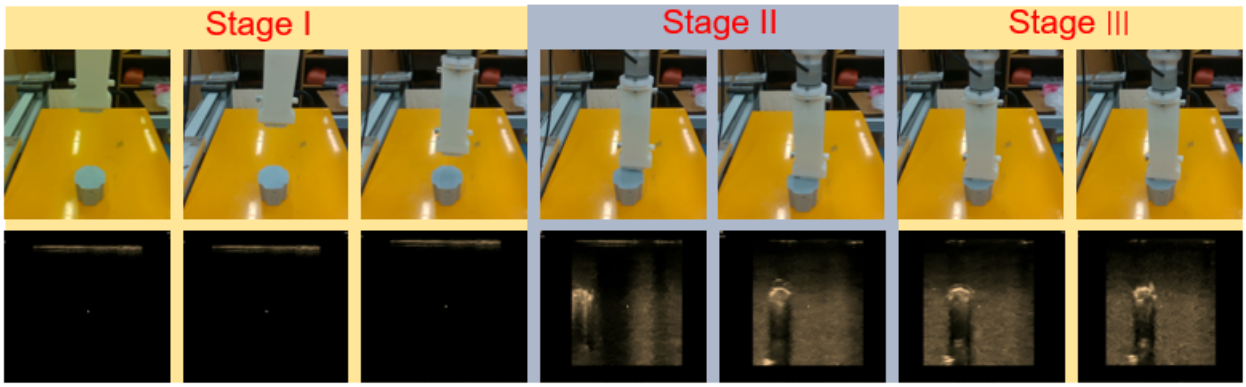

Figure 8.5: The process of robotic ultrasound scanning on Phantom. The first row is the RGB images during robot scanning on Phantom autonomously. The second row is the real-time ultrasound images. In stage I, the robot approaches the Phantom, stage II explores to find the artery, and stage III is to allow the artery in the centre of the ultrasound image.

assumption of conditional independence of individual inputs to a multimodal model has been widely used in the sensor fusion work, such as the use of Bayesian filters (Bennewitz et al., 2005) and the more recent work on multimodal generative models (Wu and Goodman, 2018).

Decode layer

The model is expected to output the desired command for the motion of the robot arm, including desired pose and desired force. After obtaining the latent z, z will be used as input to directly predict the next position/rotation and force of the end-effector through three different four-layer multilayer perceptron (MLP) layers. Again, based on this, the forces after an interval of N steps and the position/rotation of the robot are predicted by a similar structure. By knowing the next step and the next N steps of action. We create a buffer on the ROS task to store the N steps, we can then predict the continuous trajectory of the robot for the next N steps directly from the buffer after the robot has moved for more than N execution cycles. With this buffer, the trajectory profile of the control can be optimised.

Data set

For the creation of the data set, the system clock of ROS was used as a reference to ensure the uniform data input to the training set in time. Different threads were created in the ROS system and acquired at the same time interval (20hz) including force, robot pose and RGB images with ultrasound images. The dataset created contains the process of descending from an initial position to approach the phantom and adjusting the probe position after contacting the phantom to obtain the best view of the ultrasound images. A senior vascular scientist from University Hospital Bristol demonstrated the scanning on Phantom and real human subjects. The dataset of Phantom includes 12128 data, including the ultrasound images, RGB images, contact force and pose of the probe, and the dataset of the real human body includes 5832 data. We chose 2% data as the validation dataset.

8.3.2 Baseline model

We chose two ways to validate the model. 1) Validate the impact of each sensor on the predictive output data compared to the multimodal model. For the input to the model, four modal inputs were chosen for this experiment, including RGB images, ultrasound images, force data and the pose of probe. The baseline model aims to study how it will affect the model when removing the RGB, ultrasound images and force data respectively. On the other hand, it shows how reducing the dimensionality of the hidden variable Z affects the model. 2) Based on this, the single end-to-end output model with 128 dimensions of the hidden variable Z was then compared to our proposed model that adds a predicted robot motion trend after N steps to the model. This differs from the end-to-end trajectory output model of previous multimodal models in that the model is able to predict changes in robot motion over time in the future, which allows the robot to understand its next move and scan better.

8.3.3 Compliant control

The low-level compliant control, we used the impedance controller in Cartesian space, introduced in Chapter 3.

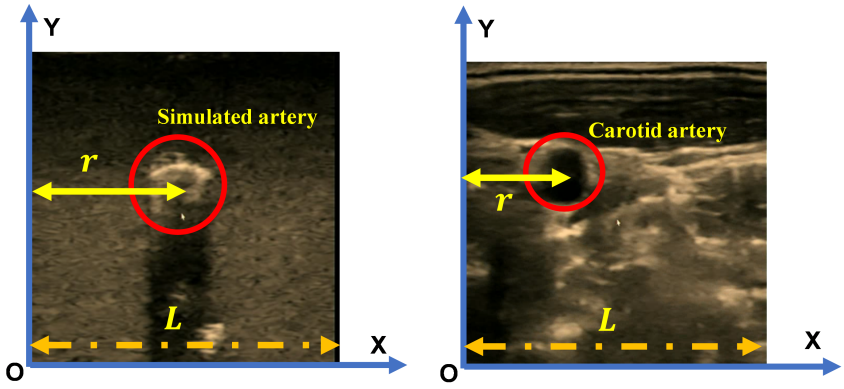

Figure 8.6: The centre deviation of the ultrasound image.The left one is the ultrasound scanning on Phantom, and the right one is the ultrasound image of human carotid artery.

8.4 Experiment on phantom and human body

We defined the centre deviation of the ultrasound image to evaluate the image performance, as shown in Fig. 8.6. The deviation of the ultrasound image is defined,

$$\Delta r = \frac{|L - 2r|}{L} \tag{8.1}$$

where L is the width of the ultrasound image, and r is the X coordinate of the centre of the artery.

8.4.1 The setup of experimental platform

The experimental setup is shown in Fig.8.7. A 7-DoF Franka Emika Panda equipped with a ultrasound probe to perform the scanning task. A Touch X was used as the teleoperation device. Realsense

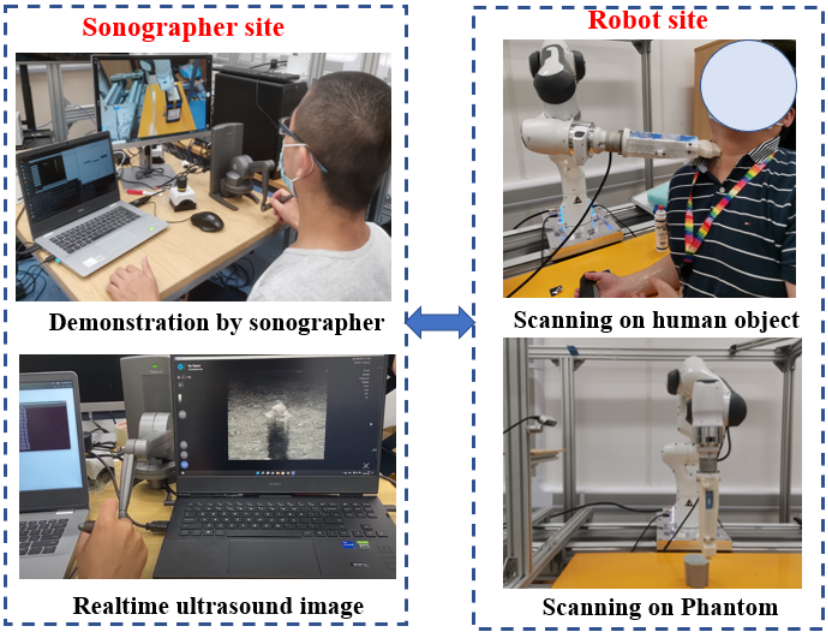

Figure 8.7: The setup of the experiment. Demonstration by a sonographer and autonomous scanning on Phantom and human objects.

camera (D435i) was used to record RGB images,which could also provide visual feedback during human teleoperation. Control computer running Ubuntu 18.04, which was connected to the Touch X device, F/T sensor, Franka Emika Panda, and the camera. F/T sensor[2] was employed to sense the contact force during the robot-assisted scanning. The SONON 300L[3] ultrasound probe was used to scan the phantom and carotid artery of human being. ROS was used to integrate different components. The whole experimental procedure was conducted in accordance with the Faculty Research Ethics Committee, and the protocol was approved by the UWE Research Ethics Committee (UWE REC REF No: FET-2122-59).

[2]http://www.nbit6d.com/product/656.html

[3]http://www.orcamedical.co.uk/product/1/Healcerion-Sonon-300L/

8.4.2 Validation of the multimodal imitation learning on Phantom

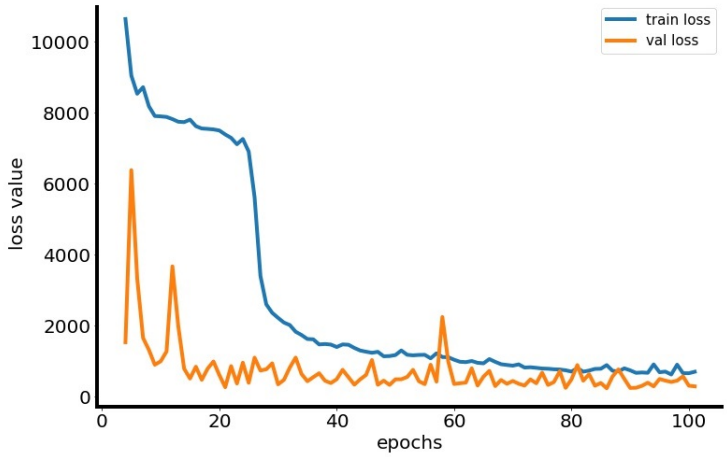

Figure 8.8: The loss of the full multimodal training.

As shown in Fig. 8.8, the loss curve of the multimodal learning process indicates that the multimodal model could learn the information from the multimodal data. On the validation dataset, the loss value also converges. In addition, we evaluated the effect of different modalities by reducing the corresponding modality input. In Fig. 8.9, the prediction along the Z axis multimodal with and without force info are compared. The prediction error along the Z axis, without the force info, is larger than that of the multimodal imitation learning model. Because we employed impedance control to track desired force, the position error in the Z axis caused force error along the Z axis.

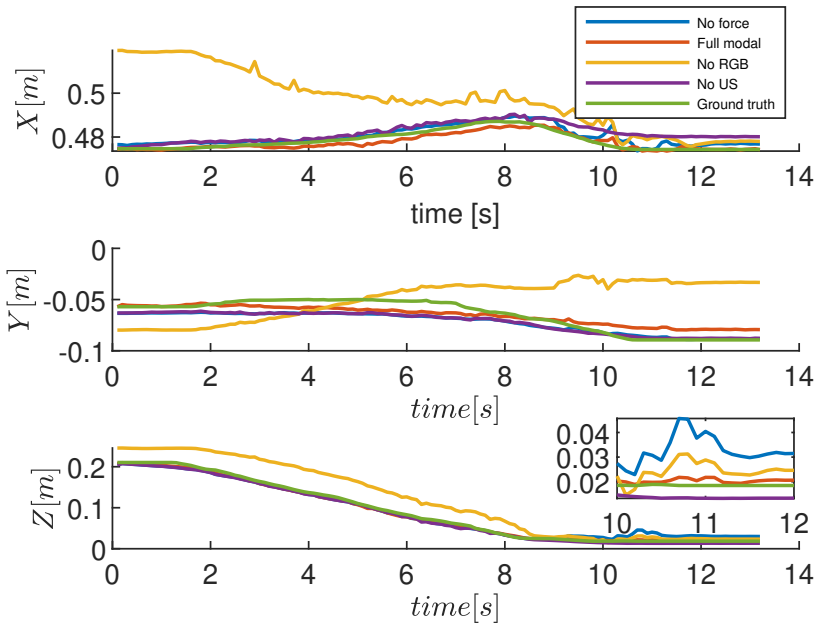

Figure 8.9: Prediction comparison among different modals.

As shown in Fig. 8.9 is the comparison between the prediction along Z axis multimodal and model without ultrasound images. We compared the prediction along Z axis multimodal with and without RGB images. We also conducted evaluation experiments on Phantom by reducing certain modal inputs, including contact force, ultrasound images, and RGB images. In experiments, the reduced model is hard to acquire good ultrasound images with compliant interaction with the Phantom. While the multimodal model method could acquire good ultrasound images, the success rate is only 75%. We further evaluate the success rate by integrating the trajectory smooth module. Fig. 8.10 demonstrates the comparison among the prediction results with different dimensions of latent variables. The results show that the dimension of latent variables has an impact on the predictions, and dimension 128 has the best performance in this work.

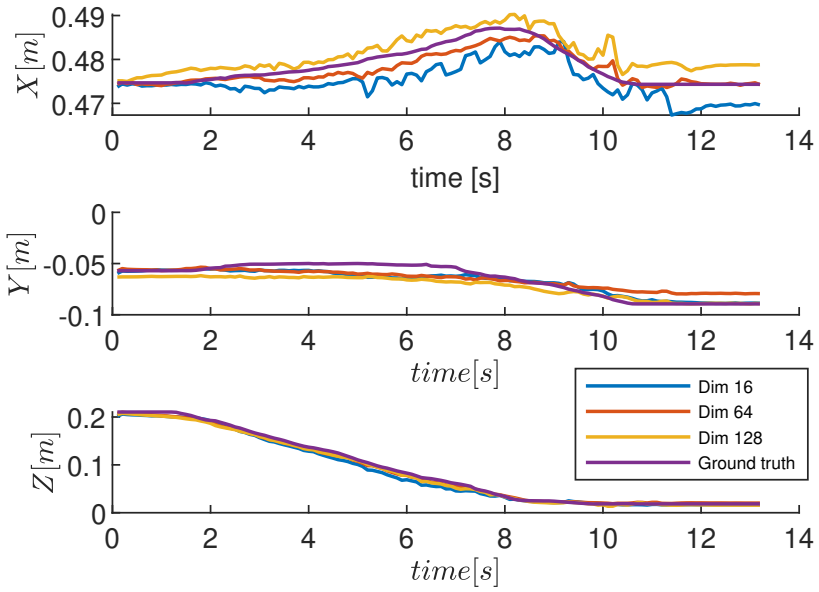

Figure 8.10: Prediction comparison among different dimensions of latent variables.

In addition, we conducted a comparison experiment on the Phantom with the proposed method, pure multimodal imitation without the smooth trajectory process. We carried out 30 times to calculate the success rate. The success rate is improved from 75% to 90%. The trajectory smooth process allows the generated desired trajectory to be smooth and stable.

8.4.3 Generalisation performance

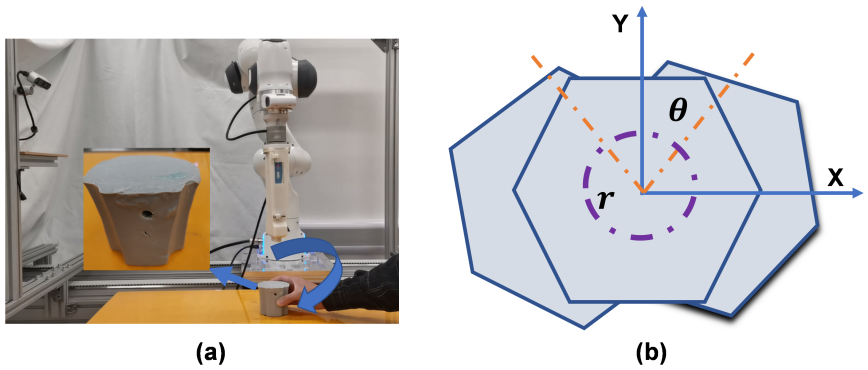

Figure 8.11: Generalisation performance evaluation by rotating the Phantom.

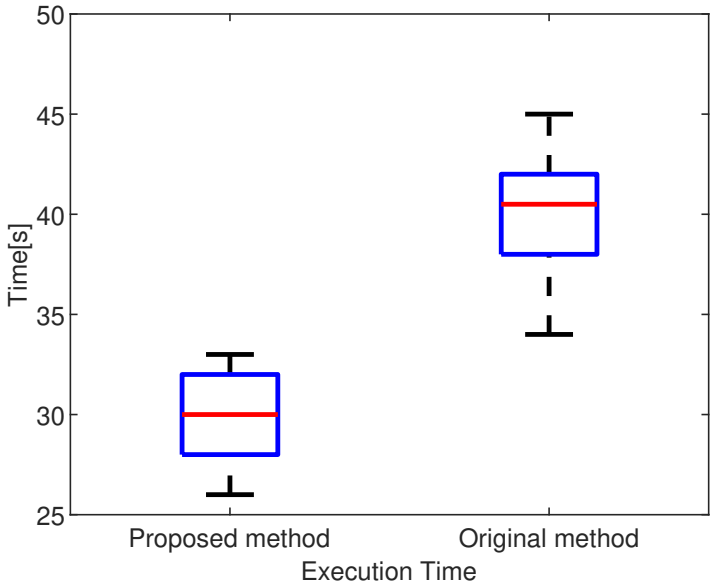

Figure 8.12: The results of execution time.

The generalisation capability of the learned model is essential. Although the patients are asked to lay in the same position and orientation, there are still differences in the position and orientation in practice. Thus, we need to evaluate the generalisation ability to different pose. To evaluate the generalisation performance of the skill model, we change the orientation of the phantom, as shown in Fig. 8.11. The

Phantom is rotated within θ and r. We conducted the experiment on different rotation angles. For each case, we conducted ten times, and the performance result is shown in Table.8.1. The success rate is higher than 78%, and the complete time within 40s. The result demonstrates that the efficiency and success of different cases. The experiment results by the third participant are presented. The complete time of the proposed method is reduced 33%, from 45s to 30s, as shown in Fig.8.12. The comparison of the baseline model and the proposed framework is shown in Table.8.2

Table 8.1: Generalisation performance evaluation.

Rotation angle θ	-20°	-10°	-10°	20°	30°
Success rate	0.80	0.90	0.88	0.85	0.78
Time (s)	35	32	30	34	40
Force error (N)	0.60	1.2	0.4	0.8	1.5
Image deviation	0.85	0.88	0.94	0.92	0.84

Table 8.2: Performance evaluation on Phantom.

	Success rate	Time mean (s)	Time variance (s)	Force error (N)	Force variance (N)
Proposed	0.90	30	3	2	0.53
Baseline	0.75	45	6	3	1.3

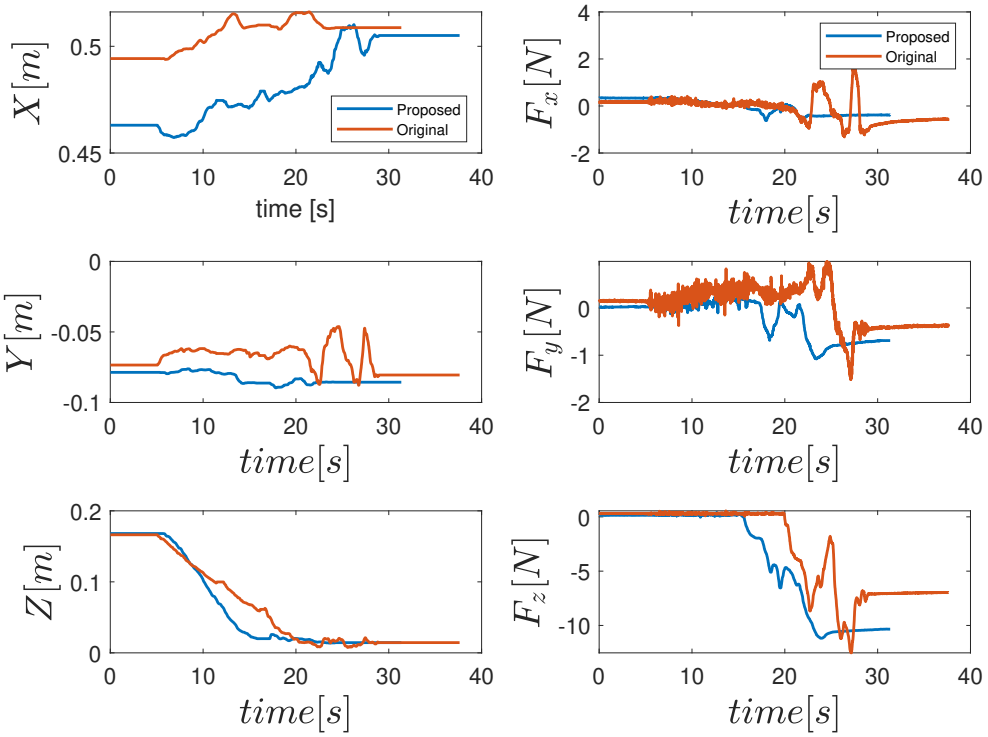

Figure 8.13: The results of the proposed method and the original network.

8.4.4 Validation on human subject

The trajectory and contact force results by the fourth participant are presented. The performance of the proposed method is validated on human subjects, as shown in Fig. 8.13. The predicted trajectory and the contact force are smoother than the original model. In addition, the contact force error along the Z axis is below 1N, while the original force error is 2.7N (the desired force $F_z$is 10N). As shown in Fig. 8.14, from (a) to (c) the robot could adjust the probe to place the artery (black circle) in the center of the ultrasound image. The robot could control the probe to acquire good ultrasound images. We chose the result of one experiment as an example to illustrate that the robot automatically adjusts the probe to make the carotid artery image in the center of the image, as shown in Fig. 8.14.

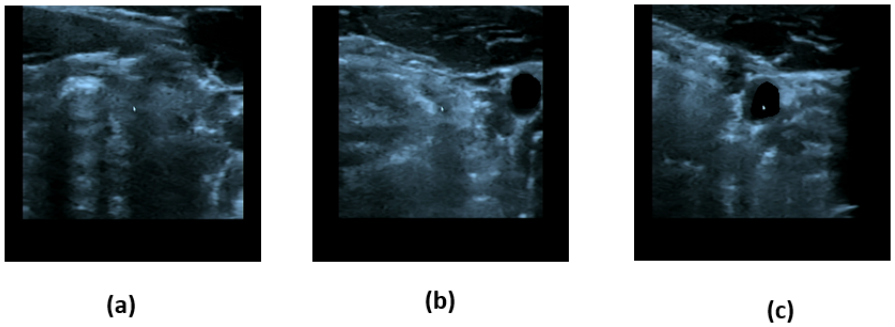

Figure 8.14: The results of ultrasound images on human subject. The ultrasound images of artery when robot scan autonomously. From (a) to (c), the robot gradually adjusts the probe to allow the artery (black circle) in the centre.

8.5 Summary

In this chapter, we proposed a novel robot-assisted ultrasound scanning method, integrating deep multimodal imitation learning, compliant control, and trajectory smooth process. A deep neural network model was designed to encode multimodal information, including the RGB images, force data, ultrasound images, and proprioceptive information for robot-assisted ultrasound scanning artery. The experiment results show that the deep multimodal imitation model has better generalization capability than the reduced models without certain modal information. Also, a trajectory optimisation planner between the deep imitation learning module and the low-level impedance controller was designed, which was used to smooth the trajectory generated by the deep imitation learning algorithm. The trajectory optimisation module improves the success rate compared the pure multimodal imitation learning method. The results show that the proposed approach can significantly improve the success rate of procedure completion.

9 Conclusions and future work

9.1 Conclusions

In this thesis, we studied the robot manipulator skill learning and generalising through teleoperation. First, one of the contributions is the development of a multimodal teleoperation system for human-in-the-loop, combining the intelligence of human beings and the autonomy of robots and allowing human-robot skill transfer. The multimodal teleoperation system can capture the dexterous manipulation skills of human beings and achieve the human-in-the-loop mechanism for correction and demonstration online. We implemented different interfaces for human-robot interaction, teleoperation and corrections. The natural and intuitive interfaces improve the dexterity and experience of human operators, reducing the physical fatigue and cognitive workload of operators and increasing control performance.

Second, we proposed a composite dynamic movement primitive (CDMP) skill modelling based on the neural network for manipulation skills, including motion and orientation skills. The primitive motor skills, including motion, orientation and force skills, are encoded by the proposed CDMP, and the primitive motor skills are implemented by various controllers, such as impedance controller, force controller, and hybrid position/ force controller etc., forming the primitive behaviours. The dexterous and primitive behaviours are used to generate human-like and complex manipulation behaviour for various manipulation tasks.

Third, in contrast to the primitive skill theory in previous work, the novel primitive behaviour library allows robots to execute more complex and diverse tasks. Inspired by human decision and action

mechanisms, we combined the behaviour tree model with the primitive behaviour library theory. We have evaluated the feasibility and effectiveness of the primitive behaviour theory through various manipulation tasks with multi-steps, including rolling pizza dough and robot-assisted composite layup etc. The primitive behaviours can be merged and sequenced based on the task requirements and sensing feedback for contact-rich and multiple sequences tasks. This primitive behaviour library method benefits from the advantages of the behaviour tree and real-time perceptual feedback to improve the generalisation of LfD.

Last, we proposed a deep imitation learning model to deal with multimodal information, including the RGB image, force profile, ultrasound image, and proprioceptive information for robot-assisted ultrasound scanning artery. The deep imitation learning module predicts reference motion and force command. We designed a compliant controller in Cartesian space to track reference trajectory and desired force. To smooth the trajectory and ensure safety, we employed a trajectory optimization planner between the deep imitation learning module and the low-level compliant controller. The generalization capability of the deep multimodal imitation learning module and control performance and the quality of the acquired ultrasound image through Phantom and the human subject were evaluated. The results show that the proposed approach is able to significantly improve the success rate of procedure completion, and the complete time is reduced.

In summary, we developed an intuitive teleoperation-based system for human-robot skill transfer and proposed various methods for manipulation skills learning and generalising.

9.2 Limitations and future work

Although we have implemented an intuitive teleoperation-based system for human-robot skill transfer and proposed various methods for manipulation skills learning and generalising, several questions can

be further investigated in the future.

• The multimodal teleoperation robot system can be further optimised by integrating the robot hand, bimanual arms, tactile sensors etc. For dexterous manipulation tasks in practice, an arm-hand or mobile arm-hand system are necessary to perform these tasks, such as picking up fruits and robot-assisted healthcare etc. In addition, the inclusion of additional sensors, such as tactile sensors, facilitates the acquisition of richer contact information. Such modality information proves crucial for human beings to execute dexterous manipulation tasks effectively.

• Simulation environments that are quite similar to the real environments, such as digital twins, can be investigated to replace the real robot environments in which data-driven robot learning methods, such as deep reinforcement learning, can be employed to train robots. The learned skills through simulation environments can be transferred to real robots system with less effort. Reducing the gap between the simulated environments and real robots will benefit the robot skill learning process, such as requiring less real robot data, parallel training robots etc.

• In this project, we focused on exploring the learning of primitive manipulation skills and implementing compliant control to execute these acquired skills. Nevertheless, when dealing with complex and long-horizon manipulation tasks, there arises a necessity to conduct the segmentation and merging of a diverse range of primitive skills. Recently, large language models (LLMs), like ChatGPT, have demonstrated remarkable efficacy in decision-making and planning. Therefore, the investigation of LLMs can be integrated with the primitive skill theory to address the long-horizon robot manipulation tasks.

• We developed human-robot interfaces with various devices and compared the performance of different interfaces via robot-assisted medical examination tasks in this project. However, there are various constraints to performing human-robot interaction in practice, such as workspace limitations, contact

force constraints, etc. How to design the control system to facilitate human operation? When robots are deployed in practice, studying the teleoperation interface is still open for dexterous manipulation. Adaptive and shared control algorithms can be investigated during human teacher demonstration, which may benefit the human experience and control performance.

10 Appendix

In chapter 3, we conduct the user study, and the NASA Task load index (Hart, 2006) is shown as follows.

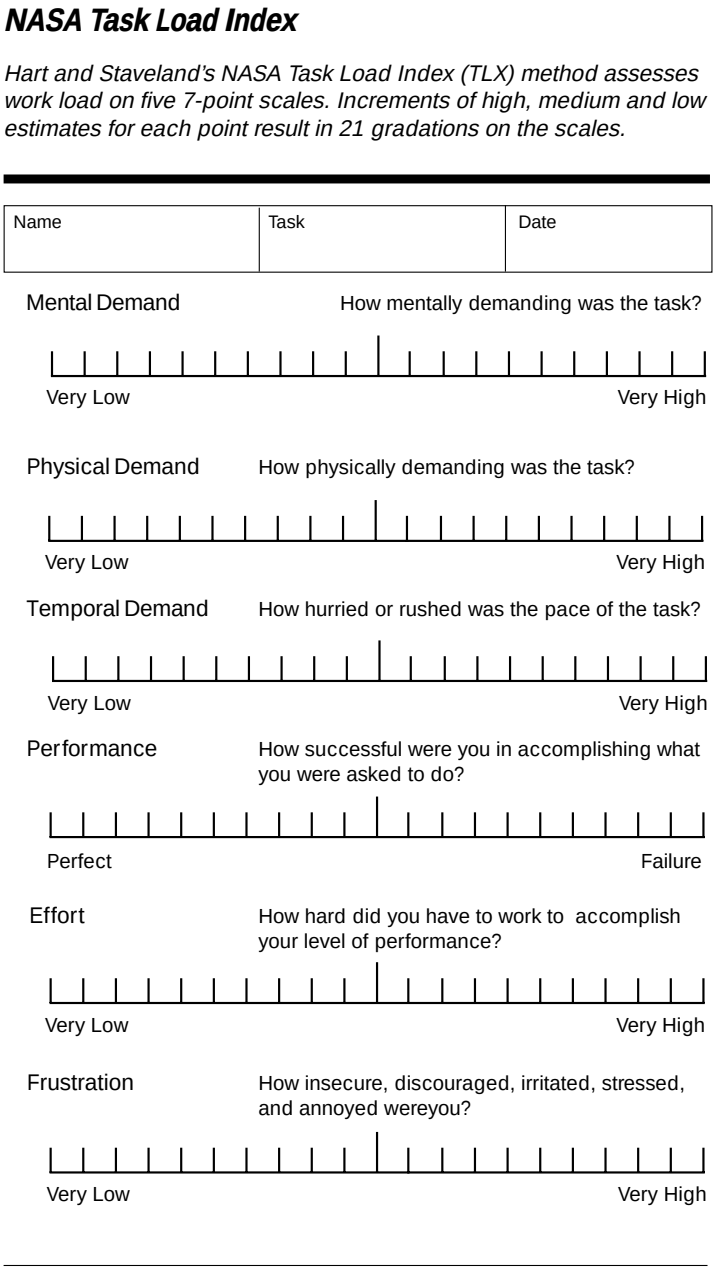

NASA Task Load Index

Hart and Staveland's NASA Task Load Index (TLX) method assesses work load on five 7-point scales. Increments of high, medium and low estimates for each point result in 21 gradations on the scales.

Name	Task	Date

Mental Demand — How mentally demanding was the task?

Very Low — Very High

Physical Demand — How physically demanding was the task?

Very Low — Very High

Temporal Demand — How hurried or rushed was the pace of the task?

Very Low — Very High

Performance — How successful were you in accomplishing what you were asked to do?

Perfect — Failure

Effort — How hard did you have to work to accomplish your level of performance?

Very Low — Very High

Frustration — How insecure, discouraged, irritated, stressed, and annoyed wereyou?

Very Low — Very High

References

Abbeel, P., Coates, A., and Ng, A. Y. (2010). Autonomous helicopter aerobatics through apprenticeship learning. *The International Journal of Robotics Research*. 29.13, pp. 1608–1639.

Ahmadzadeh, S. R., Kormushev, P., Jamisola, R. S., and Caldwell, D. G. (2014). "Learning reactive robot behavior for autonomous valve turning". In: *2014 IEEE-RAS International Conference on Humanoid Robots*. IEEE, pp. 366–373.

Argall, B. D., Chernova, S., Veloso, M., and Browning, B. (2009). A survey of robot learning from demonstration. *Robotics and autonomous systems*. 57.5, pp. 469–483.

Aronson, R. M., Santini, T., Kübler, T. C., Kasneci, E., Srinivasa, S., and Admoni, H. (2018). "Eye-hand behavior in human-robot shared manipulation". In: *Proceedings of the 2018 ACM/IEEE International Conference on Human-Robot Interaction*, pp. 4–13.

Asami, R., Sawai, Y., Sato, N., Morita, Y., Endo, T., and Matsuno, F. (2016). "Teleoperation system with virtual 3D diorama for moving operation of a tracked rescue robot". In: *2016 International Conference on Advanced Mechatronic Systems (ICAMechS)*. IEEE, pp. 90–95.

Bae, J., Zhang, W., and Tomizuka, M. (2012). Network-based rehabilitation system for improved mobility and tele-rehabilitation. *IEEE Transactions on Control Systems Technology*. 21.5, pp. 1980–1987.

Baek, I., Jeon, G., Yu, C., Kim, K., and Kim, S. (2017). Wireless active finger rehabilitation method using three-axis electromagnetic manipulation. *IEEE Transactions on Magnetics*. 53.11, pp. 1–5.

Bennewitz, M., Burgard, W., Cielniak, G., and Thrun, S. (2005). Learning motion patterns of people for compliant robot motion. *The International Journal of Robotics Research*. 24.1, pp. 31–48.

Bimbo, J., Pacchierotti, C., Aggravi, M., Tsagarakis, N., and Prattichizzo, D. (2017). "Teleoperation in cluttered environments using wearable haptic feedback". In: *2017 IEEE/RSJ International Conference on Intelligent Robots and Systems (IROS)*. IEEE, pp. 3401–3408.

Bizzi, E., Accornero, N., Chapple, W., and Hogan, N. (1984). Posture control and trajectory formation during arm movement. *Journal of Neuroscience*. 4.11, pp. 2738–2744.

Björnsson, A., Jonsson, M., and Johansen, K. (2018). Automated material handling in composite manufacturing using pick-and-place systems–a review. *Robotics and Computer-Integrated Manufacturing* [online]. 51, pp. 222–229. DOI: 10.1016/j.rcim.2017.12.003.

Black, D. G., Hosseinabadi, A. H. H., and Salcudean, S. E. (2020). 6-DOF Force Sensing for the Master Tool Manipulator of the da Vinci Surgical System. *IEEE Robotics and Automation Letters*. 5.2, pp. 2264–2271.

Bojarski, M., Del Testa, D., Dworakowski, D., Firner, B., Flepp, B., Goyal, P., Jackel, L. D., Monfort, M., Muller, U., Zhang, J., et al. (2016). End to end learning for self-driving cars. *arXiv preprint arXiv:1604.07316*.

Bolopion, A., Dahmen, C., Stolle, C., Haliyo, S., Régnier, S., and Fatikow, S. (2012). Vision-Based Haptic Feedback for Remote Micromanipulation in–SEM Environment. *International Journal of Optomechatronics*. 6.3, pp. 236–252.

Bolopion, A., Xie, H., Haliyo, D. S., and Régnier, S. (2010). Haptic teleoperation for 3-D microassembly of spherical objects. *IEEE/ASME Transactions on Mechatronics*. 17.1, pp. 116–127.

Calinon, S. (2016). A tutorial on task-parameterized movement learning and retrieval. *Intelligent Service Robotics*. 9.1, pp. 1–29.

Calinon, S. (2018). Learning from demonstration (programming by demonstration). *Encyclopedia of Robotics*, pp. 1–8.

Calinon, S. (2020). Gaussians on Riemannian Manifolds: Applications for Robot Learning and Adaptive Control. *IEEE Robotics & Automation Magazine*. 27.2, pp. 33–45.

Calinon, S., D'halluin, F., Sauser, E. L., Caldwell, D. G., and Billard, A. G. (2010). Learning and reproduction of gestures by imitation. *IEEE Robotics & Automation Magazine*. 17.2, pp. 44–54.

Calinon, S., Guenter, F., and Billard, A. (2007). On learning, representing, and generalizing a task in a humanoid robot. *IEEE Transactions on Systems, Man, and Cybernetics, Part B (Cybernetics)*. 37.2, pp. 286–298.

Calinon, S., Pistillo, A., and Caldwell, D. G. (2011). "Encoding the time and space constraints of a task in explicit-duration hidden Markov model". In: *2011 IEEE/RSJ International Conference on Intelligent Robots and Systems*. IEEE, pp. 3413–3418.

Callens, T., Have, T. van der, Van Rossom, S., De Schutter, J., and Aertbeliën, E. (2020). A Framework for Recognition and Prediction of Human Motions in Human-Robot Collaboration Using Probabilistic Motion Models. *IEEE Robotics and Automation Letters*. 5.4, pp. 5151–5158.

Cardenas, I. S. and Kim, J. (2019). "Design of a Semi-Humanoid Telepresence Robot for Plant Disaster Response and Prevention". In: *2019 IEEE/RSJ International Conference on Intelligent Robots and Systems (IROS)*, pp. 2748–2753.

Chatelain, P., Krupa, A., and Navab, N. (2017). Confidence-driven control of an ultrasound probe. *IEEE Transactions on Robotics*. 33.6, pp. 1410–1424.

Chatzilygeroudis, K., Vassiliades, V., Stulp, F., Calinon, S., and Mouret, J.-B. (2019). A survey on policy search algorithms for learning robot controllers in a handful of trials. *IEEE Transactions on Robotics*. 36.2, pp. 328–347.

Chebotar, Y., Kroemer, O., and Peters, J. (2014). "Learning robot tactile sensing for object manipulation". In: *2014 IEEE/RSJ International Conference on Intelligent Robots and Systems*. IEEE, pp. 3368–3375.

Chua, Z., Jarc, A. M., Wren, S., Nisky, I., and Okamura, A. M. (2020). Task Dynamics of Prior Training Influence Visual Force Estimation Ability During Teleoperation of a Minimally Invasive Surgical Robot. *arXiv preprint arXiv:2004.13226*.

Cohn, D. A., Ghahramani, Z., and Jordan, M. I. (1996). Active learning with statistical models. *Journal of Artificial Intelligence Research*. 4, pp. 129–145.

Conkey, A. and Hermans, T. (2019). "Active Learning of Probabilistic Movement Primitives". In: *2019 IEEE-RAS 19th International Conference on Humanoid Robots (Humanoids)*. IEEE, pp. 1–8.

Conti, F., Park, J., and Khatib, O. (2014). "Interface design and control strategies for a robot assisted ultrasonic examination system". In: *experimental robotics*. Springer, pp. 97–113.

Dahlin, A. and Karayiannidis, Y. (2019). Adaptive Trajectory Generation Under Velocity Constraints Using Dynamical Movement Primitives. *IEEE Control Systems Letters*. 4.2, pp. 438–443.

Dragan, A. D., Srinivasa, S. S., and Lee, K. C. (2013). Teleoperation with intelligent and customizable interfaces. *Journal of Human-Robot Interaction*. 2.2, pp. 33–57.

El Saddik, A. (2007). The potential of haptics technologies. *IEEE Instrumentation & Measurement Magazine*. 10.1, pp. 10–17.

Enayati, N., Ferrigno, G., and De Momi, E. (2018). Skill-based human–robot cooperation in tele-operated path tracking. *Autonomous Robots*. 42.5, pp. 997–1009.

Espiau, B., Chaumette, F., and Rives, P. (1992). A new approach to visual servoing in robotics. *ieee Transactions on Robotics and Automation*. 8.3, pp. 313–326.

Falco, P., Lu, S., Natale, C., Pirozzi, S., and Lee, D. (2019). A transfer learning approach to cross-modal object recognition: From visual observation to robotic haptic exploration. *IEEE Transactions on Robotics*. 35.4, pp. 987–998.

Freschi, C., Ferrari, V., Melfi, F., Ferrari, M., Mosca, F., and Cuschieri, A. (2013). Technical review of the da Vinci surgical telemanipulator. *The International Journal of Medical Robotics and Computer Assisted Surgery*. 9.4, pp. 396–406.

Gams, A., Nemec, B., Ijspeert, A. J., and Ude, A. (2014). Coupling movement primitives: Interaction with the environment and bimanual tasks. *IEEE Transactions on Robotics*. 30.4, pp. 816–830.

Gao, J., Zhou, Y., and Asfour, T. (2020). Learning Compliance Adaptation in Contact-Rich Manipulation. *arXiv preprint arXiv:2005.00227*.

Garate, V. R., Gholami, S., and Ajoudani, A. (2021). A scalable framework for multi-robot tele-impedance control. *IEEE Transactions on Robotics*. 37.6, pp. 2052–2066.

Gholami, S., Lorenzini, M., De Momi, E., and Ajoudani, A. (2022). Quantitative Physical Ergonomics Assessment of Teleoperation Interfaces. *IEEE Transactions on Human-Machine Systems*. 52.2, pp. 169–180.

Gilbertson, M. W. and Anthony, B. W. (2015). Force and position control system for freehand ultrasound. *IEEE Transactions on Robotics*. 31.4, pp. 835–849.

Gribovskaya, E., Khansari-Zadeh, S. M., and Billard, A. (2011). Learning non-linear multivariate dynamics of motion in robotic manipulators. *The International Journal of Robotics Research*. 30.1, pp. 80–117.

Guan, C., Vega-Brown, W., and Roy, N. (2018). "Efficient planning for near-optimal compliant manipulation leveraging environmental contact". In: *2018 IEEE International Conference on Robotics and Automation (ICRA)*. IEEE, pp. 215–222.

Gutiérrez-Giles, A., Ruggiero, F., Lippiello, V., and Siciliano, B. (2019). "Closed-loop Control of a Nonprehensile Manipulation System Inspired by the Pizza-Peel Mechanism". In: *2019 18th European Control Conference (ECC)*. IEEE, pp. 1580–1585.

Hagenow, M., Senft, E., Radwin, R., Gleicher, M., Mutlu, B., and Zinn, M. (2021). Corrective Shared Autonomy for Addressing Task Variability. *IEEE Robotics and Automation Letters*. 6.2, pp. 3720–3727.

Han, L., Kang, P., Chen, Y., Xu, W., and Li, B. (2019). "Trajectory Optimization and Force Control with Modified Dynamic Movement Primitives under Curved Surface Constraints". In: *2019 IEEE International Conference on Robotics and Biomimetics (ROBIO)*. IEEE, pp. 1065–1070.

Hart, S. G. (2006). "NASA-task load index (NASA-TLX); 20 years later". In: *Proceedings of the human factors and ergonomics society annual meeting*. Vol. 50. 9. Sage publications Sage CA: Los Angeles, CA, pp. 904–908.

Hart, S. G. and Staveland, L. E. (1988). Development of NASA-TLX (Task Load Index): Results of empirical and theoretical research. In: *Advances in psychology*. Vol. 52. Elsevier, pp. 139–183.

Havoutis, I. and Calinon, S. (2019). Learning from demonstration for semi-autonomous teleoperation. *Autonomous Robots*. 43.3, pp. 713–726.

Hoffmann, H., Pastor, P., Park, D.-H., and Schaal, S. (2009). "Biologically-inspired dynamical systems for movement generation: automatic real-time goal adaptation and obstacle avoidance". In: *2009 IEEE International Conference on Robotics and Automation*. IEEE, pp. 2587–2592.

Hogan, F. R. and Rodriguez, A. (2020). Reactive planar non-prehensile manipulation with hybrid model predictive control. *The International Journal of Robotics Research*, p. 0278364920913938.

Hogan, N. (1985). Impedance control: An approach to manipulation: Part I—Theory.

Hokayem, P. F. and Spong, M. W. (2006). Bilateral teleoperation: An historical survey. *Automatica*. 42.12, pp. 2035–2057.

Hu, Z., Sun, P., and Pan, J. (2018). Three-dimensional deformable object manipulation using fast online gaussian process regression. *IEEE Robotics and Automation Letters*. 3.2, pp. 979–986.

Huang, H., Zhang, T., Yang, C., and Chen, C. P. (2019a). Motor Learning and Generalization Using Broad Learning Adaptive Neural Control. *IEEE Transactions on Industrial Electronics*. 67.10, pp. 8608–8617.

Huang, Y., Zheng, Y., Wang, N., Ota, J., and Zhang, X. (2020). Peg-in-hole assembly based on master-slave coordination for a compliant dual-arm robot. *Assembly Automation*. 40.2, pp. 189–198.

Huang, Y., Rozo, L., Silvério, J., and Caldwell, D. G. (2019b). Kernelized movement primitives. *The International Journal of Robotics Research*. 38.7, pp. 833–852.

Huang, Y., Silvério, J., Rozo, L., and Caldwell, D. G. (2018). "Generalized task-parameterized skill learning". In: *2018 IEEE International Conference on Robotics and Automation (ICRA)*. IEEE, pp. 1–5.

Huang, Y., Xiao, W., Wang, C., Liu, H., Huang, R., and Sun, Z. (2021). Towards fully autonomous ultrasound scanning robot with imitation learning based on clinical protocols. *IEEE Robotics and Automation Letters*. 6.2, pp. 3671–3678.

Ijspeert, A. J., Nakanishi, J., Hoffmann, H., Pastor, P., and Schaal, S. (2013). Dynamical movement primitives: learning attractor models for motor behaviors. *Neural Computation*. 25.2, pp. 328–373.

Ijspeert, A. J., Nakanishi, J., and Schaal, S. (2001). "Trajectory formation for imitation with nonlinear dynamical systems". In: *Proceedings 2001 IEEE/RSJ International Conference on Intelligent Robots and Systems. Expanding the Societal Role of Robotics in the the Next Millennium (Cat. No. 01CH37180)*. Vol. 2. IEEE, pp. 752–757.

Ijspeert, A. J., Nakanishi, J., and Schaal, S. (2002). "Movement imitation with nonlinear dynamical systems in humanoid robots". In: *Proceedings 2002 IEEE International Conference on Robotics and Automation (Cat. No. 02CH37292)*. Vol. 2. IEEE, pp. 1398–1403.

Javdani, S., Admoni, H., Pellegrinelli, S., Srinivasa, S. S., and Bagnell, J. A. (2018). Shared autonomy via hindsight optimization for teleoperation and teaming. *The International Journal of Robotics Research*. 37.7, pp. 717–742.

Jiang, Z., Danis, N., Bi, Y., Zhou, M., Kroenke, M., Wendler, T., and Navab, N. (2022). Precise Repositioning of Robotic Ultrasound: Improving Registration-based Motion Compensation using Ultrasound Confidence Optimization. *IEEE Transactions on Instrumentation and Measurement*.

Jiang, Z., Grimm, M., Zhou, M., Esteban, J., Simson, W., Zahnd, G., and Navab, N. (2020). Automatic normal positioning of robotic ultrasound probe based only on confidence map optimization and force measurement. *IEEE Robotics and Automation Letters*. 5.2, pp. 1342–1349.

Karlsson, M., Robertsson, A., and Johansson, R. (2018). "Convergence of dynamical movement primitives with temporal coupling". In: *2018 European Control Conference (ECC)*. IEEE, pp. 32–39.

Kawai, Y., Honda, K., Kawai, H., Miyoshi, T., and Fujita, M. (2017). "Tele-rehabilitation system for human lower limb using electrical stimulation based on bilateral teleoperation". In: *2017 IEEE Conference on Control Technology and Applications (CCTA)*. IEEE, pp. 1446–1451.

Kelso, J. S. (1995). *Dynamic patterns: The self-organization of brain and behavior*. MIT press.

Khansari-Zadeh, S. M. and Billard, A. (2011). Learning stable nonlinear dynamical systems with gaussian mixture models. *IEEE Transactions on Robotics*. 27.5, pp. 943–957.

Khansari-Zadeh, S. M., Kronander, K., and Billard, A. (2012). Learning to play minigolf: A dynamical system-based approach. *Advanced Robotics*. 26.17, pp. 1967–1993.

Kim, D.-H., Kim, K., Kim, K.-Y., and Cha, S.-M. (2001). "Dexterous teleoperation for micro parts handling based on haptic/visual interface". In: *MHS2001. Proceedings of 2001 International Symposium on Micromechatronics and Human Science (Cat. No. 01TH8583)*. IEEE, pp. 211–217.

Kim, J.-T., Ruggiero, F., Lippiello, V., and Siciliano, B. (2022). Planning framework for robotic pizza dough stretching with a rolling pin. In: *Robot Dynamic Manipulation*. Springer, pp. 229–253.

Kim, W., Lee, C., and Kim, H. J. (2018). "Learning and generalization of dynamic movement primitives by hierarchical deep reinforcement learning from demonstration". In: *2018 IEEE/RSJ International Conference on Intelligent Robots and Systems (IROS)*. IEEE, pp. 3117–3123.

Kober, J., Mohler, B., and Peters, J. (2008). "Learning perceptual coupling for motor primitives". In: *2008 IEEE/RSJ International Conference on Intelligent Robots and Systems*. IEEE, pp. 834–839.

Kober, J., Oztop, E., and Peters, J. (2011). "Reinforcement learning to adjust robot movements to new situations". In: *Twenty-Second International Joint Conference on Artificial Intelligence*.

Kober, J., Wilhelm, A., Oztop, E., and Peters, J. (2012). Reinforcement learning to adjust parametrized motor primitives to new situations. *Autonomous Robots*. 33.4, pp. 361–379.

Koutras, L. and Doulgeri, Z. (2020a). "A correct formulation for the Orientation Dynamic Movement Primitives for robot control in the Cartesian space". In: *Conference on Robot Learning*, pp. 293–302.

Koutras, L. and Doulgeri, Z. (2020b). "Dynamic Movement Primitives for moving goals with temporal scaling adaptation". In: *2020 IEEE International Conference on Robotics and Automation (ICRA)*. IEEE, pp. 144–150.

Kroemer, O., Niekum, S., and Konidaris, G. (2019). A review of robot learning for manipulation: Challenges, representations, and algorithms. *arXiv preprint arXiv:1907.03146*.

Kronander, K. and Billard, A. (2014). Learning Compliant Manipulation through Kinesthetic and Tactile Human-Robot Interaction. *IEEE Transactions on Haptics*. 7.3, pp. 367–380.

Kronander, K. and Billard, A. (2012). "Online learning of varying stiffness through physical human-robot interaction". In: *2012 IEEE International Conference on Robotics and Automation*. Ieee, pp. 1842–1849.

Kronander, K. and Billard, A. (2016). Stability considerations for variable impedance control. *IEEE Transactions on Robotics*. 32.5, pp. 1298–1305.

Lamon, E., De Franco, A., Peternel, L., and Ajoudani, A. (2019). A capability-aware role allocation approach to industrial assembly tasks. *IEEE Robotics and Automation Letters* [online]. 4.4, pp. 3378–3385. DOI: 10.1109/LRA.2019.2926963.

Lee, D. and Ott, C. (2011). Incremental kinesthetic teaching of motion primitives using the motion refinement tube. *Autonomous Robots*. 31.2-3, pp. 115–131.

Lee, D. and Park, Y. S. (2018). "Implementation of augmented teleoperation system based on robot operating system (ROS)". In: *2018 IEEE/RSJ International Conference on Intelligent Robots and Systems (IROS)*. IEEE, pp. 5497–5502.

Lee, M. A., Zhu, Y., Zachares, P., Tan, M., Srinivasan, K., Savarese, S., Fei-Fei, L., Garg, A., and Bohg, J. (2020). Making sense of vision and touch: Learning multimodal representations for contact-rich tasks. *IEEE Transactions on Robotics*.

Leidner, D. (2019). On Cognitive Reasoning for Compliant Manipulation Tasks in Smart Production Environments. *KI-Künstliche Intelligenz*. 33.2, pp. 197–200.

Leidner, D., Bartels, G., Bejjani, W., Albu-Schäffer, A., and Beetz, M. (2019). Cognition-enabled robotic wiping: Representation, planning, execution, and interpretation. *Robotics and Autonomous Systems*. 114, pp. 199–216.

Li, S., Jiang, J., Ruppel, P., Liang, H., Ma, X., Hendrich, N., Sun, F., and Zhang, J. (2020). A Mobile Robot Hand-Arm Teleoperation System by Vision and IMU. *arXiv preprint arXiv:2003.05212*.

Li, S., Ma, X., Liang, H., Görner, M., Ruppel, P., Fang, B., Sun, F., and Zhang, J. (2019). "Vision-based teleoperation of shadow dexterous hand using end-to-end deep neural network". In: *2019 International Conference on Robotics and Automation (ICRA)*. IEEE, pp. 416–422.

Li, Y., Ganesh, G., Jarrassé, N., Haddadin, S., Albu-Schaeffer, A., and Burdet, E. (2018). Force, impedance, and trajectory learning for contact tooling and haptic identification. *IEEE Transactions on Robotics*. 34.5, pp. 1170–1182.

Lichiardopol, S. (2007). A survey on teleoperation. *Technische Universitat Eindhoven, DCT report*. 20, pp. 40–60.

Lin, T.-C., Krishnan, A. U., and Li, Z. (2019). "Physical fatigue analysis of assistive robot teleoperation via whole-body motion mapping". In: *2019 IEEE/RSJ International Conference on Intelligent Robots and Systems (IROS)*. IEEE, pp. 2240–2245.

Liu, D., Wang, Z., Lu, B., Cong, M., Yu, H., and Zou, Q. (2020a). A Reinforcement Learning-Based Framework for Robot Manipulation Skill Acquisition. *IEEE Access*. 8, pp. 108429–108437.

Liu, N., Zhou, X., Liu, Z., Wang, H., and Cui, L. (2020b). Learning peg-in-hole assembly using Cartesian DMPs with feedback mechanism. *Assembly Automation*. 40.6, pp. 895–904.

Luo, J., He, W., and Yang, C. (2020). Combined perception, control, and learning for teleoperation: key technologies, applications, and challenges. *Cognitive Computation and Systems*.

Luo, J., Lin, Z., Li, Y., and Yang, C. (2019a). A teleoperation framework for mobile robots based on shared control. *IEEE Robotics and Automation Letters*. 5.2, pp. 377–384.

Luo, J., Liu, C., Feng, Y., and Yang, C. (2020). A method of motion recognition based on electromyographic signals. *Advanced Robotics*, pp. 1–9.

Luo, J., Yang, C., Li, Q., and Wang, M. (2019b). A task learning mechanism for the telerobots. *International Journal of Humanoid Robotics*. 16.02, p. 1950009.

Ma, X., Zhang, Z., and Zhang, H. K. (2021). "Autonomous Scanning Target Localization for Robotic Lung Ultrasound Imaging". In: *2021 IEEE/RSJ International Conference on Intelligent Robots and Systems (IROS)*. IEEE, pp. 9467–9474.

Madhani, A. J., Niemeyer, G., and Salisbury, J. K. (1998). "The black falcon: a teleoperated surgical instrument for minimally invasive surgery". In: *Proceedings. 1998 IEEE/RSJ International Conference on Intelligent Robots and Systems. Innovations in Theory, Practice and Applications (Cat. No. 98CH36190)*. Vol. 2. IEEE, pp. 936–944.

Magrini, E., Flacco, F., and De Luca, A. (2015). "Control of generalized contact motion and force in physical human-robot interaction". In: *2015 IEEE International Conference on Robotics and Automation (ICRA)*, pp. 2298–2304.

Malhan, R. K., Joseph, R. J., Shembekar, A. V., Kabir, A. M., Bhatt, P. M., and Gupta, S. K. (2020). "Online grasp plan refinement for reducing defects during robotic layup of composite prepreg sheets". In: *2020 IEEE International Conference on Robotics and Automation (ICRA)*. IEEE, pp. 11500–11507. DOI: 10.1109/ICRA40945.2020.9196876.

Malhan, R. K., Shembekar, A. V., Kabir, A. M., Bhatt, P. M., Shah, B., Zanio, S., Nutt, S., and Gupta, S. K. (2021). Automated planning for robotic layup of composite prepreg. *Robotics and Computer-Integrated Manufacturing* [online]. 67, p. 102020. DOI: 10.1016/j.rcim.2020.102020.

Marin, A. G. and Weitschat, R. (2016). "Unified impedance and hybrid force-position controller with kinestatic filtering". In: *2016 IEEE/RSJ International Conference on Intelligent Robots and Systems (IROS)*, pp. 3353–3359. DOI: 10.1109/IROS.2016.7759516.

Matas, J., James, S., and Davison, A. J. (2018). Sim-to-real reinforcement learning for deformable object manipulation. *arXiv preprint arXiv:1806.07851*.

Mezirow, J. (1978). Perspective transformation. *Adult education*. 28.2, pp. 100–110.

Michel, Y., Rahal, R., Pacchierotti, C., Giordano, P. R., and Lee, D. (2021). Bilateral teleoperation with adaptive impedance control for contact tasks. *IEEE Robotics and Automation Letters*. 6.3, pp. 5429–5436.

Nikolaidis, S., Zhu, Y. X., Hsu, D., and Srinivasa, S. (2017). "Human-robot mutual adaptation in shared autonomy". In: *2017 12th ACM/IEEE International Conference on Human-Robot Interaction (HRI)*. IEEE, pp. 294–302.

Ochoa, H. and Cortesao, R. (2021). Impedance Control Architecture for Robotic-Assisted Mold Polishing based on Human Demonstration. *IEEE Transactions on Industrial Electronics* [online]. 69.4, pp. 3822–3830. DOI: 10.23919/ICAC50006.2021.9594192.

Oktay, O., Schlemper, J., Folgoc, L. L., Lee, M., Heinrich, M., Misawa, K., Mori, K., McDonagh, S., Hammerla, N. Y., Kainz, B., et al. (2018). Attention u-net: Learning where to look for the pancreas. *arXiv preprint arXiv:1804.03999*.

Pairet, È., Ardón, P., Mistry, M., and Petillot, Y. (2019). Learning Generalizable Coupling Terms for Obstacle Avoidance via Low-Dimensional Geometric Descriptors. *IEEE Robotics and Automation Letters*. 4.4, pp. 3979–3986.

Paraschos, A., Daniel, C., Peters, J. R., and Neumann, G. (2013). "Probabilistic movement primitives". In: *Advances in Neural Information Processing Systems*, pp. 2616–2624.

Paraschos, A., Rueckert, E., Peters, J., and Neumann, G. (2015). "Model-free probabilistic movement primitives for physical interaction". In: *2015 IEEE/RSJ International Conference on Intelligent Robots and Systems (IROS)*. IEEE, pp. 2860–2866.

Pastor, P., Righetti, L., Kalakrishnan, M., and Schaal, S. (2011). "Online movement adaptation based on previous sensor experiences". In: *2011 IEEE/RSJ International Conference on Intelligent Robots and Systems*. IEEE, pp. 365–371.

Peng, J., Qiao, H., and Xu, Z.-b. (2002). A new approach to stability of neural networks with time-varying delays. *Neural networks*. 15.1, pp. 95–103.

Peternel, L., Petrič, T., and Babič, J. (2018). Robotic assembly solution by human-in-the-loop teaching method based on real-time stiffness modulation. *Autonomous Robots*. 42.1, pp. 1–17.

Petit, A., Lippiello, V., Fontanelli, G. A., and Siciliano, B. (2017). Tracking elastic deformable objects with an RGB-D sensor for a pizza chef robot. *Robotics and Autonomous Systems*. 88, pp. 187–201.

Pomerleau, D. A. (1989). "Alvinn: An autonomous land vehicle in a neural network". In: *Advances in neural information processing systems*, pp. 305–313.

Qin, F., Xu, D., Zhang, D., and Li, Y. (2019). Robotic skill learning for precision assembly with microscopic vision and force feedback. *IEEE/ASME Transactions on Mechatronics*. 24.3, pp. 1117–1128.

Quek, Z. F., Provancher, W. R., and Okamura, A. M. (2018). Evaluation of skin deformation tactile feedback for teleoperated surgical tasks. *IEEE Transactions on Haptics*. 12.2, pp. 102–113.

Racca, M., Pajarinen, J., Montebelli, A., and Kyrki, V. (2016). "Learning in-contact control strategies from demonstration". In: *2016 IEEE/RSJ International Conference on Intelligent Robots and Systems (IROS)*. IEEE, pp. 688–695.

Rai, A., Meier, F., Ijspeert, A., and Schaal, S. (2014). "Learning coupling terms for obstacle avoidance". In: *2014 IEEE-RAS International Conference on Humanoid Robots*. IEEE, pp. 512–518.

Rai, A., Sutanto, G., Schaal, S., and Meier, F. (2017). "Learning feedback terms for reactive planning and control". In: *2017 IEEE International Conference on Robotics and Automation (ICRA)*. IEEE, pp. 2184–2191.

Rajeswaran, A., Kumar, V., Gupta, A., Vezzani, G., Schulman, J., Todorov, E., and Levine, S. (2017). Learning complex dexterous manipulation with deep reinforcement learning and demonstrations. *arXiv preprint arXiv:1709.10087*.

Ravichandar, H., Polydoros, A. S., Chernova, S., and Billard, A. (2020). Recent advances in robot learning from demonstration. *Annual Review of Control, Robotics, and Autonomous Systems*. 3.

Rodriguez, I., Nottensteiner, K., Leidner, D., Kaßecker, M., Stulp, F., and Albu-Schäffer, A. (2019). Iteratively refined feasibility checks in robotic assembly sequence planning. *IEEE Robotics and Automation Letters*. 4.2, pp. 1416–1423.

Ronneberger, O., Fischer, P., and Brox, T. (2015). "U-net: Convolutional networks for biomedical image segmentation". In: *International Conference on Medical image computing and computer-assisted intervention*. Springer, pp. 234–241.

Rozo, L. D., Calinon, S., Caldwell, D., Jiménez, P., and Torras, C. (2013). "Learning collaborative impedance-based robot behaviors". In: *Twenty-Seventh AAAI Conference on Artificial Intelligence*.

Santos, L., Cortesão, R., and Quintas, J. (2019). "Twin Kinematics Approach for Robotic-Assisted Tele-Echography". In: *2019 IEEE/RSJ International Conference on Intelligent Robots and Systems (IROS)*, pp. 1339–1346.

Santos, L. and Cortesão, R. (2018). Computed-torque control for robotic-assisted tele-echography based on perceived stiffness estimation. *IEEE Transactions on Automation Science and Engineering*. 15.3, pp. 1337–1354.

Saracino, A., Deguet, A., Staderini, F., Boushaki, M. N., Cianchi, F., Menciassi, A., and Sinibaldi, E. (2019). Haptic feedback in the da Vinci Research Kit (dVRK): A user study based on grasping, palpation, and incision tasks. *The International Journal of Medical Robotics and Computer Assisted Surgery*. 15.4, e1999.

Satici, A. C., Ruggiero, F., Lippiello, V., and Siciliano, B. (2016). "A coordinate-free framework for robotic pizza tossing and catching". In: *2016 IEEE International Conference on Robotics and Automation (ICRA)*. IEEE, pp. 3932–3939.

Saveriano, M., Franzel, F., and Lee, D. (2019). "Merging position and orientation motion primitives". In: *2019 International Conference on Robotics and Automation (ICRA)*. IEEE, pp. 7041–7047.

Saveriano, M. and Piater, J. (2020). Combining decision making and dynamical systems for monitoring and executing manipulation tasks. *Elektrotech. Inftech.* 137.6, pp. 309–315.

Schwarz, M., Rodehutskors, T., Droeschel, D., Beul, M., Schreiber, M., Araslanov, N., Ivanov, I., Lenz, C., Razlaw, J., Schüller, S., et al. (2017). NimbRo Rescue: Solving disaster-response tasks with the mobile manipulation robot Momaro. *Journal of Field Robotics*. 34.2, pp. 400–425.

Selvaggio, M., Giordano, P. R., Ficuciellol, F., and Siciliano, B. (2019). "Passive task-prioritized shared-control teleoperation with haptic guidance". In: *2019 International Conference on Robotics and Automation (ICRA)*. IEEE, pp. 430–436.

Şen, H. T., Cheng, A., Ding, K., Boctor, E., Wong, J., Iordachita, I., and Kazanzides, P. (2016). Cooperative control with ultrasound guidance for radiation therapy. *Frontiers in Robotics and AI*. 3, p. 49.

Shams, L. and Seitz, A. R. (2008). Benefits of multisensory learning. *Trends in Cognitive Sciences*. 12.11, pp. 411–417.

Sharma, R. S., Shukla, S., Karki, H., Shukla, A., Behera, L., and Venkatesh, K. (2019). "DMP based trajectory tracking for a nonholonomic mobile robot with automatic goal adaptation and obstacle avoidance". In: *2019 International Conference on Robotics and Automation (ICRA)*. IEEE, pp. 8613–8619.

Si, W., Guan, Y., and Wang, N. (2022). Adaptive Compliant Skill Learning for Contact-Rich Manipulation With Human in the Loop. *IEEE Robotics and Automation Letters*. 7.3, pp. 5834–5841.

Si, W., Wang, N., and Yang, C. (2021a). A review on manipulation skill acquisition through teleoperation-based learning from demonstration. *Cognitive Computation and Systems*. 3.1, pp. 1–16.

Si, W., Wang, N., and Yang, C. (2021b). Composite dynamic movement primitives based on neural networks for human–robot skill transfer. *Neural Computing and Applications*, pp. 1–11.

Sidhik, S., Sridharan, M., and Ruiken, D. (2021). Towards a Framework for Changing-Contact Robot Manipulation. *arXiv preprint arXiv:2106.10969*.

Silvério, J., Calinon, S., Rozo, L., and Caldwell, D. G. (2018). Learning task priorities from demonstrations. *IEEE Transactions on Robotics*. 35.1, pp. 78–94.

Steinmetz, F., Nitsch, V., and Stulp, F. (2019). Intuitive Task-Level Programming by Demonstration Through Semantic Skill Recognition. *IEEE Robotics and Automation Letters*. 4.4, pp. 3742–3749.

Stotko, P., Krumpen, S., Schwarz, M., Lenz, C., Behnke, S., Klein, R., and Weinmann, M. (2019). A VR system for immersive teleoperation and live exploration with a mobile robot. *arXiv preprint arXiv:1908.02949*.

Stulp, F., Theodorou, E. A., and Schaal, S. (2012). Reinforcement learning with sequences of motion primitives for robust manipulation. *IEEE Transactions on Robotics*. 28.6, pp. 1360–1370.

Su, H., Sandoval, J., Makhdoomi, M., Ferrigno, G., and De Momi, E. (2018). "Safety-enhanced human-robot interaction control of redundant robot for teleoperated minimally invasive surgery". In: *2018 IEEE International Conference on Robotics and Automation (ICRA)*. IEEE, pp. 6611–6616.

Su, H., Yang, C., Ferrigno, G., and De Momi, E. (2019). Improved human–robot collaborative control of redundant robot for teleoperated minimally invasive surgery. *IEEE Robotics and Automation Letters*. 4.2, pp. 1447–1453.

Theodoridis, T. and Hu, H. (2012). Toward intelligent security robots: A survey. *IEEE Transactions on Systems, Man, and Cybernetics, Part C (Applications and Reviews)*. 42.6, pp. 1219–1230.

Todorov, E. and Jordan, M. I. (2002). Optimal feedback control as a theory of motor coordination. *Nature Neuroscience*. 5.11, pp. 1226–1235.

Triantafyllidis, E., McGreavy, C., Gu, J., and Li, Z. (2020a). Multimodal Interfaces for Effective Teleoperation. *arXiv preprint arXiv:2003.14392*.

Triantafyllidis, E., Mcgreavy, C., Gu, J., and Li, Z. (2020b). Study of Multimodal Interfaces and the Improvements on Teleoperation. *IEEE Access*. 8, pp. 78213–78227.

Ude, A., Nemec, B., Petrić, T., and Morimoto, J. (2014). "Orientation in cartesian space dynamic movement primitives". In: *2014 IEEE International Conference on Robotics and Automation (ICRA)*. IEEE, pp. 2997–3004.

Wang, F., Guo, D., Liu, H., Zhou, J., and Sun, F. (2019). "Sound-Indicated Visual Object Detection for Robotic Exploration". In: *2019 International Conference on Robotics and Automation (ICRA)*. IEEE, pp. 8070–8076.

Wang, N., Chen, C., and Di Nuovo, A. (2020). A framework of hybrid force/motion skills learning for robots. *IEEE Transactions on Cognitive and Developmental Systems*.

Wang, N., Chen, C., and Yang, C. (2020). A robot learning framework based on adaptive admittance control and generalizable motion modeling with neural network controller. *Neurocomputing*. 390, pp. 260–267.

Wang, X., Yang, C., Ma, H., and Cheng, L. (2015). "Shared control for teleoperation enhanced by autonomous obstacle avoidance of robot manipulator". In: *2015 IEEE/RSJ International Conference on Intelligent Robots and Systems (IROS)*. IEEE, pp. 4575–4580.

Weber, B., Balachandran, R., Riecke, C., Stulp, F., and Stelzer, M. (2019). "Teleoperating Robots from the International Space Station: Microgravity Effects on Performance with Force Feedback". In: *IEEE International Conference on Intelligent Robots and Systems*. IEEE, pp. 8138–8144.

Wen, X. and Chen, H. (2020). 3d long-term recurrent convolutional networks for human sub-assembly recognition in human-robot collaboration. *Assembly Automation*. 40.4, pp. 655–662.

Wu, M. and Goodman, N. (2018). Multimodal generative models for scalable weakly-supervised learning. *Advances in Neural Information Processing Systems*. 31.

Wu, Y., Balatti, P., Lorenzini, M., Zhao, F., Kim, W., and Ajoudani, A. (2019). A teleoperation interface for loco-manipulation control of mobile collaborative robotic assistant. *IEEE Robotics and Automation Letters*. 4.4, pp. 3593–3600.

Xu, X., Cizmeci, B., Al-Nuaimi, A., and Steinbach, E. (2014). Point cloud-based model-mediated teleoperation with dynamic and perception-based model updating. *IEEE Transactions on Instrumentation and Measurement*. 63.11, pp. 2558–2569.

Xu, X., Panzirsch, M., Liu, Q., and Steinbach, E. (2020). "Integrating Haptic Data Reduction with Energy Reflection-Based Passivity Control for Time-delayed Teleoperation". In: *2020 IEEE Haptics Symposium (HAPTICS)*. IEEE, pp. 109–114.

Xu, Y., Yang, C., Liu, X., and Li, Z. (2018a). "A teleoperated shared control scheme for mobile robot based semg". In: *2018 3rd International Conference on Advanced Robotics and Mechatronics (ICARM)*. IEEE, pp. 288–293.

Xu, Y., Yang, C., Zhong, J., Wang, N., and Zhao, L. (2018b). Robot teaching by teleoperation based on visual interaction and extreme learning machine. *Neurocomputing*. 275, pp. 2093–2103.

Yang, C., Chen, C., He, W., Cui, R., and Li, Z. (2018a). Robot learning system based on adaptive neural control and dynamic movement primitives. *IEEE transactions on neural networks and learning systems*. 30.3, pp. 777–787.

Yang, C., Chen, C., Wang, N., Ju, Z., Fu, J., and Wang, M. (2018b). Biologically inspired motion modeling and neural control for robot learning from demonstrations. *IEEE Transactions on Cognitive and Developmental Systems*. 11.2, pp. 281–291.

Yang, C., Ganesh, G., Haddadin, S., Parusel, S., Albu-Schaeffer, A., and Burdet, E. (2011). Human-like adaptation of force and impedance in stable and unstable interactions. *IEEE Transactions on Robotics*. 27.5, pp. 918–930.

Yang, C., Zeng, C., Cong, Y., Wang, N., and Wang, M. (2018c). A learning framework of adaptive manipulative skills from human to robot. *IEEE Transactions on Industrial Informatics*. 15.2, pp. 1153–1161.

Yang, C., Zeng, C., Fang, C., He, W., and Li, Z. (2018d). A dmps-based framework for robot learning and generalization of humanlike variable impedance skills. *IEEE/ASME Transactions on Mechatronics*. 23.3, pp. 1193–1203.

Yang, C., Zeng, C., Liang, P., Li, Z., Li, R., and Su, C.-Y. (2017a). Interface design of a physical human–robot interaction system for human impedance adaptive skill transfer. *IEEE Transactions on Automation Science and Engineering*. 15.1, pp. 329–340.

Yang, C., Zeng, C., and Zhang, J. (2021). *Robot Learning Human Skills and Intelligent Control Design*. CRC Press. DOI: 10.1201/9781003119173.

Yang, Y., Hua, C., Li, J., and Guan, X. (2017b). Finite-time output-feedback synchronization control for bilateral teleoperation system via neural networks. *Information Sciences*. 406, pp. 216–233.

Yu, N., Xu, C., Li, H., Wang, K., Wang, L., and Liu, J. (2016). Fusion of haptic and gesture sensors for rehabilitation of bimanual coordination and dexterous manipulation. *Sensors*. 16.3, p. 395.

Zeng, C., Su, H., Li, Y., Guo, J., and Yang, C. (2021). An Approach for Robotic Leaning Inspired by Biomimetic Adaptive Control. *IEEE Transactions on Industrial Informatics*.

Zeng, C., Yang, C., and Chen, Z. (2020). Bio-inspired robotic impedance adaptation for human-robot collaborative tasks. *Science China Information Sciences*. 63.7, pp. 1–10.

Zeng, C., Yang, C., Chen, Z., and Dai, S.-L. (2018). Robot learning human stiffness regulation for hybrid manufacture. *Assembly Automation* [online]. 38, pp. 539–547. DOI: 10.1108/AA-02-2018-019.

Zeng, C., Yang, C., Cheng, H., Li, Y., and Dai, S.-L. (2020). Simultaneously encoding movement and sEMG-based stiffness for robotic skill learning. *IEEE Transactions on Industrial Informatics*. 17.2, pp. 1244–1252.

Zeng, C., Yang, C., Zhong, J., and Zhang, J. (2019). Encoding multiple sensor data for robotic learning skills from multimodal demonstration. *IEEE Access*. 7, pp. 145604–145613.

Zhang, T., McCarthy, Z., Jow, O., Lee, D., Chen, X., Goldberg, K., and Abbeel, P. (2018). "Deep imitation learning for complex manipulation tasks from virtual reality teleoperation". In: *2018 IEEE International Conference on Robotics and Automation (ICRA)*. IEEE, pp. 1–8.

Zhu, Z. and Hu, H. (2018). Robot learning from demonstration in robotic assembly: A survey. *Robotics*. 7.2, p. 17.